# THE EFFECT OF NANOSILVER PARTICLES ON THE PHYSICO-MECHANICAL PROPERTIES OF DENTAL AMALGAM FREE OF UNBOUND MERCURY

**CHANTHIRIGA RAMASINDARUM**

**DEPARTMENT OF RESTORATIVE DENTISTRY**
**FACULTY OF DENTISTRY**
**UNIVERSITY OF MALAYA**
**KUALA LUMPUR**

**2018**

# THE EFFECT OF NANOSILVER PARTICLES ON THE PHYSICO-MECHANICAL PROPERTIES OF DENTAL AMALGAM FREE OF UNBOUND MERCURY

**CHANTHIRIGA RAMASINDARUM**

**THESIS SUBMITTED IN FULFILMENT OF THE REQUIREMENTS FOR THE DEGREE OF DOCTOR OF PHILOSOPHY**

**DEPARTMENT OF RESTORATIVE DENTISTRY**
**FACULTY OF DENTISTRY**
**UNIVERSITY OF MALAYA**
**KUALA LUMPUR**

**2018**

**UNIVERSITY OF MALAYA**

**ORIGINAL LITERARY WORK DECLARATION**

Name of Candidate: **Chanthiriga Ramasindarum**

Matric No: **DHA100003**

Name of Degree: **Doctor of Philosophy**

Title of Project Paper/Research Report/Dissertation/Thesis ("this Work"):

**The effect of nanosilver particles on the physico-mechanical properties of dental amalgam free of unbound mercury**

Field of Study: **Dental Materials**

I do solemnly and sincerely declare that:

(1) I am the sole author/writer of this Work;
(2) This Work is original;
(3) Any use of any work in which copyright exists was done by way of fair dealing and for permitted purposes and any excerpt or extract from, or reference to or reproduction of any copyright work has been disclosed expressly and sufficiently and the title of the Work and its authorship have been acknowledged in this Work;
(4) I do not have any actual knowledge nor do I ought reasonably to know that the making of this work constitutes an infringement of any copyright work;
(5) I hereby assign all and every rights in the copyright to this Work to the University of Malaya ("UM"), who henceforth shall be owner of the copyright in this Work and that any reproduction or use in any form or by any means whatsoever is prohibited without the written consent of UM having been first had and obtained;
(6) I am fully aware that if in the course of making this Work I have infringed any copyright whether intentionally or otherwise, I may be subject to legal action or any other action as may be determined by UM.

Candidate's Signature Date:

Subscribed and solemnly declared before,

Witness's Signature Date:

Name:

Designation:

## ABSTRACT

Dental amalgam has been widely used over the past 190 years in dentistry due to its low cost and durability. Silverfil™ was introduced into the Malaysian market in early 2000 as an amalgam free of unbound mercury (Hg). However, a large particle size variation of Silverfil™ alloy is the critical concern raised by its manufacturer. Therefore, the present study focuses on introducing nano-sized silver particles (AgNPs) into the manufacturing process of Silverfil™ in order to enhance its physical and mechanical properties. The aims of this research were first to characterise the Silverfil™ starting materials, followed by synthesis and characterisation of AgNPs, formulation of an experimental nanosilver amalgam based on the conceptual Silverfil™ model, and to finally compare the physical and mechanical characteristics of the optimised experimental nanosilver amalgam with those of Silverfil™ as well as GS80 and Dispersalloy as two other commercially available amalgams. The results obtained via the field emission electron microscopy indicated a particle size distribution in the range of 146-786 nm for the Silverfil™ alloy. Moreover, the X-Ray photoelectron spectroscopy analyses confirmed the absence of unbound Hg in the triturated Silverfil™, while elements such as copper and tin were present as impurities in the composition of its starting materials. AgNPs were synthesised by reaction of an aqueous silver nitrate ($AgNO_3$) solution with hydrazine hydrate as a reducing agent. The high resolution transmission electron microscopy investigations indicated the formation of AgNPs with polygonal morphology and mean particle size of 34.27±7.38 nm. The crystalline structure and size of AgNPs, investigated respectively by X-ray diffraction and small angle X-Ray scattering, were face centred cubic (FCC) and 54.20 nm. Among varied types of AgNPs synthesised with different $AgNO_3$ concentrations, those produced by a 2 M $AgNO_3$ solution were chosen for formulation of the optimised experimental nanosilver amalgam with the AgNPs:Hg ratio of 1:2.9. The manipulation and handling of the optimised experimental nanosilver

amalgam were evaluated by two dentists. The optimised experimental nanosilver amalgam was consisted of polygonal-shaped particles with mean particle size of approximately 141.55±52.12 nm and without the presence of unbound Hg in the triturated formulation. According to the XRD analyses, both Silverfil™ and the optimised experimental nanosilver amalgam showed a crystalline structure resembling "moschellandsbergite", a naturally occurring mineral ($Ag_2Hg_3$). The compressive strength, diametral tensile strength, and Vickers microhardness values of the optimised experimental nanosilver amalgam were quantified as after 24 hours and 7 days of incubation in distilled water at 37°C. The compressive strength values measured after 24 hours for the optimised experimental nanosilver amalgam, Silverfil™, GS80, and Dispersalloy were 380.62±37.10 MPa, 449.66±173.98 MPa, 447.12±18.60 MPa, and 190.68±44.18 MPa, respectively. The diametral tensile strength measured at 24 hours for the optimised experimental nanosilver amalgam was 128.77±63.59 MPa, which was significantly higher than those of Silverfil™ (72.71±10.23 MPa), GS80 (39.32±7.79 MPa), and Dispersalloy (41.66±7.79MPa). On the other hand, GS80 exhibited the highest Vickers microhardness value (233.82±15.68), followed by Dispersalloy (175.38±8.02), and Silverfil™ (103.16±4.39) whereas Vickers microhardness for the optimised experimental nanosilver amalgam was the lowest (89.77±5.55) after 24 hours. Subsequent Bonferroni post hoc tests showed significant differences ($P<0.005$) between the mean Vickers microhardness values of the tested amalgams after storage for 24 hours and 7 days. In conclusion, although no detectable unbound Hg was present in Silverfil™, the impurities existing in the starting materials might contribute to its relatively high mechanical strength. The large particle size variation of the SilverfilTM alloy was addressed by utilisation of AgNPs synthesised with a particle size of 18.81±46.12 nm. The optimised experimental nanosilver amalgam showed improved homogeneity and a significantly higher diametral strength compared to Silverfil™. The AgNPs:Hg ratio of

1:2.9 was determined as the minimum applicable ratio for producing a well-triturated dental amalgam.

**Keywords:** Silver nanoparticles, Unbound Mercury, Silverfil$^{TM}$, Experimental Nanosilver Amalgam.

## ABSTRAK

Amalgam pergigian telah digunakan secara meluas sejak 190 tahun yang lalu dalam bidang restoratif pergigian kerana kos yang rendah dan tahap ketahanannya yang tinggi. Silverfil™ iaitu amalgam pergigian tanpa raksa (Hg) tak terikat telah diperkenalkan dalam pasaran Malaysia pada awal tahun 2000. Walau bagaimanapun, pihak pengeluar menyatakan rasa tidak puas hati tentang variasi saiz zarah yang besar bagi aloi amalgam ini. Maka penyelidikan ini tertumpu pada pengenalan zarah perak bersaiz nano (AgNPs) untuk proses pengeluaran Silverfil™ bagi mempertingkatkan sifat fizikal dan mekanikalnya. Tujuan penyelidikan ini adalah pertama, mencirikan bahan permulaan Silverfil™, diikuti dengan sintesis dan pencirian AgNPs, memformulasikan amalgam pergigian nanoperak eksperimental berdasarkan model konsep Silverfil™ dan akhir sekali membandingkan ciri-ciri fizikal dan mekanikal amalgam pergigian nanoperak eksperimental yang optimum dengan Silverfil™ serta dua lagi amalgam pergigian yang didapati dipasaran iaitu GS80, dan Dispersalloy. Analisis mikroskop elektron pengimbas pancaran medan menunjukkan bahawa sebaran saiz zarah adalah dalam julat 146-786 nm bagi aloi Silverfil™. Selain itu, analisis spektroskopi sinar-X fotoelektron mengesahkan bahawa tiada Hg yang tidak terikat dalam Silverfil™ tertriturat, manakala tembaga dan timah pula hadir sebagai bendasing dalam komposisi bahan permulaannya. AgNPs telah disintesis menggunakan tindak balas larutan perak nitrat ($AgNO_3$) dengan hydrazine hydrate sebagai ejen penurunan. Hasil analisis mikroskop elektron penghantaran leraian tinggi menunjukkan pembentukan AgNPs, morfologinya berbentuk poligon dan saiz puratanya adalah 34.27±7.38 nm. Struktur kristal dan saiz zarah AgNPs masing-masing diselidik menggunakan belauansinar-X (XRD) dan penyerakan sinar-X sudut kecil (SAXS) menunjukkan bentuk kubus berpusat muka (face-centred cubic atau FCC) dan

saiznya 54.20 nm. Antara pelbagai jenis AgNPs yang disintesis dengan kepekatan $AgNO_3$ yang berbeza, AgNPs yang dihasilkan melalui 2 M $AgNO_3$ telah dipilih untuk fomulasi amalgam pergigian nanoperak eksperimental dengan nisbah optimum AgNPs kepada Hg adalah 1:2.9. Manipulasi dan pengendalian amalgam pergigian nanoperak eksperimental dilakukan oleh dua orang doktor pergigian. Amalgam pergigian nanoperak eksperimental yang optimum terdiri daripada zarah-zarah berbentuk poligon dengan saiz puratanya lebih kurang 141.55±52.12 nm dan tiada Hg yang tidak terikat dikesan dalam pemformulaan setelah tertriturat. Menurut analisis XRD, kedua-dua Silverfil™ dan amalgam pergigian nanoperak eksperimental yang optimum telah dihasilkan dalam struktur kristal yang menyerupai mineral semulajadi "moschellandsbergite" ($Ag_2Hg_3$). Sifat mekanikal seperti kekuatan mampatan, kekuatan tegangan diametral dan kekerasan Vickers amalgam pergigian nanoperak eksperimental yang optimum telah diukur selepas 24 jam dan 7 hari diinkubasi dalam air suling pada suhu 37°C. Nilai kekuatan mampatan selepas 24 jam untuk amalgam pergigian nanoperak eksperimental yang optimum, Silverfil™, GS80, dan Dispersalloy masing-masing adalah 380.62±37.10 MPa, 449.66±173.98 MPa, 447.12±18.60 MPa, dan 190.68±44.18 MPa. Kekuatan tegangan diametral selepas 24 jam untuk amalgam pergigian nanoperak eksperimental yang optimum adalah 128.77±63.59 MPa, iaitu lebih tinggi dan signifikan berbanding dengan Silverfil™ (72.71±10.23 MPa), GS80 (39.32±7.79 MPa), dan Dispersalloy (41.66±7.79 MPa). Di samping itu, GS80 pula mempamerkan nilai kekerasan Vickers tertinggi (233.82±15.68), diikuti oleh Dispersalloy (175.38±8.02) dan Silverfil™ (103.16±4.39) manakala amalgam pergigian nanoperak eksperimental yang optimum menunjukkan kekerasan Vickers yang terendah (89.77±5.55) selepas 24 jam. Ujian post hoc Bonferroni telah menunjukkan perbezaan yang signifikan ($P<0.005$) antara nilai min kekerasan Vickers untuk pelbagai jenis amalgam pergigian selepas 24 jam dan 7 hari inkubasi. Kesimpulannya, walaupun tiada Hg yang tidak terikat dikesan dalam komposisi Silverfil™, bendasing yang ada di dalam

bahan permulaan Silverfil™ mungkin menyumbang kepada kekuatan mekanikalnya yang agak tinggi secara relatif. Pelbagai saiz zarah yang besar dalam aloi Silverfil™ telah dikenalpasti manakala apabila menggunakan AgNPs, purata saiz zarah adalah 18.81±46.12 nm. Amalgam nanoperak eksperimental yang optimum, menujukkan penambahbaikan dalam keseragaman bahan dan kekuatan diametral yang tinggi dan signifikan berbanding dengan Silverfil™. Nisbah AgNPs:Hg adalah 1:2.9 telah ditentukan sebagai nisbah minimum untuk menghasilkan amalgam pergigian nanoperak yang memuaskan.

**Kata kunci:** zarah perak bersaiz nano, Hg tidak terikat, Silverfil™, amalgam pergigian nanoperak eksperimental.

## ACKNOWLEDGEMENTS

I would like to express my deepest gratitude to my supervisor, Professor Dr. Noor Hayaty Abu Kasim, for giving me the opportunity to be one of her students at University of Malaya and letting my dream comes true. Her expertise, brilliant ideas, and full supports have made this research possible. Her kindness and continuous optimism for this research have always been encouraging and supporting through the project. I would like to thank her again for introducing me to the "dental world". I also would like to also thank Dr. Ali Dabbagh, my co-supervisor, for his guidance and warm encouragement. Both helped me a lot to improve my knowledge and complete this study. I really appreciate their valuable companions, suggestions and comments.

I could never carry out this research without the financial support received from the University of Malaya and Ministry of Science, Technology, and Innovation (MOSTI) under the Science Fund scheme (03-01-03-SF536). I would like to thank all the lab staff for their assistance in this project.

Not forgetting to thank my sons Nitheesh (3 years) and Shasvinth (8 months) for their patience, as well as my amma, daddy, and sisters Saritha, Anusiah, and Wong Xiang Xiang who have been sources of inspiration, prayer, and support all the while till today. Special thanks to my mother-in-law and father-in-law for taking care of my sons during the thesis write-up. May God bless all of you.

Last but not least my husband, Vegentheran, I want to express my utmost gratefulness to you for your continue support, care, and love.

## TABLE OF CONTENTS

## LIST OF TABLES

## LIST OF FIGURES

## LIST OF SYMBOLS AND ABBREVIATIONS

| | | |
|---|---|---|
| γ | : | $Ag_3Sn$ |
| γ1 | : | Ag-Hg |
| γ2 | : | Sn-Hg |
| η | : | $Cu_6Sn_5$ |
| wt.% | : | Weight percentage |
| v/v% | : | Volume to volume percentage |

| | | |
|---|---|---|
| Ag | : | Silver |
| Ag-Cu | : | Silver copper eutectic |
| Ag-Hg | : | Silver mercury |
| Ag-R | : | Reactive silver |
| Ag-Sn | : | Silver tin |
| $Ag_2Hg_3$ | : | Silver mercury |
| AgNPs | : | Silver nanoparticles |
| CTAB | : | Cetyl trimethylammonium bromide |
| Cu | : | Copper |
| DLS | : | Dynamic light scattering |
| FESEM | : | Field emission scanning electron microscope |
| FWHM | : | Full width at the half maximum |
| HCl | : | Hydrochloric acid |
| Hg | : | Mercury |
| HRTEM | : | High resolution transmission electron microscope |
| ICDD | : | The International centre for diffraction data |

| | | |
|---|---|---|
| In | : | Indium |
| JCPDS | : | Joint Committee for Powder Diffraction Standard |
| $NaBH_4$ | : | Sodium borohydride |
| OSHA | : | Occupational Safety and Health Administration |
| Pd | : | Palladium |
| PDF | : | Powder Diffraction Files Database |
| PPE | : | Personal protective equipment |
| SDS | : | Sodium dodecylbenzenesulfonate |
| Sn | : | Tin |
| UNEP | : | The United Nations environment programme |
| US FDA | : | The United States Food and Drug Administration |
| VHN | : | Vickers hardness number |
| WHO | : | The World Health Organization |
| XPS | : | X-ray photoelectron spectroscopy |
| XRD | : | X-ray diffraction |
| Zn | : | Zinc |

# CHAPTER 1: INTRODUCTION

## 1.1 Background and Rational of the Study

Dental restorations are generally categorised either as direct type, where the filling material is placed into the prepared tooth before being hardened, or the indirect restorations, which are fabricated in laboratories using impressions of the prepared tooth. Dental amalgams, composite resins, and glass ionomers are among the most commonly used direct restorative materials, whereas the gold alloys, base metal alloys, porcelain, and porcelain fused to metal are mostly employed as indirect restorative materials.

Among the varied direct restorative materials, dental amalgam has been widely used over the past two centuries for restoration of premolars and molars (Kasacka et al., 2010). Dental amalgam has been used for replacement of the tooth structure, and in particular for treatment of the large cavities. The amalgam alloys, which provide excellent mechanical properties, wear resistance, and durability are mostly used in public funded clinics due to their relatively low cost compared to their other indirect counterparts (Correa et al., 2012). Dental amalgam placement is not technically difficult due to its excellent conformation to the cavity shape and facile manipulation following amalgamation, making this filling material applicable for a broad range of clinical situations that require long term clinical performance (Brunthaler et al., 2003; Manhart et al., 2004).

In general, dental amalgams are still the preferred filling materials in most low- and middle-income countries (Petersen et al., 2010). According to the report of a meeting on future use of materials for dental restorations convened at the World Health Organization (WHO) headquarter in Geneva, Switzerland in 2009, the filling materials used in the

Philippines included 70% dental amalgams, 20% composite resins, and 10% glass ionomers up to that year. In Jordan, dental amalgam accounted for 90% of the filling materials used in their government clinics, 70-80% in the dental schools, and 60-70% in the private sector. While in Kuwait, the percentage usage of dental amalgam was reported to be 50%, 25%, and 20%, in the public dental clinics, dental schools, and private practice, respectively. In Malaysia, the data for the usage of dental amalgam is only available for private practices, constituting 50% of the applied filling materials, followed by composite resins (30%), and glass ionomers (20%).

In spite of the desirable mechanical performance, the toxicity risks of dental amalgams have raised public concerns due to the presence of residual unbound mercury (Hg) upon setting (Saghiri et al., 2014). Although the quantity of Hg released from dental amalgam is considered as "minute" by the American Dental Associations (Richardson et al., 2011), a series of studies has been carried out to address the exposure levels of Hg released from the dental amalgam restorations (Al-Saleh, 2011; Berdouses et al., 1995; Dutton et al., 2013; Richardson et al., 2011). The reports indicated the absorption and accumulation of the released Hg in various organs such as kidney, brain, lung, and liver. The Hg presence in the body can be detected by examination of saliva (Fakour et al., 2010; Melchart et al., 2008; Zimmer et al., 2002), blood (Abraham et al., 1984; Zimmer et al., 2002), urine (Dye et al., 2005), and faeces (Björkman et al., 1997).

Several attempts have been made to reduce the Hg quantity of the dental amalgam restorations. Incorporation of the spherical-shaped alloy is often considered as the first step in reducing the Hg quantity to 43% compared to 50% for lathe-cut amalgam (Bracho-Troconis et al., 2000). The Hg amount can further be reduced by size optimisation of the alloy particles. A number of studies have also reported the positive effects of some elements such as palladium (Pd), indium (In), and gallium (Ga) on reducing the emission

of the Hg vapour from the dental amalgams (Neme et al., 1999; Powell et al., 1989). In another attempt to address this shortcoming of the dental amalgam, Silverfil™ was also commercially introduced in 2000 to the Malaysian market as an alternative material in the public dental clinics. Silverfil™ formulation is based on 'reactive silver' (Ag-R) particles, partially amalgamated silver mercury (Ag-Hg) compound, and Hg, which produce a chemical structure alike the naturally occurring moschellandsbergite ($Ag_2Hg_3$) mineral. According to the manufacturer, this product, which conforms to the International Standards (ISO 24234:2004, BS EN 1641:2004), is free of unbound Hg following amalgamation due to a complete Hg absorption by Ag-R upon setting. A number of unpublished technical reports provided by the manufacturer confirmed the absence of unbound Hg in Silverfil™ through varied assessments including optical absorption, scanning electron microscope (SEM), energy dispersive X-ray spectroscopy (EDX), X-ray mapping, and metallographic examinations. An electrochemical study further indicated a high rate of Hg diffusion into the Ag-R and Ag-Hg particles during the amalgamation process, resulting in no residual Hg ion the amalgam composition (Abu Kassim et al., 2007). The skin sensitisation and irritation tests according to the ISO 10993-10 criteria also confirmed the Silverfil™ biocompatibility. Furthermore, this product showed insignificant cytotoxicity and genotoxic effects through the tests carried out in accordance to the ISO 10993-5 and ISO 10993-3 standards, respectively.

### 1.2 Problem Statement

In 2010, the Silverfil™ manufacturer raised a concern regarding their difficulties in controlling the size of Ag particles, which ranged between 146 to 786 nm. The inconsistency in the particle size the starting materials might result in variation of the physical, chemical, and mechanical characteristics of the alloy in differed production

batches and difficulties in prediction of the clinical outcomes. Incorporation of raw materials with nano-sized particles is a potential approach to overcome the inconsistency of particle sizes and to further enhance the physical and mechanical properties of Silverfil™. Nanoparticles are being widely used in design and development of various dental materials (Beun et al., 2007; De Souza, 2015; Kaur et al., 2016; Moszner et al., 2004), resulting in outstanding clinical performances compared to those incorporating larger particles (De Souza, 2015; Ernst et al., 2006; Khurshid et al., 2015). The increased surface area endowed by the nano-sized particles may also lead to improved reaction of the Ag particles with Hg and thus, reduced Hg quantity and enhanced mechanical properties.

### 1.3 Aims and Objectives

The current study investigates the effects of nano-sized Ag particles on the physical, chemical, and mechanical characteristics of Silverfil™ through the following aims and objectives:

Aim I: Characterisation of Silverfil™ starting materials;

1. To analyse the elemental composition, phase structure, and the chemical state of Silverfil™ starting materials.
2. To investigate the morphological characteristics of the alloy including the particle size, distribution, and shape.

Aim II: Synthesis and characterisation of Ag nanoparticles (AgNPs);

1. To synthesise AgNPs via the precipitation method.
2. To characterise the chemical and morphological properties of the synthesised AgNPs.

Aim III: Formulation of an experimental nanosilver amalgam using Silverfil™ as the conceptual model;

1. To determine the appropriate amount of AgNPs for formulation of the optimised experimental nanosilver amalgam.
2. To determine the optimal Alloy: Hg ratio for the experimental nanosilver amalgam formulation.
3. To evaluate the manipulation and handling capabilities of the optimised experimental nanosilver amalgam.

Aim IV: A comparative investigation on the chemical, physical, and mechanical properties of the optimised experimental nanosilver amalgam relative to those of Silverfil™ as well as GS80, and Dispersalloy as two commercially available conventional amalgams;

1. To compare the chemical, physical, and morphological features of the optimised experimental nanosilver amalgam with Silverfil™, GS80, and Dispersalloy.
2. To compare the compressive strength, diametral tensile strength, and Vickers microhardness of the optimised experimental nanosilver amalgam with Silverfil™, GS80, and Dispersalloy.

## 1.4 Null Hypothesis

The null hypothesis of the study is that the incorporation of AgNPs with varied concentrations will not influence the physical, chemical, and mechanical characteristics of the resulting dental amalgams free of unbound Hg.

## 1.5 Research Framework

This thesis is prepared in six chapters to comprehensively investigate the varied effects of AgNPs on the physico-mechanical properties of the produced dental amalgams. The current chapter introduced the research subject and provided an overview on the current usages of the dental amalgams and particularly Silverfil™, followed by outlining the aim and objectives of this study. The second chapter presents a comprehensive review on different types of dental amalgams, their various chemical, morphological, and mechanical characteristics, as well as the current challenges in clinical application of these restorative materials. Methods concerning the synthesis of AgNPs and the factors affecting their morphological properties are also outlined in this chapter. Chapter 3 describes the methods applied for characterisations of the Silverfil™ starting materials, Silverfil™, GS80 and Dispersalloy. The experimental steps for producing AgNPs and their characterisation as well as the protocols used for formulation, characterisation, and optimisation of the experimental nanosilver amalgam have also been outlined in this chapter. The results obtained from all the experiments throughout this study are presented in Chapter 4, followed by discussion of the results in Chapter 5. Chapter 6 finally states the limitations of this study, followed by conclusion and recommendations for future works. The research framework illustrated in **Figure 1.1** summarises the protocol applied in this study to achieve the targeted research aims and objectives.

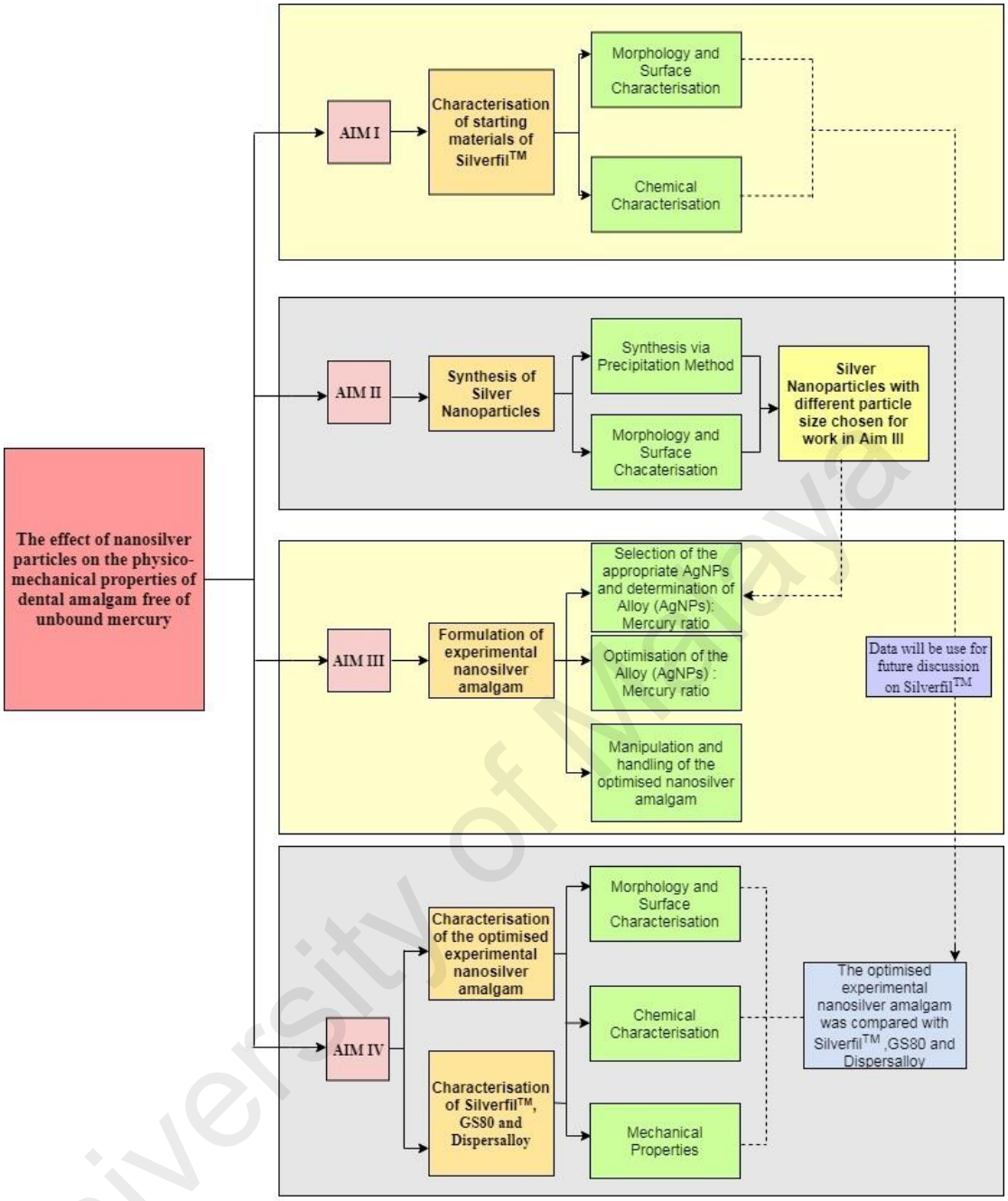


**Figure 1.1: The research framework applied in the present study.**

# CHAPTER 2: LITERATURE REVIEW

This chapter presents a comprehensive review on different types of dental amalgams, their various chemical, morphological and mechanical characteristics, as well as the current challenges in clinical application of these restorative materials. The methods concerning the synthesis of silver nanoparticles (AgNPs) and the factors affecting their morphological properties are also outlined in this chapter.

## 2.1 Dental Amalgam

Amalgam, an alloy of Hg with one or more metals, was invented by the Crawcours brothers in 1833 using shaved French silver coins mixed with Hg and known as "Royal Mineral Succedaneum" (Bharti et al., 2010). However, a high expansion upon setting was the main limitation of this amalgam. In 1895, another generation of amalgam alloy powder consisting 65 wt.% silver (Ag), 29 wt.% tin (Sn) and less than 6 wt.% copper (Cu) was developed by G.V. Black to overcome the high expansion problem (Marquez et al., 2000). Black extensively investigated the physical properties such as dimensional change, strength, and flow ability of the developed amalgam. In 1960, the conventional amalgam comprised of low-copper lathe-cut alloy was introduced, followed by production of the single composite spherical shape amalgam in 1970 with ternary system of Ag, Sn, and Cu (Mahler, 1997).

The dental amalgams available in the market follow the requirements of the International Organization for Standardization, ISO 24234:2015 (International Organization for Standardization, 2015). Numerous factors such as alloy composition, alloy:Hg ratio, size, shape, and the production method of the alloy particles could affect

the clinical performance of the dental amalgam restorations (Anusavice et al., 2013; Chen et al., 1999).

The amalgam formulations generally vary in their Hg content, where 43% to 50% Hg is mixed with metals such as Ag (40-70%), Sn (12-30%), Cu (12- 30%), In (0-4%), Pd (0-5%), and zinc (Zn) (0-1%) (Berry et al., 1994), which are each added to play a specific role in the dental amalgam formulation. The Ag element is a critical component of the amalgam alloy, which enhances the mechanical strength and increases the setting expansion. Sn is also added to decrease the expansion ratio and prolong the setting time (Anusavice et al., 2013). Furthermore, Sn could minimise the Hg evaporation through formation of a protective oxide film on the amalgam surface (Marek, 1997). On the other hand, Cu is incorporated to increment the mechanical strength and surface hardness as well as to reduce the tarnishing, corrosion, and creep in the alloy (Hasheminethad et al., 2012; Shaini et al., 2001). Furthermore, Cu improves the marginal integrity and moderates the plastic deformation (Marquez et al., 2000). However for the high-copper amalgams, research is mostly highlighted the significant effect of this metallic element on the corrosion behaviour of the resulting amalgam (Acciari et al., 1998; Acciari et al., 2005; Solanki, 2012). Zn is used in small portions as a sacrificial anode in the alloy to decrease oxidation of other elements (Anusavice et al., 2013) as well as to improve strength, fatigue resistance, and creep resistance of the dental amalgam (Watkins et al., 1995) as well as to decrease the surface tension, Hg evaporation, and marginal break down (Powell et al., 1989). Incorporation of Pd in the amalgam composition results in reduced corrosion and increased amalgam lustring (Colon et al., 2003; Mahler et al., 1990), where addition of less than 0.5 wt.% of Pd in a high-copper amalgam improves the corrosion behaviour up to a period of 10 years (Colon et al., 2003).

Dental amalgam serves as a versatile filler for the premolar and molar cavities (Kasacka et al., 2010). This restorative material is mainly used for direct, permanent, posterior restorations, and as large foundation restoration or core prior to placing the crown. The dental amalgams endow a high wear resistance, desirable mechanical properties, excellent durability, low sensitivity to clinical techniques, and low cost (Correa et al., 2012). Due to its high mechanical strength and long-term clinical performance, dental amalgam is the preferred material for posterior restorations where masticatory loads are high (Cenci et al., 2004). Dental amalgam highly conforms to the shape of cavity upon hardening, making this material applicable for a broad range of clinical situations (Brunthaler et al., 2003; Manhart et al., 2004).

## 2.2 Types of Dental Amalgam

Many types of amalgam alloys have been produced, which are broadly classified into low-copper and high-copper alloys (Letzel et al., 1997).

### 2.2.1 Low-copper Amalgam

Low-copper or conventional amalgams are the alloys that contain less than 6% Cu, 63-70% Ag, 26-28% Sn, and below 2% Zn (Powers et al., 2006), prepared by dissolution and precipitation methods. Hg diffusion into the Ag-Sn particles forms the Ag-Hg phase ($\gamma 1$), followed by production of the Sn-Hg ($\gamma 2$) phase (Powers et al., 2006). The general setting reaction of the conventional amalgam is presented in Equation (2.1) (Manappallil, 2015).

$$Ag_3Sn + Hg = Ag_2Hg_3 + Sn_8Hg + Ag_3Sn \text{ (unreacted)} \quad \textbf{(2.1)}$$

The $Ag_3Sn$, designated as γ phase, is the strongest phase with the lowest corrosion, which forms about 30 v/v% of the set amalgam. $Ag_2Hg_3$ ($\gamma_1$) is the second strongest phase in the material, which acts as a matrix for the unreacted alloy and forms about 60 v/v% of the set material. The $Sn_8Hg$ ($\gamma_2$) is the weakest and softest phase with high corrosion rate. The volume of this phase decreases with time due to corrosion, resulting in formation of voids in the amalgam structure.

A relatively high corrosion rate is the main disadvantage of the conventional amalgam formulation, caused largely by presence of the $\gamma_2$ phase. This phenomenon can be reduced by adding a powder with globules of eutectic Ag-Cu alloy in portion of 9-33% (Städtler, 1991). The term eutectic refers to an alloy in which the elements are completely soluble in liquid solution, while completely separate into distinct areas upon solidification.

### 2.2.2 High-copper Amalgam

A high-copper amalgam is an alloy with a Cu content more than 6%, which comprises of two types; admixed alloy powder and single-composition alloy powder. The admixed alloy contains 69% Ag, 17% Sn, 13% Cu, and 1% Zn (Manappallil, 2015). During amalgamation, the Ag element originated from the Ag-Cu spherical eutectic particles dissolves into the Hg phase to form the $\gamma_1$ phase. The general setting reaction in the admixed alloy is given in Equation (2.2).

$$Ag_3Sn + Ag\text{-}Cu + Hg = Ag_3Sn + Ag\text{-}Cu + Ag_2Hg_3 + Cu_6Sn_5 \quad \textbf{(2.2)}$$

In this process, the Sn atoms diffuse into the Ag-Cu particles and react with Cu to form the $Cu_6Sn_5$ (η) phase, resulting in γ1 phase surrounded by η and γ phases. The admixed

alloy could facilitate achieving tight contacts and suitable polishability. However, the admixed alloy is hardened slowly.

Unlike the admixed alloy power, the composition of each particle in the single-composition alloy is constant. The Cu content in various single-composition alloys ranges from 13-30 wt.%. In some single-composition alloys, small amounts of In or Pd are included. Equation (2.3) shows the simplified setting reaction in the single-composition alloy.

$$AgSnCu + Hg = Cu_6Sn_5 + Ag_2Hg_3 + AgSnCu \text{ (unreacted)} \quad \textbf{(2.3)}$$

In this process, Ag and Sn dissolve in the Hg phase during trituration, while the Cu-rich phases do not dissolve. The growth of $\gamma_1$ crystals forms a matrix that binds together with the partially dissolved alloy particles. However, the η phase develops crystals on the surface of γ particles dispersed in the matrix (Manappallil, 2015). These phenomena reduce creeps and prevent formation of $\gamma_2$ phase. A study proved that the Cu concentrations above 12% are necessary to eliminate $\gamma_2$ phase and consequently result in reduced corrosion and marginal fracture of the amalgam restorations during their clinical service (Mahler, 1997).

A number of studies have been carried out to compare the low- and high-copper amalgams in terms of marginal fracture (Mahler et al., 1980), microleakage (Gottlieb et al., 1985) and corrosion behaviour (Acciari et al., 1998). In general, the high-copper amalgams show more desirable mechanical strength, durability, corrosion resistances, and tarnishing compared to their low-copper counterparts (Solanki, 2012). The chance of creep is also minimised in the restored teeth when high-copper amalgam is used (Solanki, 2012).

## 2.3 Morphology of the Dental Amalgam Alloy

In addition to the copper content, the dental amalgam alloys can also be categorised as the lathe-cut alloys, spherical alloys, or their combination according to the morphological properties of their particles (**Figure 2.1**).

### 2.3.1 Lathe-cut Amalgam Alloys

Lathe-cut amalgams consist of fine or coarse particles with irregular shapes. These amalgams are prepared by melting together and cooling the alloy components, followed by heat treatment at about 400°C for 8 hours. The bulk alloy is then ground and milled into three different grades of particle sizes. The regular-graded alloys contain particle sizes of above 50 µm, while the fine-graded and micro-graded alloys contain particle sizes of approximately 35 µm and less than 26 µm, respectively. The fine-graded lathe-cut alloy is mostly favoured as it is easily manipulated. Lathe-cut alloy has a higher resistance to condensation compared to their spherical counterparts (Anusavice et al., 2013).

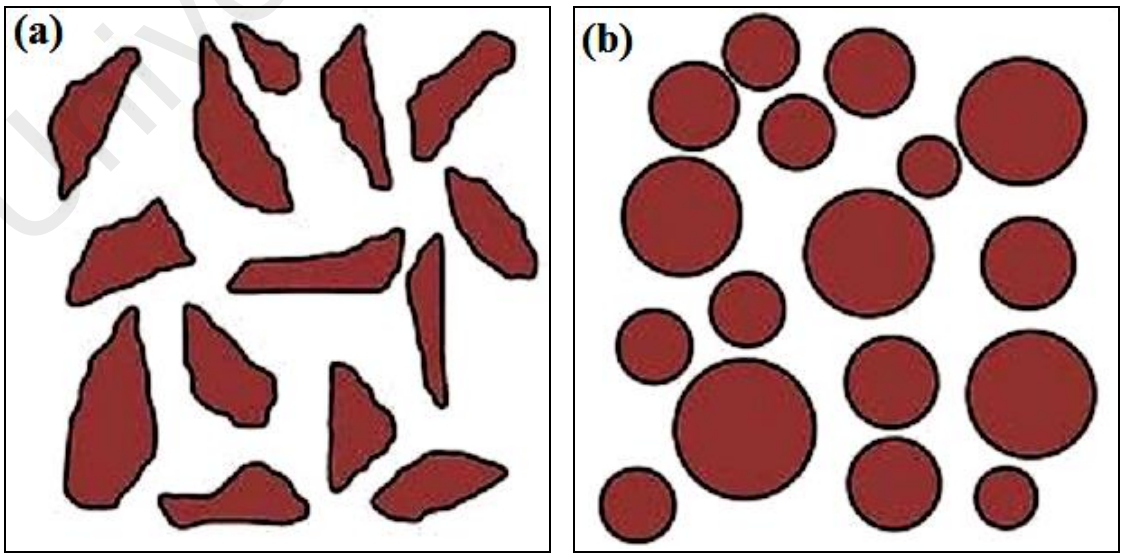


**Figure 2.1: Schematic representations of the lathe-cut and spherical shaped particles of the amalgam alloys; adapted from (Wordpress Theme, 2014).**

### 2.3.2 Spherical Amalgam alloys

In the spherical type amalgam, the alloys are melted, atomised, and cooled to produce spheres with particle sizes of 5-40 μm. The spherical alloys possess smaller surface area per volume ratios compared to the lathe-cut alloys, thus requiring less Hg amount during trituration. Moreover, spherical alloys show higher condensation, faster hardening, and smoother polish. However, these alloys are highly plastic and the clinicians cannot rely on the condensation pressure to establish proximal contour. Further, their overhang tendency is high and achieving tight contacts is challenging (Anusavice et al., 2013).

## 2.4 Durability of the Amalgam Restorations

In 1972, the clinical performance of the dental amalgam and commercial composite direct-filling resin in Class II cavities were compared (Phillips et al., 1972). In this study, 124 paired restorations were placed in 73 patients and only 92 pairs were evaluated in a period of two years. The results showed no changes in anatomic form of the amalgam restorations, while in the composite resin restorations, moderate changes were observed probably due to their occlusal wear (Phillips et al., 1972). Anatomic form is the surface contour of the ridge when it is not supporting an occlusal load.

In 1993, (Mjör et al., 1993) conducted a five-year clinical study on the Class II restorations in permanent teeth using amalgam, glass polyalkenoate cermet, and resin-based composite materials. This study involved 274 Class II restorations with 88 amalgams, 95 cermets, and 91 resin-composites placed in 142 teenager patients. The obtained results indicated the failure of 4 amalgam restorations, 22 cermets, and 9 resin composite restorations. The failure of amalgam and glass ionomer cermet restorations was due to the bulk fractures, whereas the resin composite restorations failed because of both the secondary caries and bulk fractures.

In 1998, Plasman et al. investigated the long-term survival of the extensive amalgam restorations over a 100-months period. The analyses revealed that the survival rate and the functional survival of the extensive amalgam restoration were 88±2% and 92±2%, respectively. There were no statistically significant manipulates of the survival rates for the tooth type, retention method, operator, and extension of the extensive amalgam restoration except for the patient age variable ($p \leq 0.05$).

Van Nieuwenhuysen et al. (2003) conducted a long-term evaluation on the amalgam performance in 428 adults using 722 amalgam restorations, followed by 115 composite resin restorations and 89 crowns. According to the results, 48% of the restorations showed satisfactory performances, while 24% were lost due to the lack of follow up, and 28% failed mainly due to fracture (8%), secondary caries (6%), as well as cusp fracture (5%). The number of failures in the premolars (34%) were relatively higher compared to the molars (27%). It was concluded that amalgam could be considered as a favourable alternative to crowns due to the longevity of this restorative material.

**Table 2.1: The selected studies on durability of amalgam restorations.**

| Authors (years) | Years of studies | Total restorations | No. of patients | AM survival (%) | CR survival (%) | Failed/total restorations |
|---|---|---|---|---|---|---|
| (Phillips et al., 1972) | 1-2 | 124 | 73 | No change in anatomic | Moderate change in anatomic | - |
| (Mjör et al., 1993) | 5 | 274 | 142 | - | - | 4/88 AM<br>22/95 CM<br>9/91 CR |
| (Plasmans et al., 1998) | 8 years, 4 months | - | - | 88±2 | - | - |
| (Van Nieuwenhuysen et al., 2003) | | 722 AM<br>115 CR<br>89 CW | 428 | - | - | - |
| (Bernardo et al., 2007) | 7 | - | - | 94.4 | 85.5 | - |
| (De Amorim et al., 2014) | 2 | - | - | 77.3 | 73.5 | - |

AM=Amalgam, CR=Composite Resin, CM=Cerment, CR=Composite Resin

Bernardo et al. (2007) studied the durability of amalgam and composite restorations in a 7-years follow-up period. The survival rates of amalgam and composite restorations were respectively 94.4% and 85.5%, indicating a better performance of the dental amalgams compared to the composite restorations.

De Amorim et al. (2014) performed a comparative investigation on the survival rates of amalgam and atraumatic restoration treatment and reported the 2-years cumulative survival rates of 77.3% and 73.5% for the amalgam and atraumatic restoration treatment, respectively. Although the difference was not statistically significant, the influences of "type of surface" and "cavity filling time" on the survival rates were indicated. In conclusion, all these studies confirmed the excellent longevity and durability of the dental amalgams compared to other restorative materials. The selected studies carried out for investigation of the durability of amalgam restorations are summarised in **Table 2.1.**

## 2.5 Current Limitations of Dental Amalgams

A major challenge in the clinical application of dental amalgams is the presence of Hg as a heavy metal with high toxicity. Hg exists in inorganic and organic forms. The inorganic form includes the elemental or metallic Hg ($Hg^0$) and mercurous ($Hg^{2++}$) or mercuric ions ($Hg^{++}$). The Hg vapour released from the amalgam is the major source of the inorganic Hg. The organic form includes Hg bonded to carbon-based structures such as methyl, ethyl, phenyl, or similar groups (Bernhoft, 2012).

The Hg vapour has a great binding affinity to the sulphur-containing amino acids present in the body, which further results in its transportation into the brain or deposition in the thyroid, breast, muscles, liver, kidney, lungs, and skin (Bernhoft, 2012). Chronic exposure in a group of people who are regularly or occupationally exposed to high levels

of Hg can produce neurological dysfunction, while the lower exposure levels contribute to a number of non-specific symptoms like weakness, fatigue, anorexia, and weight loss (Bernhoft, 2012).

The released Hg comes from the excess Hg that is not chemically bound to the metal in the set amalgam at lower levels. The rate of Hg release depends on size of the filling, type of tooth, surface area, food texture, chewing and brushing, tooth grinding, as well as the amalgam composition and age (Bates, 2006; Ganss et al., 2000; Hansen et al., 2004). According to the WHO report in 1991 and Berglund et al. (1988), about 2 to 28 mg per facet surface per day is absorbed through inhalation of $Hg^0$ evaporated from the amalgam.

Numerous studies showed that the Hg concentrations in urine (Barregard et al., 2007; Dye et al., 2005), faeces (Engqvist et al., 1998), blood (Gerhardsson et al., 2010; Melchart et al., 2008) and saliva (Fakour et al., 2010; Melchart et al., 2008) are higher in the groups with amalgam fillings than those without this materials. Dye et al. (2005) reported that the total Hg concentration in urine of 1616 female adults aged between 16 to 49 years showed an increment of 0.07±0.004 µg $Hg.g^{-1}$ creatinine per amalgam filled surface. Similar results were found among 267 children aged between 6 to 10 years by Maserejian et al. (2007), where an increase of 0.082±0.022 µg $Hg.g^{-1}$ creatinine per amalgam filled surface was observed. In another study by Melchart et al. (2008), the urine excretion of Hg in patients with amalgam filling was higher (2.21 $ng.ml^{-1}$) after application of 300 mg of 2,3-dimercapto-1-propanesulfonic acid compared to the patients without amalgam filling (0.62 $ng,ml^{-1}$). Moreover, the Hg concentration in erythrocytes (blood) was significantly higher (128 $ng.ml^{-1}$) for the patients treated by amalgam compared to those without amalgam fillings (0.96 $ng.ml^{-1}$) (Melchart et al., 2008). It was also reported in this study that the total Hg in saliva after chewing gum was 0.89 $ng.ml^{-1}$ for the patients with amalgam filling compared to 0.74 $ng.ml^{-1}$ before chewing gum, indicating almost

similar Hg concentrations in saliva prior and after chewing gum. For patients without amalgam filling, the Hg concentration after extensive usage of chewing gum was 0.02 $ng.ml^{-1}$ (Melchart et al., 2008). Therefore, it was concluded that the Hg contents of the blood, urine, and saliva were significantly different between the patients with and without using amalgam restorations.

Due to its potential toxicity to the human health, the use of Hg in dental amalgam has been controversial over the last 25 years. This metallic compound was recognised as the cause of public health disaster in Minamata Bay, Japan, and Iraq (Bernhoft, 2012). The Minamata Convention was termed after a neurological syndrome observed in Minamata City, Japan in 1956, due to consumption of seafood contaminated by the industrial Hg wastes. This Hg poisoning known as "Minamata disease" incurred a public health disaster, resulting in thousands of demises and congenital disorders (Tsuda et al., 2009). The Minamata treaty implements several controls over the mining, trading, storage, as well as disposal of Hg sources in order to reduce the Hg emissions (Unep, 2013). In addition, a number of commitments for health promotion and education, building healthcare capacity, technical supports, and transfer of technology are urged by this treaty with particular consideration of the less developed countries (Unep, 2013). Implementation of a worldwide ban on importation and exportation of certain Hg-containing products including batteries, switches, fluorescent lamps, relays, soaps, and cosmetics) is the most crucial provision of the Minamata treaty, which is set to commence in 2020. However, the dental amalgam fillings have been exempted from the 2020 ban (Unep, 2013).

Application of dental amalgam has been banned in several countries such as Sweden and Norway due to the controversy of their Hg content (Richardson et al., 2011). In Germany, the use of amalgam has been restricted in young children, pregnant women, and patients

with kidney problems (Al-Saleh, 2011). However, this material is still used in the United States of America (USA) (Richardson et al., 2011) and considered as the preferred filling material in many developing countries such as Malaysia, Philippines, Jordan, and Kuwait (Petersen et al., 2010) due to its relatively low cost, durability, and ease to use (Bates, 2006). In spite of the proven health hazards of Hg, it is important to note that the potential health risks due to the Hg release from the dental amalgams is often referred to as "minute" or "very small" by the American Dental Associations (Richardson et al., 2011). It is believed that the amount of Hg release from the dental amalgam is minimal compared to its daily intake through water, food, air, ingestion of contaminated fish, and occupational exposure (Bernhoft, 2012; Kasacka et al., 2010).

## 2.6 Silverfil™

In accordance with the trend to reduce the amount of released Hg vapour, a new formulation of amalgam alloy has been recently developed, which is claimed to contain no unbound Hg upon setting (Radakrishnan, 2008). This dental amalgam, namely, Silverfil™, was launched in April 2001 by the Prime Minister, Dato' Seri Dr. Mahathir Mohamed and secured the United State Food and Drug Administration (US FDA) (510K) approval for sale in USA as well as the European Conformity, CE mark, for distribution in the United Kingdom (UK) and Europe. According to the manufacturer, Silverfil™ has been tested and conformed to the ISO 1559: 1995 (Dental Material-Alloys for Dental Amalgam), EN 1641:2004 (Dentistry- Medical Devices for Dentistry), and ISO 24234:2004 (Dental Mercury) standards (Radakrishnan, 2008). Furthermore, Silverfil™ has undergone the usability tests at both government and private dental sectors in Malaysia to evaluate its clinical performance. The Institute of Medical Research, Kuala Lumpur has confirmed that Silverfil™ is biocompatible without producing irritation and

skin sensitisation (ISO 10993-10) and no cytotoxicity effects in accordance to ISO 10993-5. Moreover, a study carried out at the University of Science Malaysia reported that Silverfil™ is biocompatible with no toxicity and genotoxicity effects (ISO 10993-3) (Radakrishnan, 2008).

### 2.6.1 Formulation and Preparation of Silverfil™

Silverfil™ differs from other commercially available dental amalgams in term of composition where it is purely manufactured from silver tin (Ag-Sn), 'reactive silver' (Ag-R), silver mercury (Ag-Hg), as well as silver mercury plus 'reactive silver' (Ag-Hg+Ag-R). The set Silverfil™ is structurally similar to moschellandsbergite, a natural mineral mostly found in the Landberg district, Obermoschel, Rhineland-Palatinate, Germany (Radakrishnan, 2008). This mineral is made of silver-white amalgam of Hg and Ag with the chemical formula of $Ag_2Hg_3$. Moschellandsbergite has metallic bonds similar to those of pure metallic elements and thus, it could be classified in the class of native elements.

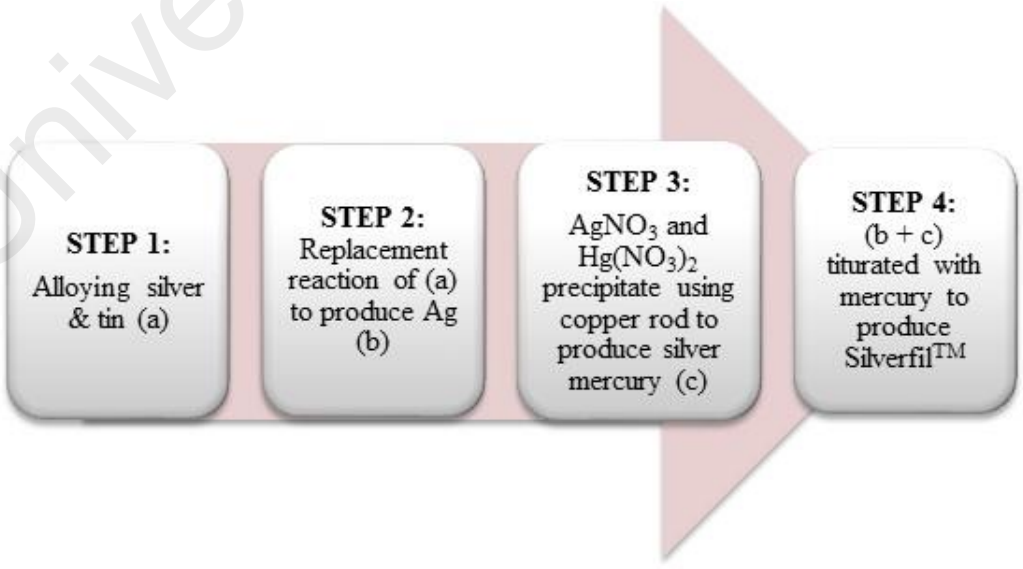


**Figure 2.2: A schematic flow of the experimental steps applied for preparation of Silverfil™.**

**Figure 2.2** illustrates the preparation process of Silverfil™ according to the manufacturer's instruction. In the first step, the metallic Ag and Sn with high purities are alloyed and ground into a fine powder (constituent a). In order to produce Ag, the Ag-Sn alloy is then dissolved in hydrochloric acid (HCl). The acid treatment is repeatedly performed on the solid Ag-Sn particles till a colour alteration from dark grey to yellowish brown is observed. The particles are further filtrated and rinsed several times with warm water to eliminate the acid traces. The treated product is then formed by drying the particles in an oven. The produced Ag in this step is claimed by the manufacturer as 'reactive silver' (constituent b). In order to produce Ag-Hg (constituent c) in the third step, the Ag granules and Hg are separately reacted with nitric acid, resulting in formation of silver nitrate ($AgNO_3$) and mercury nitrate [$Hg(NO_3)_2$] solutions, respectively. After mixing the ($AgNO_3$) and $Hg(NO_3)_2$ solution and diluting the obtained mixture with water, a highly-pure Cu rod is placed to initiate precipitation of the metallic elements and thus produce the Ag-Hg alloy. The precipitation is further filtrated and repeatedly rinsed with warm water to wash out the acid traces, and dehydrated in an oven. Finally, the Ag-R and Ag-Hg components are blended with a weight ratio of 65:35 to produce the compound powder. The mixture is triturated with Hg in the ratio of 1:1.76 and then triturated using high-speed amalgamator for 3s, forming an amalgam paste. This Silverfil™ production technology is patented internationally in countries like Malaysia, USA, Australia, Europe, Hong Kong, South Korea, Russia, Japan, and Latin America. The current Malaysian Utility Innovation Patent number for Silverfil™ is UI 2014000441.

### 2.6.2 The Hg State in Silverfil™

A number of unpublished technical reports (**Appendix A**) have confirmed the absence of free Hg in Silverfil™ using X-ray mapping and metallographic examinations carried

out at City University London as well as the optical absorption, scanning electron microscope (SEM), and energy dispersive X-ray spectroscopy (EDX) performed at University of Malaya (Radakrishnan, 2008). An electrochemical study showed that the diffusion rate of Hg into the Ag particles after amalgamation was higher (Abu Kassim et al., 2007). This study also confirmed that the Hg amount used for the amalgamation process was completely absorbed by Ag and no unbound Hg was present upon setting (Abu Kassim et al., 2007).

### 2.6.3 Antibacterial Performance of Silverfil™

Hassan et al. (2010) used the Ames test to study the genotoxicity effect of Silverfil™ on a mutated strain of *Salmonella typhimurium* (TA1538), with and without an external metabolic activation system. The results depicted that the quantity of revertant colonies, either with or without the external metabolic activation system, were below two-fold of the negative control, even when a high amalgam concentration of 5.0 $ug.ml^{-1}$ was present. These results indicated that Silverfil™ possesses no genotoxic effect (Hassan et al., 2010).

The antibacterial effects of Silverfil™ on two types of oral bacteria including *Streptococcus sobrinus* and *Lactobacillus salivarius* have been evaluated and compared with that of a resin-modified glass ionomer cement (Ketac™ Nano), a composite resin (Amaris), and a glass ionomer cement (Ionofil Molar AC/Quick) (Mohd Azmi et al., 2013). It was observed that Silverfil™ demonstrated the greatest antibacterial effect towards both the studied microorganisms, with the median inhibition zone of 22.41 mm for *Streptococcus sobrinus* and 11.99 mm for *Lactobacillus salivarius*, followed by Ketac™ Nano (12.23 mm and 9.79 mm), and Ionofil Molar (11.65 mm and 1.72 mm) respectively. Amaris was more sensitive towards *Lactobacillus salivarius* (8.86 mm)

rather than *Streptococcus sobrinus* (0.00 mm) (Mohd Azmi et al., 2013). A Similar comparative study was carried out by Jaafar et al. (2013) to investigate the antibacterial effects of Silverfil™, conventional amalgam (Nu Alloy® dp), composite resin (nanohybrid Filtek™ Z350 XT), and glass ionomers (GC Fuji II LC and GC Fuji IX) towards *Enterococcus feacalis* and *Staphylococcus aureus*. It was found that Silverfil™ exhibited the most significant antibacterial effect toward *Enterococcus faecalis* (24.44 mm), followed by GC Fuji II LC (10.46), Nu Alloy® dp (7.92 mm), and GC Fuji IX (5.85 mm). Silverfil™ also showed the greatest inhibition activity toward *Staphylococcus aureus* (29.41 mm), followed by GC Fuji II LC (10.90 mm), GC Fuji IX (8.97 mm), and Nu Alloy® dp (6.95 mm). However, no detectable antibacterial activity was observed by the studied composite resin towards both the strains. Moreover, there was no significant differences between the inhibition activities of Nu Alloy® dp, GC Fuji II LC, and Z350 against two studied strains (Jaafar et al., 2013).

### 2.6.4 Hardness of Silverfil™

Yahya et al. (2013) evaluated the hardness of Silverfil™ amalgam containing different amounts of zinc oxide (ZnO) or aluminium oxide ($Al_2O_3$) nanoparticles produced at different temperatures. They reported an increased hardness of the Silverfil™ amalgam with incorporation of ZnO nanoparticles annealed at 250°C, where incorporation of 0, 10, and 20 wt.% of ZnO led to hardness values of 27.40, 52.03, and 68.53, respectively. However, an opposite effect was observed by annealing of the ZnO particles at 350°C, which resulted in hardness values of 43.20, 23.50, and 15.85 in the amalgams containing 0, 10, and 20 wt.% of ZnO, respectively. The decreased hardness by using ZnO particles annealed at 350°C may be due to the particle agglomeration and formation of coarser ZnO grains (1.2 µm to 2.0 µm) at this annealing temperature. When finer grains of ZnO (800-

900 nm) were added, the hardness was increased. Similar results were also observed when $Al_2O_3$ particles were incorporated into the Silverfil™ amalgam.

### 2.6.5 Microleakage in Silverfil™

More recently, a comparative study was conducted to evaluate the gingival microleakage in Class II open-sandwich restorations for Silverfil™, Z350, and resin-modified nanoionomer Ketac™ N 100 (Malik Masudi et al., 2015). The prepared cavities were filled with four different groups of materials and the gaps between dentin and the materials were measured. Group I consisted of Silverfil™ with Panavia F (amalgam binding agent) and Z35 XT; Group II was restored with Ketac N100 nanoionomer RMGI and Z35 XT; Group III consisted of Conventional Fuji II™ GIC and Z35 XT, and in Group IV, only Z350 XT was applied. The results showed the mean gaps of 4.6±2.2, 5.2±2.7, 20.6±6.9, and 3.8±2.1 between dentin and the materials in groups I to IV, respectively (Malik Masudi et al., 2015). No significant difference was reported between the micro gaps at interfaces of Ketac N100 nanoionomer and Silverfil™ with Z350 XT. Therefore, it was concluded that all the tested restorative materials show similar microleakage outcomes in dentine-material interfaces at gingival margin of class II open-sandwich restorations (Malik Masudi et al., 2015).

## 2.7 Nanomaterials in Dentistry

The utilisations of nanomaterials in various fields of dentistry are listed in **Table 2.2**. In restorative dentistry, nanomaterials have been used to fabricate dental nanocomposites (Huey, 2010), nano-ionomers (Killian et al., 2010), tooth regeneration (Mitsiadis et al., 2012), and endodontic sealers (Abramovitz et al., 2012).

**Table 2.2: The commercialised nano-products in various fields of dentistry. The table is adapted from Khurshid et al. (2015).**

| Field | Products (Company/Manufacturer/City/Country) |
|---|---|
| **Restorative Dentistry** | Nano-ionomers (3M ESPE, St.Paul, MN), Filtek Supreme XT (3M ESPE, Auckland, New Zeland), Ceram X™ (DENTSPLY International, Milford, CT) |
| **Regenerative Dentistry and Tissue Engineering** | Ostim® (Osartis GmbH, Elsenfeld, Germany), Nano-Bone® (ARTOSS, Rostock, Germany) |
| **Periodontics** | Aresin® (Valent, Bridgewater, MA), Nanogen® (Orthogen, Springfield, IL) |
| **Preventive Dentistry** | Nanocare® Gold (Nano-care, Saarwellingen, Germany) |
| **Orthodontics** | Ketac™ N100 Light Curing Nano-Isomers (3M ESPE, St. Paul, MN), Filtek Supreme Plus Universal (3M ESPE, St.Paul, MN) |
| **Prosthodontics** | Nanotech Elite HD plus (Zhermack, Badia Polesine, Italy), GC OPTIGLAZE Color® (GC, Leuven, Belgium) |
| **Oral Implantology** | Nanolite™ Nano-coated implant (BIOMET 3i, Palm Beach Gardens, FL) |
| **Endodontic** | AH plus™ (DENTSPLY International Inc, Wong Chuk Hang, Hong Kong), Guttaflow® (Coltène, Altstätten, Switzerland) |

Several restorative products which contain nanofillers such as 3M ESPE Filtek™ Supreme XT, Grandio, Kalore™, i-Flow^N, Tetric EvoCeram®, and Venus® Diamond are currently available in the market (Takahashi et al., 2011). The nanofilled (3M ESPE Filtek™ Supreme XT) and nanohybrid (Grandio and Venus® Diamond) resin composite have higher mechanical performance compared to microhybrid and microfilled resin composites (Takahashi et al., 2011). A comparative study on the mechanical properties

of nanofilled resin composites, universal hybrid, and microfilled composite showed that the nanofilled resin composites possessed higher mechanical properties such as in flexural strength, elastic moduli, and Vickers microhardness than those of other tested nanohybrids except for the Z-100 hybrid composite. This is derived from the higher surface to volume ratios provided by the nano-sized particles, which result in higher filler loadings in the composite system (Beun et al., 2007). The nanofillers have been integrated in impression materials to obtain superior flow, enhanced hydrophilicity, and improved detail precision (Chandki et al., 2012). Nanofillers have also been used in resin-based restorative dental materials to improve the aesthetic aspect of composites.

Nanomaterials are generally synthesised using either the bottom-up or top-down methods (Iqbal et al., 2012). The bottom-up approach involves synthesis of nanomaterials via assembly of atoms or molecules. The formation of nanoparticles from the colloidal dispersion is an example of the bottom-up approach (Verma et al., 2009). In the top-down approach, nanomaterials are produced by breaking a bulk material into the desired nano-sized particles. Examples of top-down approach are lithographic, etching, and ball milling (Biswas et al., 2012). One of the best examples of the top-down approach is photolithography silicon technology (Pease et al., 2008), which was originally developed for microelectronics, while further used to also fabricate the miniature machines. Nanomaterials can be prepared by various chemical, physical, and biological methods. **Figure 2.3** illustrates different approaches and methods used for synthesis of nanoparticles (Patra et al., 2014).

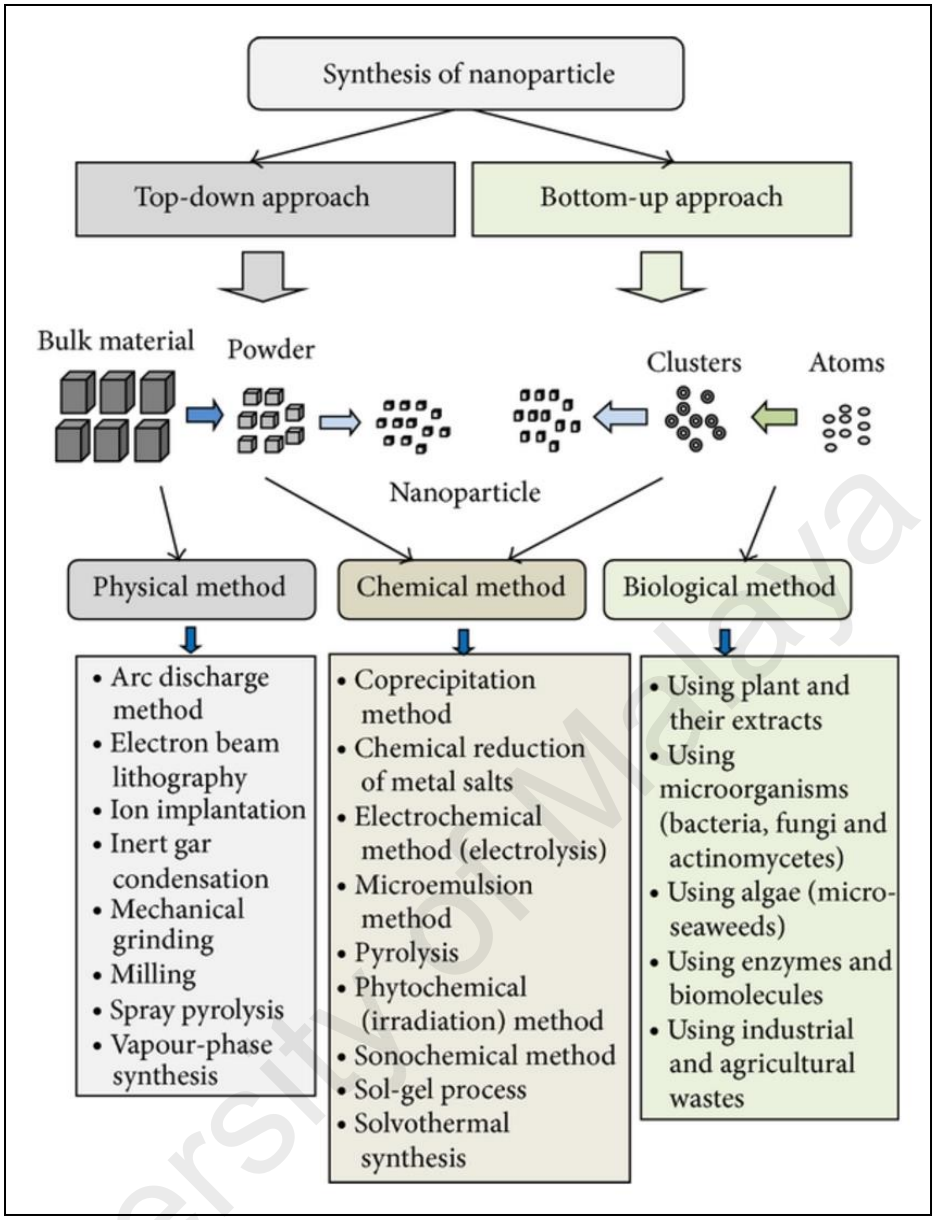


**Figure 2.3: The different methods and approaches introduced for synthesis of nanoparticles. Adapted from (Patra et al., 2014)**.

## 2.8 AgNPs

Ag is a metallic element with atomic number of 47, located in group 11 and period 5 of the periodic table, which occurs in four different states of $Ag^0$, $Ag^+$, $Ag^{2+}$ and $Ag^{3+}$ (Wijnhoven et al., 2009). Although Ag in its metallic state is inert, the ionised Ag is highly reactive with a high binding affinity s to the tissue proteins. The ionised Ag could induce alterations in structure of the bacterial cells walls and nuclear membranes, thus promoting their distortion and death (Rai et al., 2009).

**Table 2.3: Some biomedical applications of AgNPs.**

| Field | Application |
|---|---|
| **Pharmaceutical and Medicine** | Inhibition of HIV-1 replication.<br>Treatment of ulcerative colitis and acne.<br>Molecular imaging of cancer cells.<br>Coating of hospital textiles (surgical gowns and face masks).<br>Coating of breathing masks.<br>Coating of implants for joint replacement. |
| **Dentistry** | Additive in polymerisable dental materials.<br>Nanocomposite resin filler |

In contrast to bulk Ag, AgNPs are of interest due to their unique properties such as lower resistivity ($1.59 \times 10^{-8}$ Ωm) (Song et al., 2009), antimicrobial properties (Franci et al., 2015), improved catalytic performance, and optical properties towards different types of reactions (Venkatesham et al., 2014). AgNPs are also gaining importance in a number of biomedical areas such as pharmaceutical, medicine, and dentistry as summarised in **Table 2.3** (Iravani et al., 2014). AgNPs are being used as bactericidal compounds in water filters, pillows, toothpastes, soaps, and shampoos, as well as antimicrobial agents in air sanitiser sprays, resulting in its increased market value (Prabhu et al., 2012; Tran et al., 2013). According to a survey, 24% of nanotechnology-related products listed around the world are utilising AgNPs (Tran et al., 2013), making AgNPs the largest and fastest growing class of nanoparticles in consumer products applications.

In dentistry, AgNPs have found varied applications in certain areas of restorative dentistry (Cheng et al., 2012a; Cheng et al., 2012b; Durner et al., 2011), implantology (Flores et al., 2010; Zhao et al., 2011), endodontics (Lotfi et al., 2011; Samiei et al., 2013) and dental prostheses (Nam, 2011). The AgNPs incorporated with dental materials have attracted increasing attention especially for their antibacterial effect, smaller particles size, and large surface area (Çınar et al., 2009; Corrêa et al., 2015; Odabaş et al., 2011; Sarraf et al., 2018a; Sarraf et al., 2018b; Sodagar et al., 2016). The particles penetration

through cell membranes is easier when their size is smaller, ensuring higher antimicrobial activity (Corrêa et al., 2015).

The AgNPs have also been incorporated into the composite resins and adhesive systems have been developed to improve the quality, durability, and antimicrobial properties of the polymeric restorative materials (Corrêa et al., 2015). Cheng et al. (2012b) reported that incorporation of AgNPs into the dental composite resins containing amorphous calcium phosphate nanoparticles results in remarkable mechanical properties and enhanced antimicrobial potential. In this study, five nanocomposites were fabricated with different mass fractions of AgNPs (0%, 0.028%, 0.042%, 0.088%, and 0.175%). The results showed that the nanocomposites containing 0-0.042% AgNPs could provide similar mechanical properties with those of commercial composites without any antibacterial activity. An enhanced antibacterial potency was achieved with higher mass fractions of AgNPs. Yoshida et al. (1999) showed that the incorporation of AgNPs into the resin composite could endow a long term inhibitory effect against *Streptococcus mutan* (*S.mutan)*. In another study, Sodagar et al. (2016) reported that the composite discs comprising 5-10% of Ag/hydroxyapatite nanocomposites were able to inhibit the growth of different bacteria types and thus exhibit antibacterial properties against the biofilms.

In another research, Monteiro et al. (2012) incorporated different concentrations of AgNPs (0.05 wt.%, 0.5 wt.%, and 5 wt.% ) in the commercial acrylic resin. Comparison of the mechanical properties of the modified and unmodified resins (0 wt.% AgNPs) revealed that all the specimens showed similar flexural resistant values and therefore, incorporation of AgNPs did not affect the mechanical properties of the acrylic resin.

**Table 2.4: Summary of prior works on the benefits and limitations of the methods used for synthesis of AgNPs.**

| Method | Details | Benefits | Limitations | Techniques | Ref. |
|---|---|---|---|---|---|
| **Physical** | Using external energy sources (e.g. radiation and sonication) | Quick process, high precision over thin films. | Costly, complex experiment setup. | Evaporation-condensation, laser ablation, Electrochemical deposition, Sonochemical deposition, Arc discharge, Irradiation. | (Bogle et al., 2006; Darroudi et al., 2011; Iravani et al., 2014; Natsuki et al., 2015; Zhu et al., 2000) |
| **Chemical** | Using precursor salts, reducing agents, and/or stabiliser. | Excellent control over the reaction rate, narrow distribution of sizes and shapes. | Reactants may be hazardous. | Combination of chemical reducing agents, thermal decomposition, electrochemical deposition. | (López Miranda et al., 2012; Phan et al., 2013; Yin et al., 2003) |
| **Biological** | Using plant derivatives and microorganism as reducing and stabilising agents. | Cheap, highly green, biocompatible | Slow process, wide size and shape distribution. | Bacteria Fungi Plant extracts | (Ahmed et al., 2016; Song et al., 2009) |

The bacterial infection is a major clinical challenge in the field of dental implants (Lu et al., 2010) and thus, development of a coating film that provides excellent antibacterial activity is necessary. Flores et al. (2010) suggested that the modified AgNPs on titanium implants could protect the implant surface against pathogen colonisation. Lu et al. (2010) assessed the antibacterial activity of the titanium implants integrated with four AgNPs concentrations of 0.5, 1, 1.5, and 2M. It was observed that the osteoblasts adhesion on the coating layer was initiated a day after culturing and continued to spread over a period of 7 days. The author also noted that 1M of AgNPs could significantly control the cell production and concluded that the AgNPs with lower concentrations were more favourable for growth of osteoblasts.

### 2.8.1 Synthesis Methods of AgNPs

A number of physical, chemical, biological, and photochemical methods have been developed for synthesis of AgNPs (Natsuki et al., 2015; Tran et al., 2013). A high cost of production, low scalability, as well as low controls over the crystal growth, particle size and distribution, and morphology are the general challenges encountered during the synthesis of AgNPs via these methods (Iravani et al., 2014; Tran et al., 2013). A summary of the benefits and limitations of each synthesis method is provided in **Table 2.4**.

Evaporation-condensation and laser ablation are the main techniques of the physical method for synthesis of AgNPs (Iravani et al., 2014; Natsuki et al., 2015). Evaporation-condensation, which is performed in a tube furnace under the atmospheric pressure, requires a high power consumption and large space for increase the tube temperature (Natsuki et al., 2015). Laser ablation technique has been used to fabricate AgNPs without a solution of the chemical reagents, thus pure colloids can be produced (Natsuki et al., 2015). In another technique, Tien et al. (2008) fabricated AgNPs in deionised water without surfactants using arc discharge technique. In this work, the Ag wires were used as electrodes and immersed in deionised water. As a result, metallic AgNPs with particle size of 10 nm were obtained. The photo-induced or photo-catalytic technique is also a clean method to develop AgNPs, which provides a great spatial resolution and versatility, as well as convenience of use. In addition, this method allows synthesis of AgNPs in different media such as glasses, polymer films, surfactant micelles, and cells (Iravani et al., 2014). For instance, AgNPs have been developed via photoreduction of $AgNO_3$ in a layered suspension of inorganic clays that act as stabilising agents to minimise particle agglomeration (Huang et al., 2008).

Chemical method is the most-widely used approach for synthesis of AgNPs (Lu et al., 2008; Tran et al., 2013). This method is not only the simplest synthesis route, it also

produce highly stable AgNPs with narrow size distribution and controlled shapes. Further, this method can produce large quantities of nanoparticles in a short time frame (Ahmed et al., 2016; Iravani et al., 2014). Theoretically, chemical reduction method is comprised of a metal precursor, a reducing agent, and a stabilising or capping agents (Natsuki et al., 2015). Silver nitrate ($AgNO_3$) is the most preferred Ag precursor due to its low cost and stability. According to Tolaymat et al. (2010), $AgNO_3$ has been used as the starting material in 83% of the reports on synthesis of AgNPs (Tolaymat et al., 2010).Sodium borohydride, sodium citrate, ascorbic acid, dimethyl formamide, Tollen's reagent, elemental hydrogen, and block copolymers of polyethylene glycol are examples of the various organic and inorganic compounds used as reducing agent (Ahmed et al., 2016) to reduce $Ag^+$ ions present in the synthesis medium to the metallic Ag ($Ag^0$) (Ahmed et al., 2016; Iravani et al., 2014). A stabilising agent or surfactant is needed to control the nucleation as well as to limit the particles growth and agglomeration (Liu et al., 2009; Morsy, 2014). The steric hindrances of the surfactants prevent the metallic surfaces from contacting each other and change the surface charge of the clusters, resulting in lower vulnerability to aggregation (Morsy, 2014). **Table 2.5** summarises the common precursors, reducing agents, and surfactants used to synthesise AgNPs via the chemical reduction method.

A number of studies have also been conducted for biological synthesis of AgNPs using microorganisms such as bacteria, fungus, and yeast (Singh et al., 2016; Vigneshwaran et al., 2007) as well as varied plants parts such as green tea leaves (*Camellis sinensis*), neem leaves (*Azadirachta indica*), roots and stem (Kotakadi et al., 2013; Logeswari et al., 2015; Verma et al., 2016). In general, the AgNPs produced via the biological methods are more compatible for the medical applications compared to those synthesised by the chemical and physical methods (Verma et al., 2016).

**Table 2.5: The common precursors, reducing agents, and surfactants used in the chemical reduction of AgNPs.**

| Precursor | Reducing agent/solvent | Surfactant /Stabiliser | Size (nm) | Ref. |
|---|---|---|---|---|
| $AgNO_3$ | $NaBH_4$ | Trisodium citrate | ~5.0 | (Pinto et al., 2010) |
| | | Pluronic F127 | 12±4 | (Angelescu et al., 2012) |
| | | Surfactin (lipopeptide biosurfactant) | 4.9±1.4 | (Reddy et al., 2009) |
| | Ascorbic acid | CTAB | 50 | (Al-Thabaiti et al., 2008) |
| | | SDS | 10 | |
| | | Triton X-100 | - | |
| | Aniline | CTAB | 10-30 | (Khan, Al-Thabaiti, Obaid, & Al-Youbi, 2011) |
| | Ethanol | Polyvinyl-pyrrolidone | 10±5 | (Pal et al., 2009) |
| | Formaldehyde | CTAB | 30 | (Liguo et al., 2010) |

In conclusion among all the methods developed for synthesis of AgNPs, the chemical reduction is preferred due to its ease, cost-effectiveness, and accuracy apart from its practicability in the normal environmental conditions. The current study will also employ the chemical route for synthesis of AgNPs using $AgNO_3$ as the Ag precursor, hydrazine hydrate ($N_2H_4.H_2O$) as the reducing agent, ethylenediamine (EDA) as the capping agent, and cetyltrimethyl ammonium bromide (CTAB) as the surfactant and stabilizing agent. This synthesis method can apprehend sufficient controls over the mean and distribution of the particle size through regulation of the experimental factors. Therefore, the operation parameters including the concentrations of $AgNO_3$ and EDA concentrations will be modified to optimise the synthesis condition and obtain a proper range of Ag particle size. This technique can be executed under easy and gentle conditions and used to synthesise AgNPs on a large scale. The synthesised AgNPs will further be used to produce experimental nanosilver amalgam based on the Silverfil™ concept.

### 2.8.2 Factors Affecting the AgNPs Size

Numerous studies have been carried out to regulate the size, shape, and size distribution of AgNPs (Chitra et al., 2014; Darroudi et al., 2011; Park et al., 2007) and it has been found that a variety of factors including the concentrations of the dispersant, reducing agents, and stabilisers as well as the pH range of the reaction medium, reaction time, reaction temperature, and mixing rate could influence the size of AgNPs synthesised via the chemical route (El-Nour et al., 2010; Natsuki et al., 2015; Sharma et al., 2009).

#### 2.8.2.1 Types and Concentrations of the Chemical Reagents

The types and concentrations of the chemical precursors directly affect the size and distribution of the synthesised AgNPs. Proper adjustments of the type and molar ratios of the chemical reagents such as Ag precursor, reducing agent, and stabiliser often favour the formation of AgNPs with uniform size and morphological distributions (López Miranda et al., 2012). Kim et al. (2001) studied the synthesis of colloidal Ag particles using different Ag precursors including silver tetrafluoroborate ($AgBF_4$), $AgNO_3$, silver hexafluorophosphates ($AgPF_6$) and silver perchlorate ($AgClO_4$) and reported that $AgNO_3$ showed a slower but almost constant reaction rate due to the strong interaction between the $Ag^+$ ion and the nitrate ($NO_3^-$) component; whereas the other precursors represented rapid initial reaction rates, which reduced consequently at increased reaction intervals. On the other hand, many studies have shown that the increased concentrations of Ag precursor produce AgNPs with larger mean particle sizes (Agnihotri et al., 2014; Ajitha et al., 2013; Chen et al., 2009; Janardhanan et al., 2009). In particular, Lee et al. (2014) indicated that when the $AgNO_3$ concentration is increased, the mean particle size of the resulting AgNPs is increased and the size distribution becomes broader.

In case of the reducing agents, Tolaymat et al. (2010) reported that the stronger agents (e.g. sodium borohydride) tend to produce small monodispersed particles with a narrow range of size distribution, whereas the weak agents such as ascorbic acid produce larger particles (Tolaymat et al., 2010). In contrast, Amany et al. (2012) investigated the effects of different types of reducing agents including glucose, sodium borohydride, sodium citrate, and ascorbic acid on size of AgNPs and concluded that the strong reducing agents produced larger particle sizes.

Chaudhuri et al. (2010) also evaluated the effects of four different surfactants including octylphenol ethoxylate (TX-100), CTAB, sodium docecyl sulphate (SDS), and sodium dodecyl benzenesulfonate (SDBS) on the particle size of the produced AgNPs and concluded that the surfactants could significantly reduce the particle size without changing their shape. They also highlighted the different ability of each surfactant type in reducing the particle size of the synthesised AgNPs.

#### 2.8.2.2 pH

The particle size of AgNPs can also be controlled by adjustment of the pH value of the reaction system. Dong et al (2009) investigated the growth, size, and shape of AgNPs under different pH values (pH 5.7 to pH 11.1) using a fix molar ratio of citrate as the reducing agent and $AgNO_3$ as the Ag precursor. It was observed that at high pH values, the reduction rate of the precursor was fast and therefore, spherical, and rod shaped AgNPs were obtained. In contrast at low pH ranges, triangular or polygonal shapes of AgNPs were produced due to a low reduction rate of the Ag precursor. Qin et al. (2010) also observed that as the pH value of the reaction system was increased from 6.0 to 10.5, the mean size of AgNPs was decreased from 73 to 31 nm. Moreover, the reduction rate of Ag precursor was increased at the higher pH value and thus, the spherical shaped

AgNPs were produced. A similar study was carried out by Alqadi et al. (2014) for investigation of the effects of pH on the size, shape, and colour of the colloidal AgNPs produced via the chemical reduction method. It was again confirmed that the increased pH values could result in smaller nanoparticles with spherical morphologies, whereas at low pH ranges, rod- and triangular-shaped AgNPs were formed.

#### 2.8.2.3 Reaction Time

The reaction time and temperature also crucially affect various characteristics of the synthesised AgNPs via controlling the reaction rate as well as the nucleation and growth mechanisms of the nanoparticles. Darroudi et al. (2011) studied different properties of the colloidal AgNPs synthesised at varied reaction times (Darroudi et al., 2011) and observed that the colour of Ag ion changed from colourless to light brown over different periods of time. This observation indicated the increased concentrations of the produced AgNPs at prolonged reaction intervals. Furthermore, the longer reaction periods resulted in narrower particle size distributions and an approximate mean size of 20 nm. In another study, Pal et al. (2012) showed that by increasing the microwave irradiation heating time from 4 to 16 minutes, a larger number of AgNPs was produced.

#### 2.8.2.4 Reaction Temperature

The effect of temperature on development of AgNPs has been also widely studied. Temperature can significantly affect the rate of reaction and thus the particles properties. For instance, Liguo et al. (2010) produced AgNPs via chemical reduction using CTAB at reaction temperature range of 20°C to 60°C and found that the particle size became tinier and more uniform at increased temperatures, most likely due to the higher solubility of

CTAB and faster reaction rates. They also reported the formation of stable and uniform nanosilver flakes at pH of 6, while at higher pH values, a structural collapse and agglomeration were observed in the produced AgNPs.

Jiang et al. (2011) also studied the effect of temperature on the formation and growth of AgNPs. It was found that due to the slower reaction rates at temperature of 0°C, the reaction time must be continued for about 10 hours to complete the reducing process. However at 17°C to 55°C, the reaction rate and thus the particle size were increased. At temperature of 32°C, increased sizes from 90 nm to 180 nm for the nanoplate shape, and 25 nm to 48 nm for the spherical shape were observed. Therefore, it was concluded that the reaction temperature can greatly influence the rates of particle formation and growth, as well as their size, size distribution, and shape. Lee et al. (2014) showed that the AgNPs produced with nanodecahedra morphology at 0°C and 5°C, while at 20°C to 60°C were formed as nanoplates or nanoprisms. It was thus concluded that the reaction temperature affects the morphology of AgNPs in the plasmon-mediated photochemical reaction.

# CHAPTER 3: MATERIALS AND METHODS

## 3.1 Characterisation of Silverfil™ Starting Materials

The starting materials required to produce Silverfil™ including Ag-Sn, Ag-R, Ag-Hg, and Ag-Hg+Ag-R were supplied by the Silverfil™ manufacturer. The elemental compositions of the starting materials were characterised using the energy dispersive X-Ray analysis (EDX; INCA Energy 200, Oxford Instrument, Bristol, United Kingdom). The degree of crystallinity and phase purity of the starting materials were also determined by X-Ray powder diffraction analysis (XRD; D8 Advance, Bruker, Hamburg, Germany). In order to perform this analysis, the specimens were ground into fine powders and placed evenly on the alumina sample holders, followed by packing onto the sample holder using a quartz plate. The specimens were then analysed and the diffraction patterns were generated using a Bruker D8 Advance diffractometer, employing Cu Kα radiation ($\lambda$ = 1.5418 Å) at 2 theta range of 20° to 80° with 0.02° per step. This diffractometer was equipped with the Powder Diffraction Files database (PDF-2) for data acquisition and analysis. The relative intensities of the peaks were compared with the standard references of the International Centre for Diffraction Data (ICDD). The X-Ray photoelectron spectroscopy (XPS; AXIS Ultra DLD, Kratos, Manchester, UK) was also used to identify the chemical state of each element in the starting materials (**Figure 3.1**), followed by analysis of the generated spectra using Kratos Vision 2 Processing software.


**Figure 3.1: The XPS equipment used for chemical analyses of Silverfil™ starting materials as well as the varied set amalgams.**

**Table 3.1: The experimental parameters for preparation of Silverfil™.**

| Composition (%wt) | Hg weight (mg) | Alloy:Hg Ratio (mg:mg) | Trituration time (s) | Manufacturer | Lot No. |
|---|---|---|---|---|---|
| 60 Ag<br>40 $Ag_3Hg_2$ | 600 | 1:1.76 | 3-5 | Silverfil Dental Products Sdn. Bhd, Malaysia | SF1108 01 |

## 3.2 Preparation and Characterisation of Silverfil™

The experimental parameters applied for preparation of the Silverfil™ amalgam are listed in **Table 3.1**. A high-speed amalgamator (Ultramat 2, SDI, Victoria, Australia) was used to triturate the amalgam specimens for 5 seconds. No sample preparation was carried out for morphological and chemical characterisations of the triturated amalgams.

The chemical characterisations were carried out using EDX, XRD, and XPS analyses, while the field emission scanning electron microscopy (FESEM; Quanta FEG 250, FEI,

Eindhoven, the Netherlands) was utilised to assess the amalgam microstructure (**Figure 3.2**). For the FESEM analyses, the amalgam specimens were firstly attached to an aluminum stub using a carbon-coated double-sided adhesive tape and then mounted on the specimen stages. An accelerating voltage of 20 KeV with measuring time of 100 seconds and a working distance of 10 mm were used during the analyses.

## 3.3 Synthesis and Characterisation of AgNPs

### 3.3.1 Synthesis of AgNPs

The materials used to synthesise AgNPs are tabulated in **Table 3.2** and the varied EDA volumes used in synthesis of AgNPs are summarised in **Table 3.3**. **Figure 3.3** also shows the flowchart of the procedure applied for synthesis of AgNPs via the chemical reduction method as reported by Liu et al. (2008).

**Figure 3.2: The FESEM equipment used for morphological characterisations.**

**Table 3.2: Materials used for the synthesis of AgNPs.**

| Materials | Manufacturer | Purity (%) | Molecular weight ($g.mol^{-1}$) |
|---|---|---|---|
| Ethylenediamine (EDA) $(CH_2NH_2)_2$ | Merck, Germany | 98 | 60.10 |
| Silver nitrate ($AgNO_3$) | Sigma Aldrich, Germany | 99 | 169.87 |
| Cetyltrimethyl ammonium bromide (CTAB) $(C_{19}H_{33})N(CH_3)BrN$ | Sigma Aldrich, Germany | 99 | 364.45 |
| Hydrazine hydrate ($N_2H_4.H_2O$) | Sigma Aldrich, Germany | 60 | 50.06 |
| Ethanol absolute ($C_2H_6O$) | Merck, Germany | 99.5 | 46.07 |

**Table 3.3: Variations in the EDA volume used for the synthesis of AgNPs.**

| Sample Code | EDA (ml) | $AgNO_3$ (M) | CTAB (g) | $N_2H_4.H_2O$ (ml) |
|---|---|---|---|---|
| **A1** | 0.05 | 0.10 | 0.01 | 5.00 |
| **A2** | 0.10 | 0.10 | 0.01 | 5.00 |
| **A3** | 0.20 | 0.10 | 0.01 | 5.00 |
| **A4** | 0.40 | 0.10 | 0.01 | 5.00 |

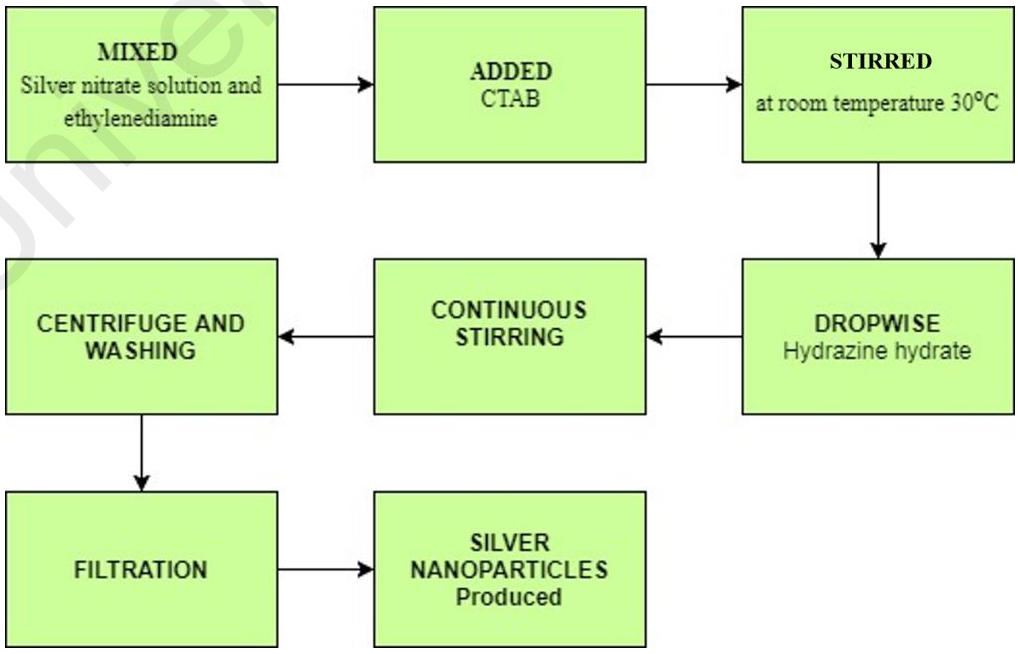


**Figure 3.3: Flowchart of the process used for synthesis of AgNPs.**

**Table 3.4: Variation of the $AgNO_3$ concentration for synthesis of AgNPs.**

| Sample Code | EDA (ml) | $AgNO_3$ (M) | CTAB (g) | $N_2H_4.H_2O$ (ml) |
|---|---|---|---|---|
| **B1** | 0.05 | 0.10 | 0.01 | 5.00 |
| **B2** | 0.05 | 0.20 | 0.01 | 5.00 |
| **B3** | 0.05 | 0.40 | 0.01 | 5.00 |
| **B4** | 0.05 | 0.60 | 0.01 | 5.00 |
| **B5** | 0.05 | 0.80 | 0.01 | 5.00 |
| **B6** | 0.05 | 1.00 | 0.01 | 5.00 |
| **B7** | 0.05 | 1.20 | 0.01 | 5.00 |
| **B8** | 0.05 | 1.60 | 0.01 | 5.00 |
| **B9** | 0.05 | 2.00 | 0.01 | 5.00 |

The $AgNO_3$ (0.1 M) solution was prepared by dissolving 1.6980 g of $AgNO_3$ into 100 ml of distilled water in a volumetric flask. Next, 0.05 ml of EDA was added into 20 ml of $AgNO_3$ solution in an Erlenmeyer flask. A magnetic stirring bar was put into the flask and placed on a stir plate. The mixture was stirred constantly at room temperature (24±1°C) for 5 minutes. Then, 0.01mg of CTAB was added into the solution under constant stirring. Then, 5 ml of 60% hydrazine hydrate solution with approximately one drop per second was added using a micropipette. The mixture was kept under constant stirring for 5 minutes at 24±1°C. The precipitates were then collected from the mixture by centrifuging at 2500 rotation per minute (rpm) for 20 minutes using Benchtop Centrifuge (ROTOFIX 46, Hettich Instruments, Beverly, MA). This centrifugation cycle was repeated several times by washing the precipitates with ethanol, followed by deionised water to remove the residual compound from the product. The final precipitate was filtrated and dried in a desiccator for 24 hours at 24±1°C to obtain AgNPs. The synthesised particles were then characterised to evaluate the effect of EDA content on their size. Once the optimum amount of EDA was determined, the experimental procedures were repeated by varying the concentration of $AgNO_3$ (**Table 3.4**).

The AgNPs prepared with different concentration of $AgNO_3$ (samples B1 to B9) were delivered to the Silverfil™ manufacturer in order to assess the nanoparticles workability

when amalgamated with the other starting materials of Silverfil$^{TM}$. According to the manufacturer's feedback, samples B1 to B4 resulted in poor amalgamations, whereas favourable amalgams were produced by samples B5 to B9. Therefore, sample B5 to B9 were further analysed to produce the optimised AgNPs.

### 3.3.2 Characterisation of AgNPs

The effect of EDA content on the AgNPs size was analysed using the dynamic light scattering (DLS) technique performed on a Zetasizer Nano ZS machine (Malvern Instruments, Malvern, UK). This instrument was equipped with a laser emitting at $\lambda_o$ = 633 nm and operating at a scattering angle of 90°. In these experiments, 0.1 mg of the synthesised AgNPs was dispersed in 5 ml of ethanol using a ultrasonic bath (UC-02, Jeio Tech, Seoul, South Korea) for 10 minutes to disintegrate the agglomerated particles and remove the air bubbles from the solution. The data were processed using the Zetasizer Software version 7.7 and the optimised sample was chosen for further analyses.


**Figure 3.4: The SAXS instrument used for size characterisation of AgNPs.**

**Figure 3.5: The HRTEM instrument used for morphological investigation of AgNPs.**

In addition, the effect of $AgNO_3$ content on size of the synthesised AgNPs was analysed using small angle X-ray spectroscopy (SAXS) and XRD. The SAXS instrument (**Figure 3.4**) equipped in the XRD machine (EMPYREAN, PANalytical, the Netherlands) was also employed to investigate the particle size, size distribution, and

crystallite size of the synthesised AgNPs. The SAXS spectra were recorded at 2 theta range of 20° to 80° with 0.02 degree per step using the Cu Kα radiation (λ=1.5418 Å). The mean crystallite size (L) was calculated through measurement of the full width at the half maximum (FWHM) values of the XRD peaks with the highest intensity. The obtained FWHM values were further transformed into radian and the particle sizes were calculated using the Debye-Scherer's equations:

$$L = \frac{k\lambda}{\beta cos\theta} \quad \textbf{(3.1)}$$

where, K is a constant, λ is the X-ray wavelength, β is FWHM in radian, and θ is the Bragg's angle.

The B5 to B9 specimens were further characterised using XPS to identify the chemical states of the AgNPs. The surface morphology and elemental composition of these specimens were determined using a FESEM machine (SU8000, Hitachi, Tokyo, Japan) equipped with EDX. The specimen preparation procedures were similar to that described earlier in Section 3.2. A high resolution transmission electron microscope (HRTEM; JEM-2100F, JEOL, Tokyo, Japan) was also used to analyse the particle size and morphology of the synthesised B5 to B9 specimens (**Figure 3.5**). For this aim, the particles were first dispersed in ethanol and ultrasonicated for 30 minutes. Then, the dispersed AgNPs were dropped onto the carbon-coated copper mesh grids (300 mesh), followed by removal of the excess liquid with a piece of filter paper and drying in desiccators for two days at 24±1°C. The specimens were mounted on the sample holder and observed under HRTEM at an accelerating voltage of 200 kV.

## 3.4 Formulation of the Experimental Nanosilver Amalgam Based on the Silverfil™ Concept

### 3.4.1 Selection of the Optimal Type of AgNPs

The experimental work for determination of the optimal AgNPs:Hg ratio in various samples (B5-B9) was carried out by the manufacturer due to their concerns about disclosure of the Silverfil™ manufacturing techiques. The samples were handed over to the manufacturer, who was also a dentist, to evaluate the manipulation and handling characteristics of each amalgam formulation. The evaluation involved trituration, condensation, and carving of each amalgam fomulation into prepared cavities in extracted human premolars. The AgNPs synthesised with 2M of $AgNO_3$ (sample B9) was then identified as the most appropriate specimen for formulation of the experimental nanosilver amalgam with AgNPs:Hg ratio of 1:3.

### 3.4.2 Confirmation of the Manufacturer's Recommended AgNPs:Hg Ratio

In order to reafirm suitability of the AgNPs:Hg ratio that was recommended by the manufacturer (1:3), the experimental nanosilver amalgam was produced using sample B9 with varying AgNPs:Hg ratios including 1:1, 1:2, and 1:3. For preparation of the amalgams with AgNPs:Hg ratio of 1:1, equal amounts of AgNPs and Hg (446.5 mg) were weighed and transfered into two separate compartments of an amalgam capsule. Then the capsules were closed and the specimens were then triturated using a high-speed amalgamator for 3 seconds. Similar calculations was done for fabrication of amalgams with AgNPs:Hg ratios of 1:2 and 1:3. Personal protective equipment (PPE) was used during handling of Hg in accordance with the Occupational Safety and Health Administration (OSHA) standard. Weighing of Hg was also performed in a fume cupboard to prevent exposure to its vapours.

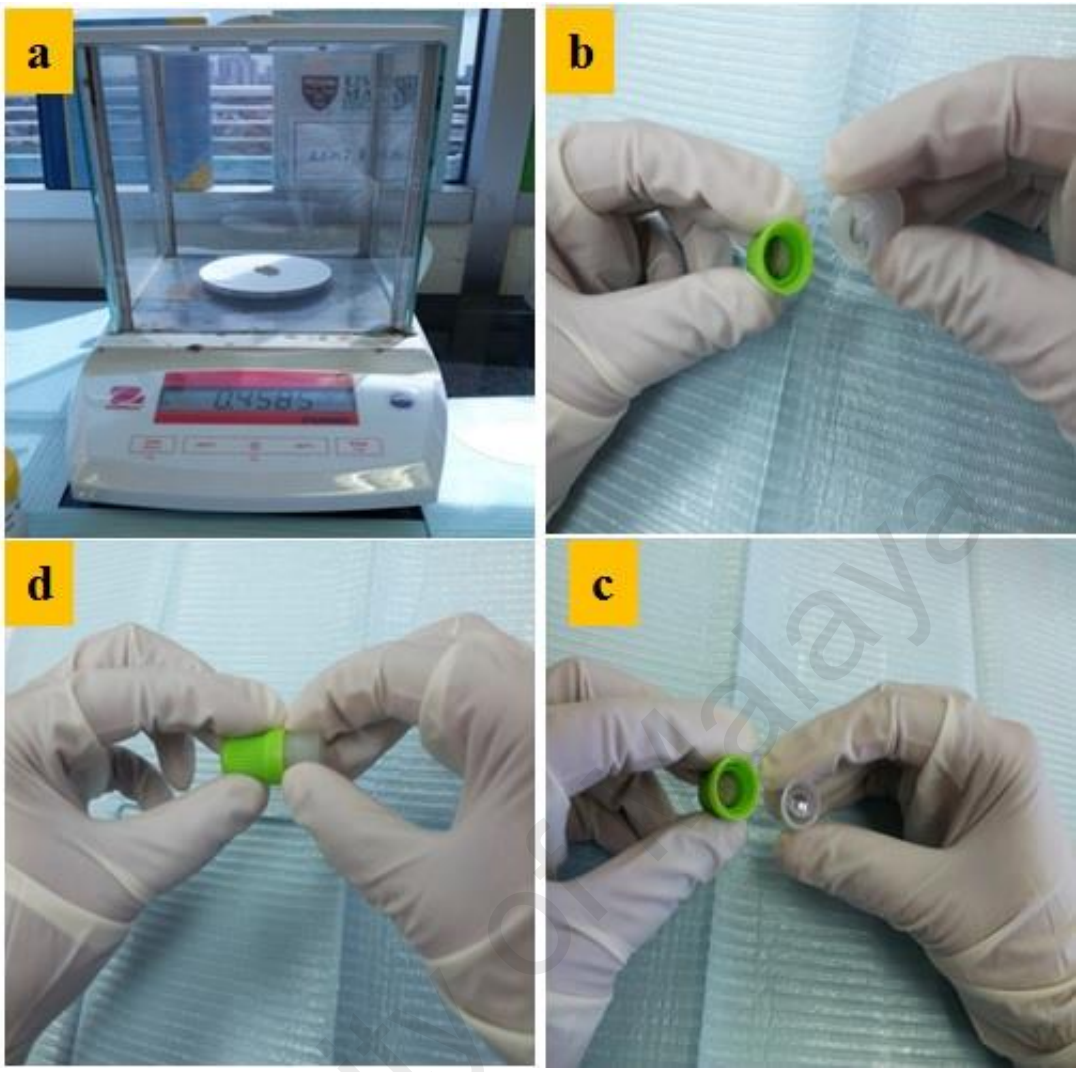


**Figure 3.6: The Encapsulation process of AgNPs and Hg for fabrication of the experimental nanosilver amalgam.** a) AgNPs were measured and b) transferred into the green compartment of the empty capsule. c) The Hg porch was inserted into the transparent compartment of the capsule, and d) the capsule was closed.

### 3.4.3 Tuning the AgNPs:Hg Ratio for Fabrication of the Optimised Experimental Nanosilver Amalgam

Following the positive feedback received from the Silverfil™ manufacturer on the experimental nanosilver amalgam produced using sample B9 and AgNPs:Hg ratio of 1:3, the Hg ratio was further reduced to determine the minimal Hg amount that could be used in formulation of the experimental nanosilver amalgam. For this aim, the amalgam preparation was repeated with the AgNPs:Hg weight ratios of 1:2.8, 1:2.9, and 1:3.0. The required Hg for this stage of the experimental works was supplied by the Silverfil™

manufacturer in the sealed pouches. The procedure applied for preparation of the experimental nanosilver amalgam is illustrated in **Figure 3.6**. The physical appearance of the triturated experimental nanosilver amalgam was then visually compared to those of Silverfil$^{TM}$, GS80, and Dispersalloy. The under-triturated amalgams are dry and crumby, while the well-triturated amalgams are cohesive and shiny with a satin-like appearance.

### 3.4.4 Manipulation and Handling of the Optimised Experimental Nanosilver Amalgam

Once the optimum ratio of AgNPs:Hg was determined, the manipulation and handling of the optimised experimental nanosilver amalgam were assessed. The needed Hg was again supplied by the Silverfil$^{TM}$ manufacturer in the sealed pouches based on the determined optimum ratio. However, addition of AgNPs into the amalgam capsule and trituration were carried out in our laboratory as illustrated in **Figure 3.6**. Two dentists including the manufacturer, who was also a dentist, were chosen to qualitatively assess the manipulation and handling of the triturated optimised experimental nanosilver amalgam in terms of its delivery into the cavity, condenstion, and carving. The dentists were instructed to restore the amalgam cavities prepared by the manufacturer on the typodont teeth using the optimised experimental nanosilver amalgam.

**Table 3.5: Details of the commercially available dental amalgams used as controls in this study.**

| Dental amalgam | Alloy composition (% wt) | Hg (mg) | Alloy:Hg Ratio (mg:mg) | Trituration time (s) | Manufacturer | Lot No. |
|---|---|---|---|---|---|---|
| GS80 | 40 Ag<br>31.3 Sn<br>28.7 Cu | 360 | 1:0.90 | 8 | SDI, Australia | 100222119 |
| Dispersalloy | 69 Ag<br>18 Sn<br>12 Cu<br>1 Zn | 400 | 1:1 | 9-12 | DENTSPLY, USA | 100517 |

### 3.5 Preparation of GS80 and Dispersalloy Amalgams

The specifications of the commercially available dental amalgams used as controls in this study are listed in **Table 3.5**. These control groups were used as indicators to compare their physical and mechanical properties with those of Silverfil™ and the experimental nanosilver amalgam. A high-speed amalgamator (Ultramat 2, SDI, Australia) was used to triturate GS80 and Dispersalloy for respectively 8 and 9 seconds, according to the requirements recommended by their corresponding manufacturers. No sample preparation was performed on the triturated amalgams for the morphological and chemical characterisations.

### 3.6 Chemical and Physical Characteristics of the Optimised Experimental Nanosilver Amalgam, Silverfil™, GS80, and Dispersalloy

The chemical characterisations were carried out using EDX, XRD, and XPS analyses, while the FESEM was utilised to compare the microstructures of different triturated dental amalgams. For the FESEM analyses, the amalgams were first attached to the aluminum stubs using a carbon-coated double-sided adhesive tape and then mounted on the specimen stage. An accelerating voltage of 20 keV was used during the analysis with measuring time of 100 seconds and a working distance of 10 mm.

### 3.7 Mechanical Properties of the Optimised Experimental Nanosilver Amalgam, Silverfil™, GS80, and Dispersalloy

The mechanical properties of the optimised experimental nanosilver amalgam, Silverfil™, GS80, and Dispersalloy amalgams including the compressive strength,

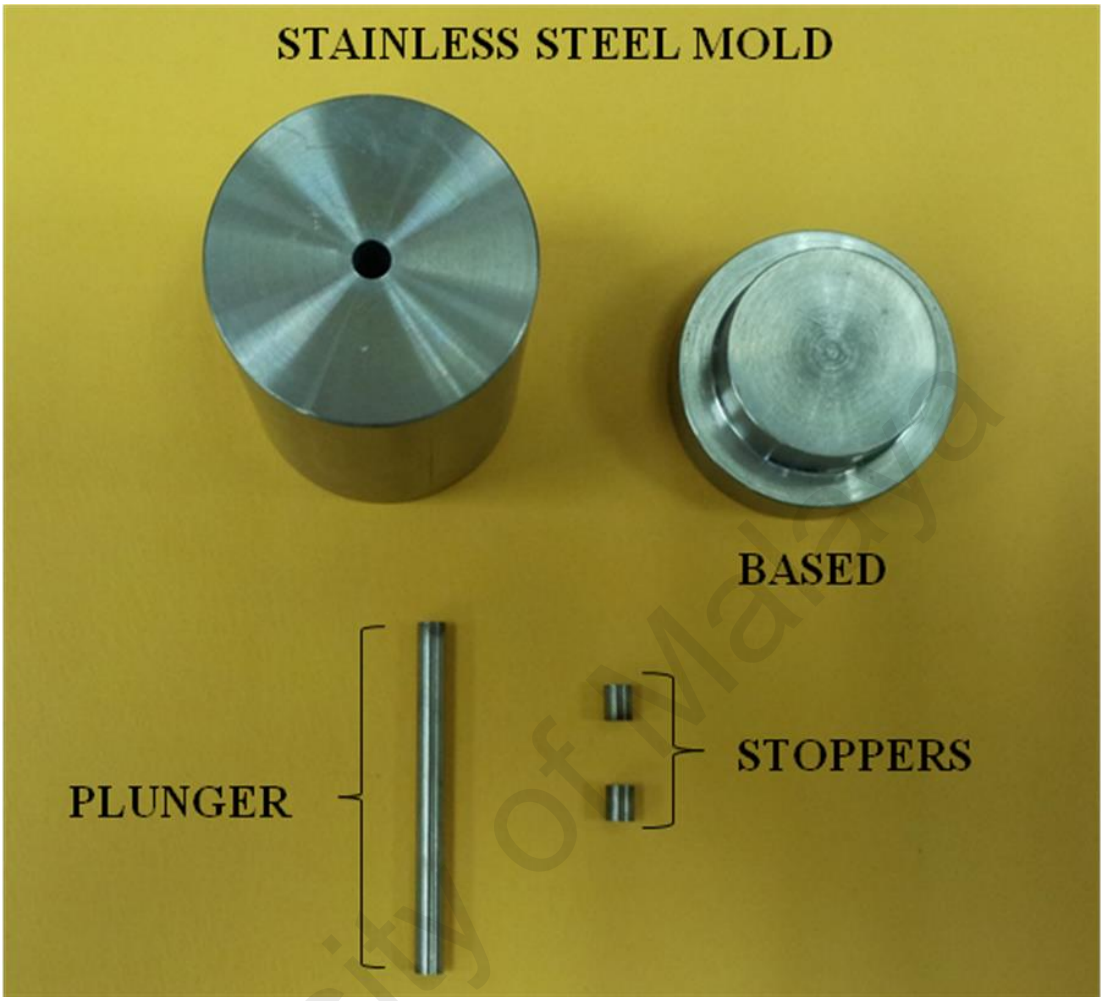


**Figure 3.7: The cylindrical stainless steel compaction die used in preparation of the samples for the compressive strength and diametral tensile strength tests.**

diametral tensile strength, and Vickers microhardness were also investigated. The results obtained for the optimised experimental nanosilver amalgam and Silverfil™ were compared with GS80 and Dispersalloy, assigned as the control groups. The sample preparations for the compressive strength and diametral tensile strength tests were carried out by hand condensation and hydraulic compression of the amalgams into a cylindrical stainless steel compaction die, which consisted of four parts as shown in **Figure 3.7**.

Prior to preparation of each sample, the mould was first cleaned with ethanol and gauze to remove any contamination, followed by lubrication with zinc stearate to facilitate removal of the specimen from the mould after the hydraulic compaction. For preparation of the samples, the first stopper was placed into the mould, followed by insertion of the triturated amalgam and its condensation using the hand pressure. Once the mould was filled, the second stopper and a plunger were placed for the final compaction. Later, the specimen was compacted for two minutes using a hydraulic press machine at 14 MPa, as recommended in the ANSI/ADA Specification No.1 (Alloy for dental amalgam) and ISO 24234:2015 standards. This process led to the fabrication of rod-shaped specimens with approximate heights and diameters of 8 mm and 4 mm, respectively.

For preparation of each specimen, one and a half spills of capsulated amalgam were used. In order to investigate the effect of oral environment on mechanical properties of the varied dental amalgams, the specimens were immersed in distilled water with temperature of 37±1°C for 24 hours and 7 days, without performing any thermocycling process on the prepared specimens. The compressive and diametral tensile strengths were determined using a Universal Testing Machine (Model 4469, Instron, Norwood, MA) (**Figure 3.8(a)**) with a cross-head speed of 0.5 $mm.min^{-1}$ at room temperature (24±1°C). The dimensions of each specimen were measured with 0.01 mm accuracy using a digital caliper (CD-6" CSX, Mitutoyo, Kawasaki, Japan). The experiments were repeated ten times for each storage condition and the obtained data were tabulated for the statistical analyses using the Statistical Package for Social Science (SPSS) software (version 22, SPSS Inc., Chicago, IL). The results obtained for the optimised experimental nanosilver amalgam and Silverfil$^{TM}$ were compared with those of the control groups.

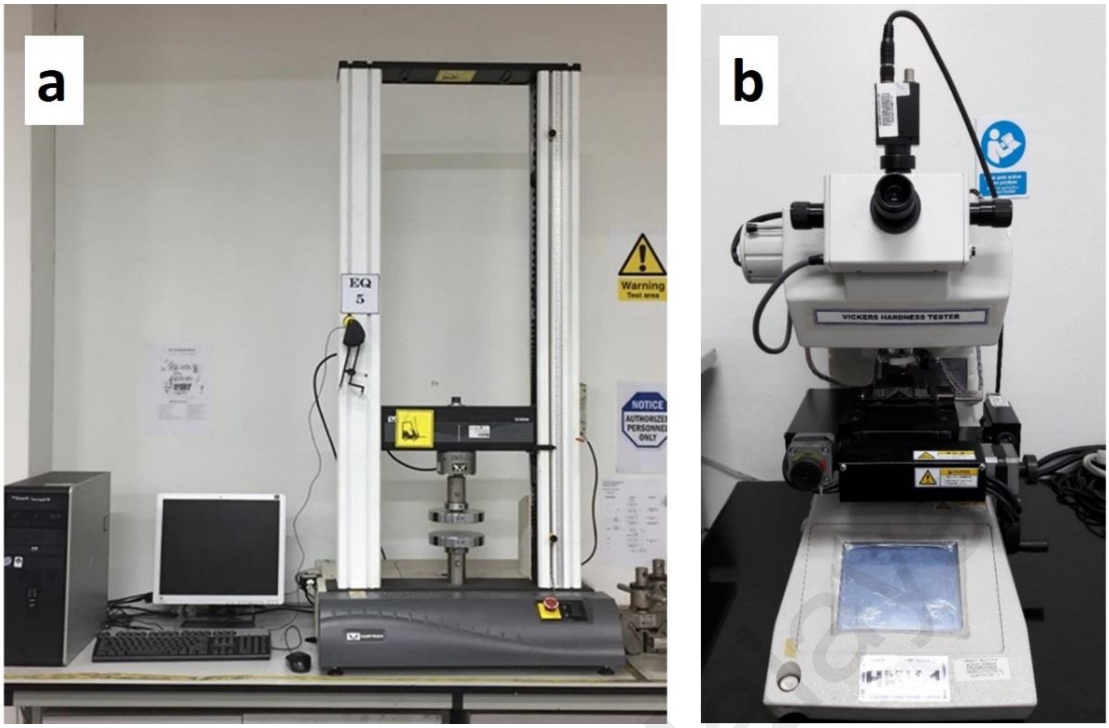


**Figure 3.8: a) The universal testing machine used to measure the compressive strength and diametral tensile strength, and b) the automated Vickers microhardness testing machine used to determine the Vicker microhardness of the set amalgams.**

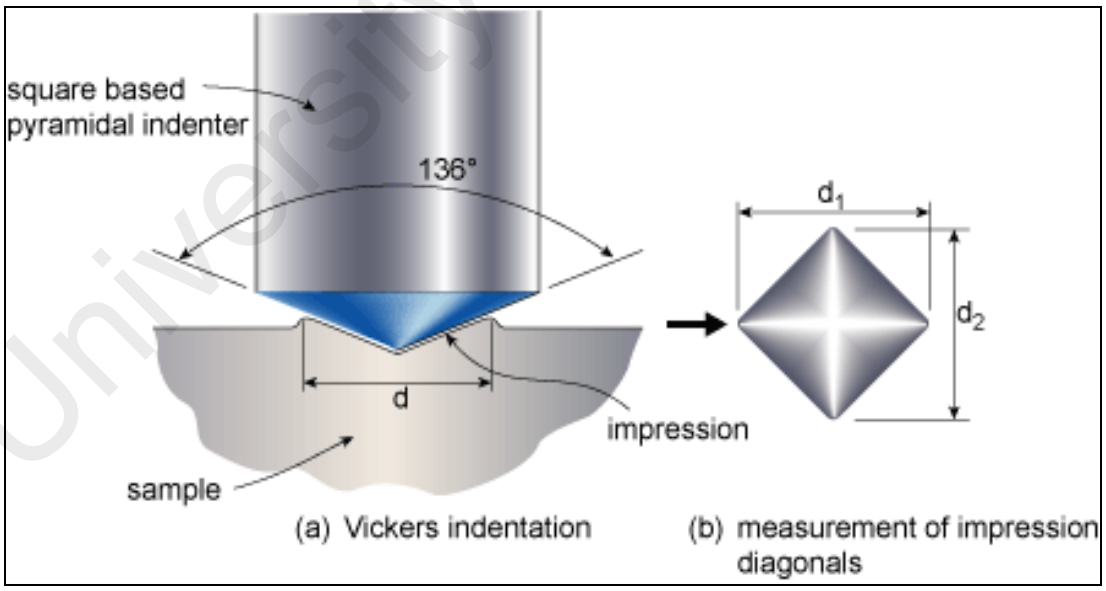


**Figure 3.9: A schematic of the diagonal approach used in the Vickers microhardness measurements. The figure was adapted from Gen (2017).**

The optimised experimental nanosilver amalgam, Silverfil™, GS80, and Dispersalloy were also subjected to surface hardness measurements using a Vickers microhardness

tester (HMV, Shimadzu, Tokyo, Japan) based on an optical measurement system (**Figure 3.8(b)**). The Vickers hardness number (VHN) was determined according to the Equation (3.2).

$$VHN = \frac{1.854\ L}{d^2} \qquad \textbf{(3.2)}$$

where L is the load in kg and d is the diagonal length in mm of the indentation impression.

A schematic of the diagonal measurements for the Vickers hardness tests is illustrated in **Figure 3.9**. In order to perform the Vickers hardness tests, ten cylindrical specimens with heights and diameters of 4mm were prepared from each amalgam via the compaction method described previously. One flat surface of the specimens was ground by hand lapping using the medium grade P800 silicon carbide papers (CarbiMet2 Abrasive, Buehler, Aachen, Germany), followed by polishing with the fine grade P1200 silicon carbide papers (CarbiMet2 Abrasive, Buehler, Aachen, Germany) for a minute. Five indentations were made on the polished surface of each specimen after incubation for 24 hours or 7 days in distilled water at 37±1°C. The indentations were created by application of a 30 g loading for 20 seconds, which were both determined in preliminary studies as the optimal experimental parameters to obtain a clear diamond indentation shape. The diagonal lengths of the resultant indentations were recorded for calculation of the VHN values according to the Equation (3.2). The data were tabulated for statistical analyses where the results obtained for the optimised experimental nanosilver amalgam and Silverfil™ were compared with those of GS80 and Dispersalloy.

# CHAPTER 4: RESULTS

## 4.1 Characterisation of Silverfil™ Starting Materials

In this study, the starting materials of Silverfil™ including Ag-Sn, Ag-R, Ag-Hg, and Ag-Hg+Ag-R were characterised in terms of their elemental composition, microstructural properties, and chemical states of the elements.

### 4.1.1 Elemental characteristics

The elemental spectra of the varied starting materials obtained by EDX analyses are presented in **Figure 4.1 and** the atomic percentages of their elements are listed in **Table 4.1**. The EDX analyses carried out on large regions of the samples revealed that no impurities were present in the Ag-Sn, Ag-R, and Ag-Hg compositions. The incidenced of the peaks at lower keV values probably corresponded to some light elements such as C and O because of their presence in the environment as well the rubber paste used for attachment of the specimens on the EDX specimen holders. The Ag-R peak showed a relatively high intensity at 3.0 keV corresponding to the binding energy of Ag, which indicated that the Ag-R composed of Ag particles.

The EDX map analyses were also performed to establish the elemental distributions of the starting materials. The EDX analysis is crutial to ensure the homogeneity of the elemental distributions, which further result in identical chemical, physical, and mechanical characteristics in different parts of the sample. Furthermore, inhomogeneous distribution of the elements may probably result in decreased interaction of the Ag and Hg atoms, leading to increased amounts of unbound Hg. The distributions of the constituent Ag and Sn atoms in Ag-Sn as well as Ag and Hg atoms in Ag-Hg, are

highlighted using different colour schemes in **Figure 4.2.** According to this figure, all the elements were homogeneously distributed without the presence of large agglomerates.

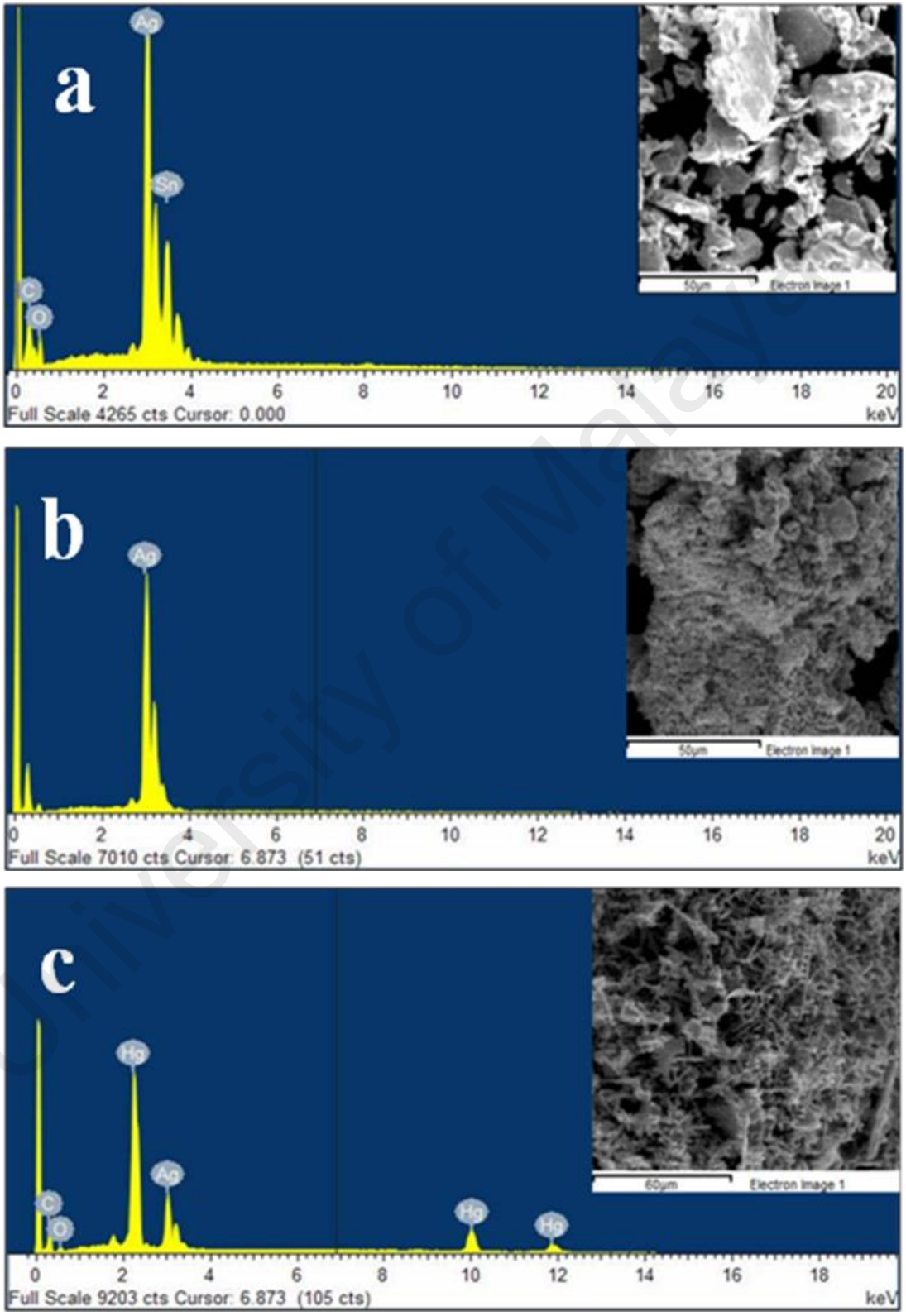


**Figure 4.1: The EDX spectra of the starting materials of Silverfil™.** a) The Ag-Sn peaks indicated the presence of Ag and Sn, b) the Ag-R peaks confirmed the presence of pure Ag, and c) Ag-Hg Peaks showed the existence of Ag and Hg.

**Table 4.1: The atomic percentages of Silverfil™ starting materials recorded by the EDX analyses.**

| Starting Materials | Atomic Percentage (%) | | | | | | |
|---|---|---|---|---|---|---|---|
| | C | O | Ag | Sn | Cu | Hg | Total |
| **Ag-Sn** | 22.08 | 44.21 | 23.56 | 10.15 | - | - | 100 |
| **Ag-R** | - | - | 100 | - | - | - | 100 |
| **Ag-Hg** | 63.48 | 8.1 | 12.92 | - | - | 15.5 | 100 |

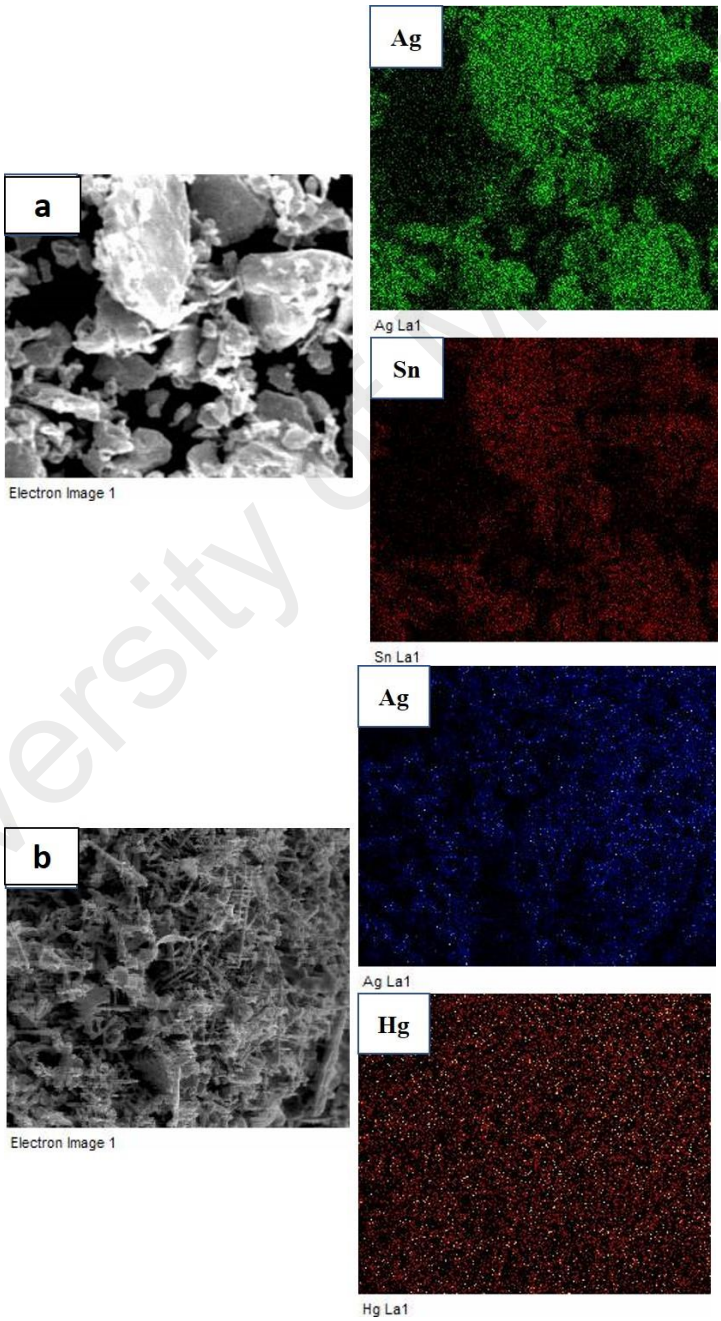


**Figure 4.2: The EDX elemental mapping of a) Ag-Sn, and b) Ag-Hg.** The elemental mappings show the homogeneous distribution of a) Ag and Sn atoms in the selected area of the Ag-Sn material, and (b) Ag and Hg in the Ag-Hg alloy (b). No impurities were detected in both the starting materials.

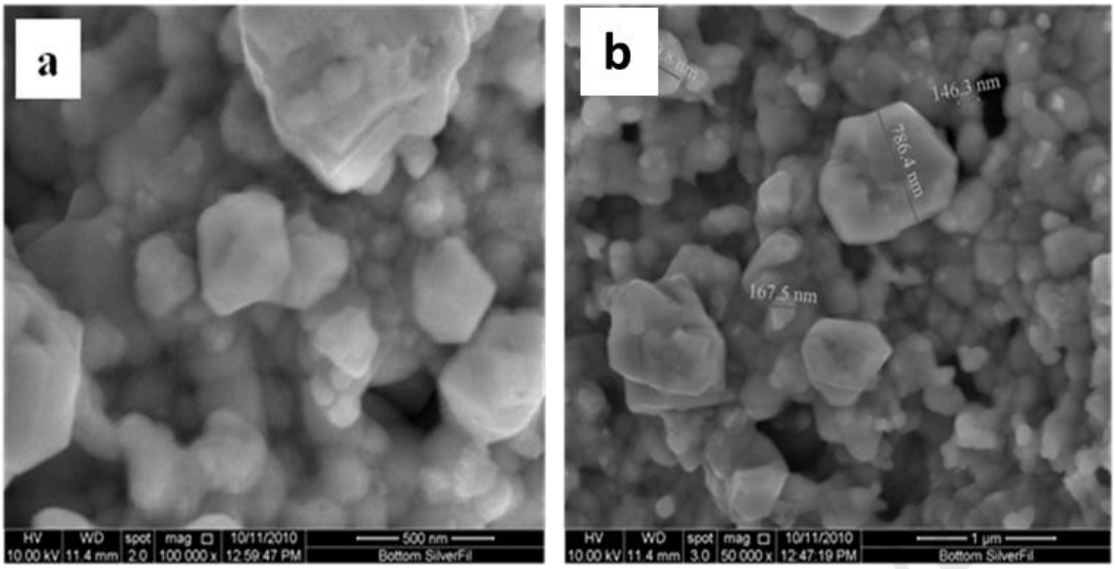


**Figure 4.3: FESEM images of the Ag-Hg+Ag-R component at a) 100k, and b) 50k magnifications.** The alloy consisted of polygonal shaped particles in a size range of 146-786 nm.

### 4.1.2 Morphological Characteristics

The microstructure of the Silverfil™ alloy (Ag-Hg+Ag-R) was analysed by FESEM as shown in **Figures 4.3(a) and 4.3(b).** The micrographs showed that the alloy was composed of particles with polygonal shapes and size range of 146-786 nm.

### 4.1.3 Phase Structures

The phase structure and crystallinity of the starting materials of Silverfil™ were also studied using the XRD analysis. All the diffraction peaks were compared with the Joint Committee for Powder Diffraction standard (JCPDS) files. **Figure 4.4** represents the XRD diffraction patterns of Ag-Sn, Ag-R, and Ag-Hg. The XRD diffraction pattern of Ag-Sn (**Figure 4.4(a))** showed two strong diffraction peaks at 39.6° and 40.0°, indicating the presence of $Ag_3Sn$ phase. All the diffraction peaks were in agreement with the standard spectrum data base of JCPDS 44-1300. The presence of crystallographic planes with miller indices of (201), (020), (211), (221), and (231) indicated that this sample was

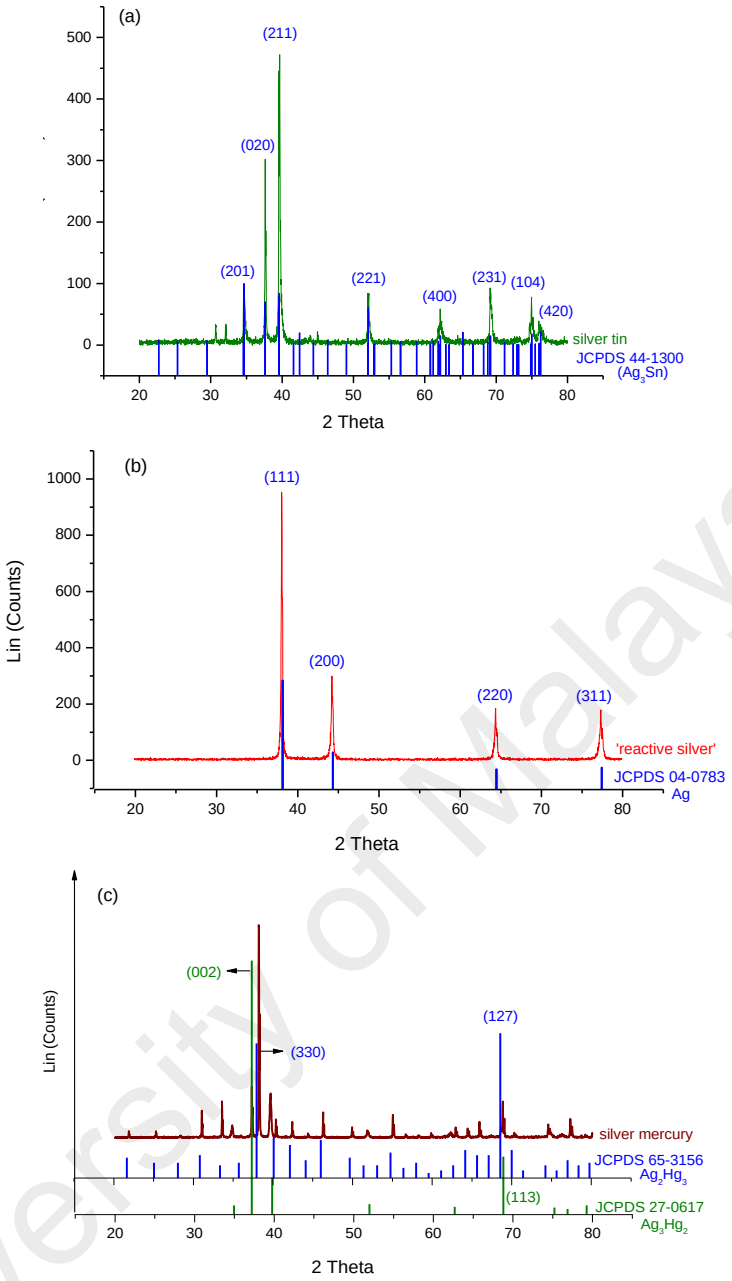


**Figure 4.4: The XRD patterns of Silverfil™ starting materials.** a) Ag-Sn was composed of $Ag_3Sn$ phase, b) Ag-R only showed the pure Ag phase, and c) Ag-Hg contained both the $Ag_2Hg_3$ and $Ag_3Hg_2$ phases.

composed of unit cells with the orthorhombic structure. Furthermore, the relatively broad peaks observed in **Figure 4.4(a)** indicated the small crystallite size of the Ag-Sn alloy, which was estimated to be 37.66 nm according to the Debye-Scherer formula.

The XRD spectrum of the Ag-R component shown in **Figure 4.4(b)** represents four sharp peaks with 2 theta values of 38.11°, 44.30°, 64.44°, and 77.40° corresponding to the (111), (200), (220), and (311) planes of pure Ag with the cubic structure. All the

diffraction peaks were sharp, while the peak corresponded to the (111) plane showed the highest intensity. The sharp diffraction peaks showed that the sample was highly crystalline. All the miller indices were well corresponded to those reported in JCPDS 04-0783 database, corroborated with the EDX results for the presence of pure Ag in this starting material. Unlike the single-phased Ag-Sn and Ag-R materials, the XRD diffraction pattern of the Ag-Hg in **Figure 4.4(c)** showed the presents of $Ag_2Hg_3$ (JCPDS 65-3156) and $Ag_3Hg_2$ (JCPDS 27-0617). Therefore, it can be concluded that Ag-Hg consisted of two different compositions where the $Ag_2Hg_3$ phase matched the majority of the observed peaks in the XRD spectrum.

The XRD pattern of the Ag-Hg+Ag-R alloy is also shown in **Figure 4.5**. This XRD spectrum exhibited broad diffraction peaks at 37.32°, 75.58°, and 79.59°corresponded to the (111), (311), and (222) planes in cubic structure of the Ag-Hg phase, according to the standard database of JCPDS 43-1465. Furthermore, four strong diffraction peaks were observed at 38.11°, 44.28°, 64.43°, and 77.48°, which confirmed the presence of metallic Ag with cubic structure (JCPDS 04-0783). Additionally, the corresponding diffraction peaks of $Ag_3Sn$ (JCPDS 71-0530) were also detected, probably due to its inclusion as impurity during production of the Ag-R particles. The broad diffraction peaks observed in this XRD spectrum suggested that the Ag-Hg+Ag-R alloy consisted of small crystallites.

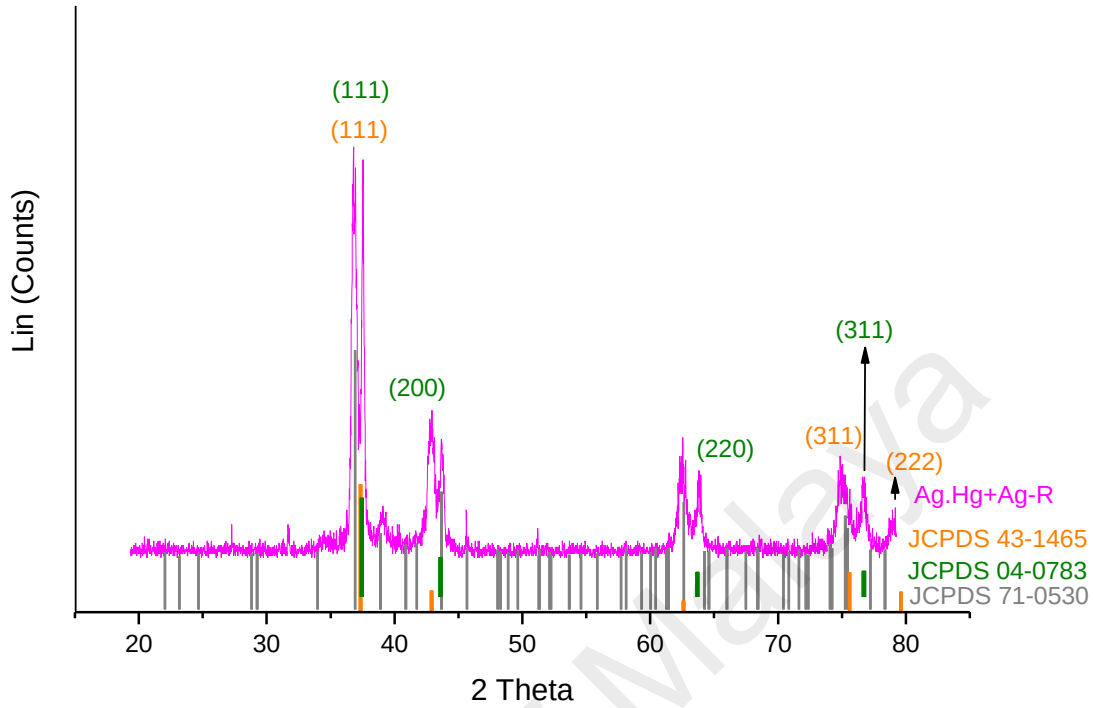


**Figure 4.5: The XRD pattern of the Ag-Hg+Ag-R component.** The spectrum matched the standard spectra of Ag-Hg, Ag, and also $Ag_3Sn$, indicating the presence of Sn as impurity.

### 4.1.4 Chemical States

The XPS technique was employed to define the surface composition and chemical state of the elements in the Silverfil™ starting materials. The position of the photoelectron peak can be confirmed by comparing the binding energy with the standard binding energy database from the XPS Handbook (Wanger et al., 1992). The XPS survey spectrum of Ag-Sn is illustrated in **Figure 4.6** and the relative atomic concentrations of its constituting elements are detailed in **Table 4.2**. All binding energies in a single data set were referenced to the C 1s line at 285.0 eV, which provided binding energy values with an accuracy of ±0.2 eV.

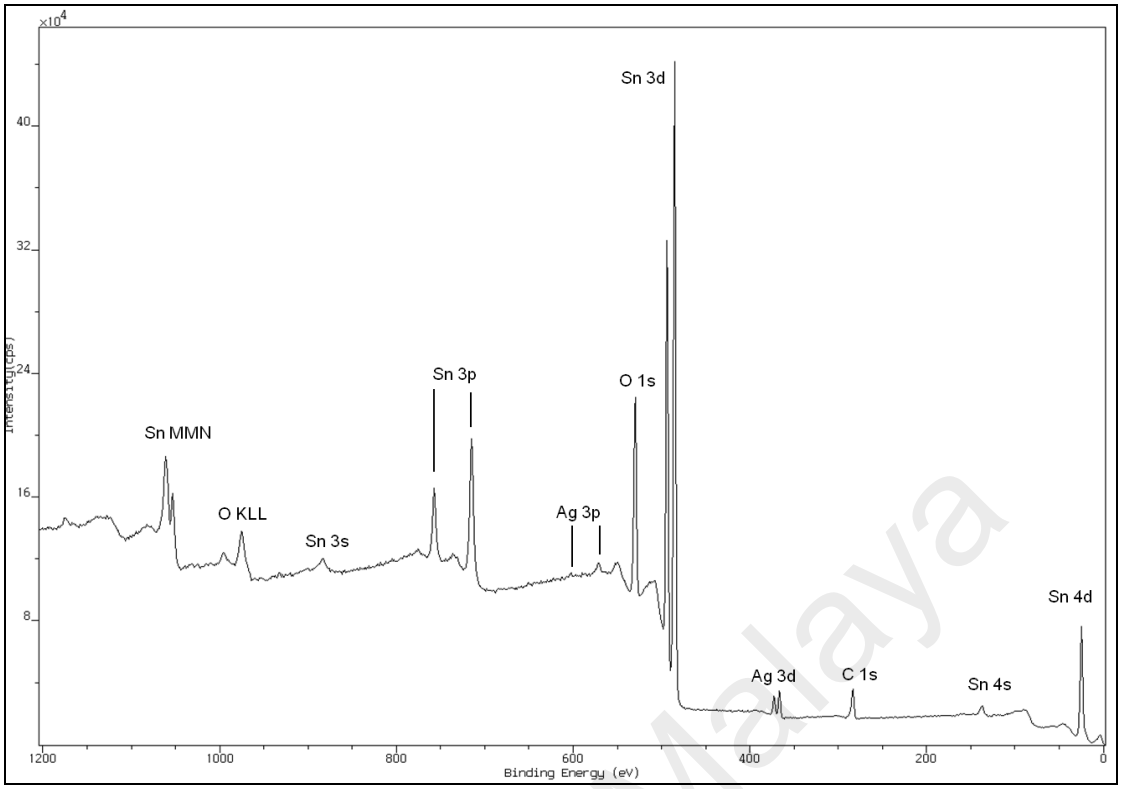


**Figure 4.6: The XPS survey spectrum of Ag-Sn.** The spectrum indicated the presence of Ag, Sn, O, and C elements.

**Table 4.2: The relative atomic concentrations of the elements present in Ag-Sn, a starting material of the Silverfil™ amalgam.**

| Element | Peak Quantified | Relative atomic concentration (%) |
|---|---|---|
| **Silver** | **Ag 3d** | 1.27 |
| **Oxygen** | O 1s | 53.13 |
| **Carbon** | C 1s | 22.94 |
| **Tin** | Sn 3d | 22.65 |
| **Total** | | **99.99** |

The survey spectrum of Ag-Sn indicated the presence of Sn (3s, 3p, 3d, 4s, and 4d), Ag (3d and 3p), O (1s), and C (1s) elements in different configurations. Apart from that, this spectrum included a sequence of peaks labeled O KLL and Sn MMN, which represented the energy of the electrons ejected from the atoms due to filling of electrons

in each shell. It was observed that Sn (3d) showed the highest intensity compared to other elements with relative atomic percentage of 22.65%.

The high-resolution XPS peaks of O 1s and Sn 3d for the Ag-Sn phase are shown in **Figure 4.7** while **Figure 4.8** shows the high-resolution XPS peaks for Ag 3d and C 1s. **Figure 4.7(a)** shows the binding energy values of 530.9 eV and 532.2 eV for O 1s, indicating the presence of a metallic oxide. **Figure 4.7(b)** also shows the presence of a doublet Sn $3d_{5/2}$ peak with binding energy of 487.0 eV ascribed to Sn (IV). The formation of $Ag^0$ with the binding energy of 368.2 eV is shown in **Figure 4.8(a)**. Furthermore, the C 1s region shown in **Figure 4.8(b)** was fitted by contributions of C-C and C-H bindings at 285.0 eV, C-O binding at 286.6 eV, and O=C-O binding at 289.1eV.

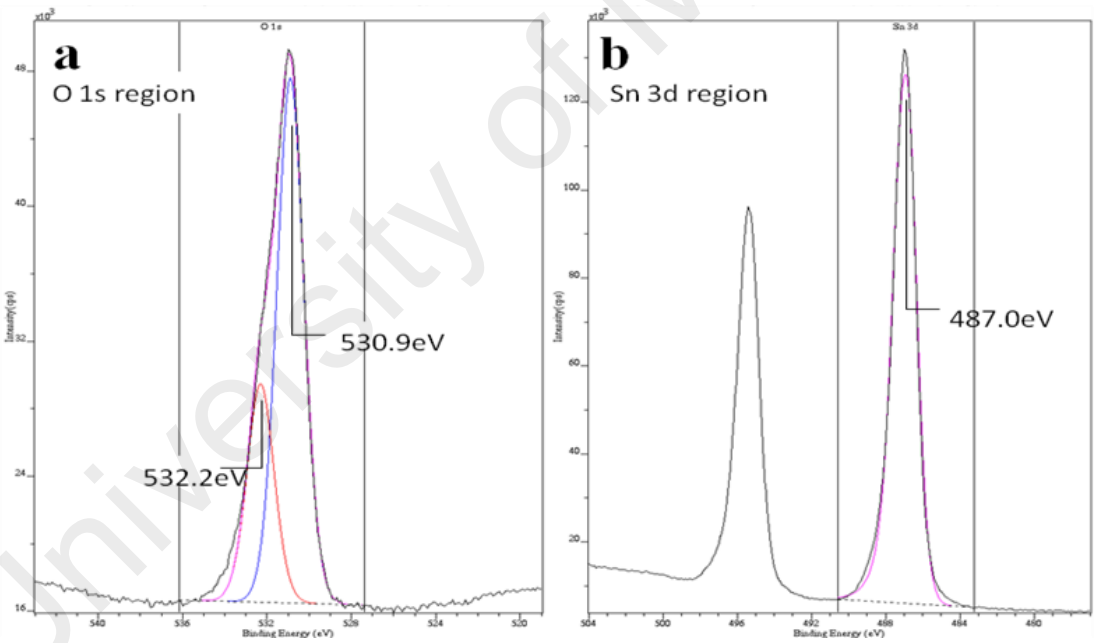


**Figure 4.7: The high-resolution XPS spectra of O 1s and Sn 3d in the Ag-Sn component.** a) the O 1s region showed the presence of a metal oxide, and b) the Sn 3d region showed the oxidation state of Sn (IV).

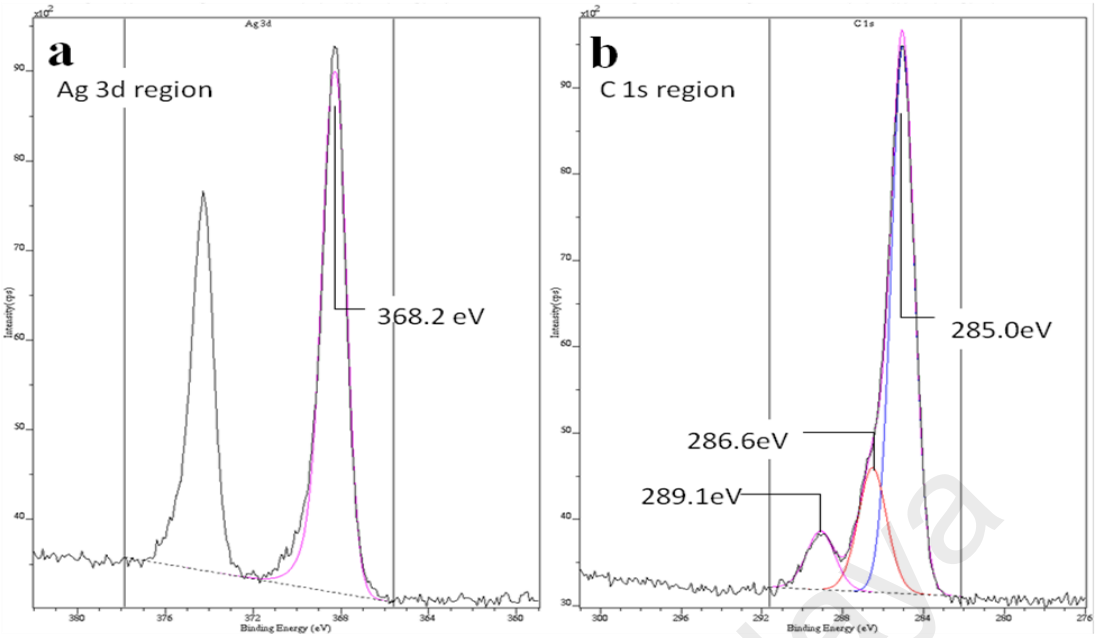


**Figure 4.8: The high-resolution XPS spectra of Ag 3d and C 1s in the Ag-Sn component.** a) The Ag 3d region represented the Ag0 state, and b) the C 1s region showed the presence of C-C, C-H, C-O, and O=C-O bounds.

The XPS survey spectrum of Ag-R is also presented in **Figure 4.9** and the relative atomic concentrations of its elements are listed in **Table 4.3**. The XPS spectrum contained the expected photoelectron peaks of Ag 3d and C 1s with relative atomic concentrations of 21.23% and 5.86%, respectively. However, this spectrum also showed the presence of other elements such as O, Cu, and Sn, which were probably entered as impurities during the displacement reactions when Ag-R was produced. The Cu 2p appeared in a small percentage, whereas the relative atomic concentrations of Sn 3d and O 1s were 20.20% and 52.7%, respectively. Therefore, due to the presence of these elements with high percentages, it was concluded that the supplied Ag-R was not purely composed of Ag.

**Figure 4.10** shows the high-resolution XPS peaks of O 1s and Sn 3d observed in Ag-R, whereas the high-resolution XPS peaks of Ag 3d and C 1s for this material are shown in **Figure 4.11**. The binding energies of both O 1s and Sn 3d shown respectively in **Figure 4.10(a)** and **Figure 4.10(b)** indicated the presence of metal oxide and the oxidation state of Sn (IV), respectively. The XPS peak of Ag 3d (**Figure 4.11(a)**)

indicated the existence of $Ag^0$ in Ag-R composition with the binding energy of 368.2 eV. For C 1s region (**Figure 4.11(b)**), the results were similar to those observed in Ag-Sn, as outlined previously.

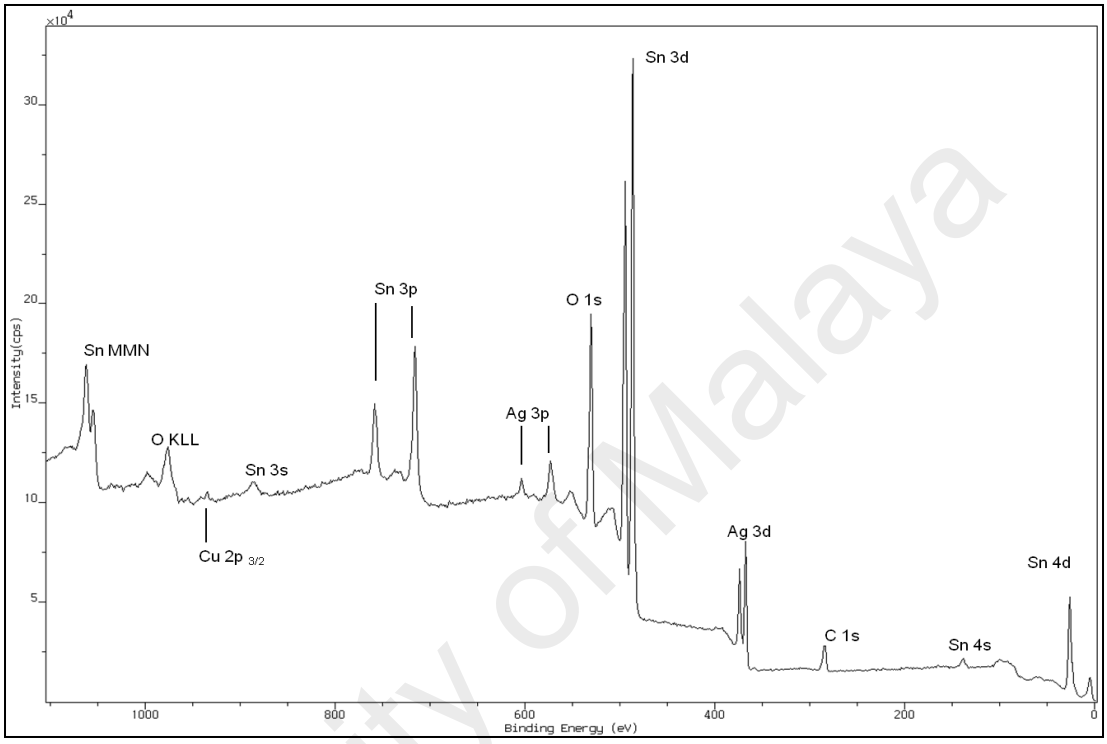


**Figure 4.9: The XPS survey spectrum of Ag-R.** The spectrum showed the presence of various elements including Ag, Sn, Cu, O, and C. Sn appeared as impurity in this sample.

**Table 4.3: The relative atomic concentrations of the elements present in Ag-R, a Silverfil™ starting material.**

| Element | Peak Quantified | Relative Atomic Concenteration (%) |
|---|---|---|
| **Copper** | Cu 2p | trace |
| **Silver** | Ag 3d | 21.23 |
| **Oxygen** | O 1s | 52.71 |
| **Carbon** | C 1s | 5.86 |
| **Tin** | Sn 3d | 20.20 |
| **Total** | | **100.00** |

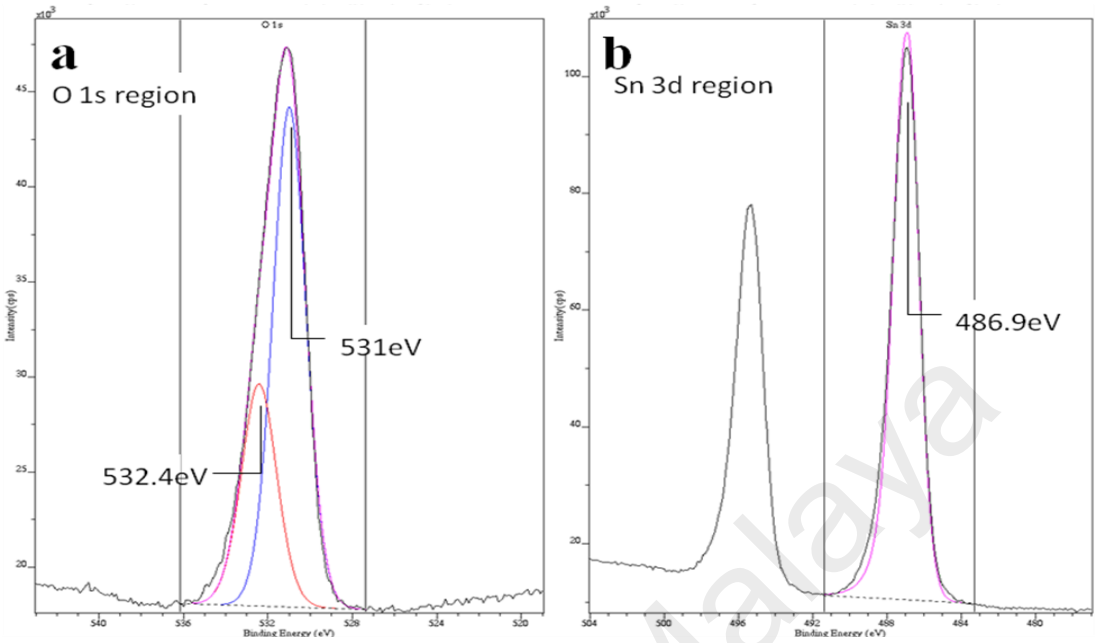


**Figure 4.10: The high-resolution XPS spectra of O 1s and Sn 3d for the Ag-R component.** a) The O 1s region showed the presence of metal oxide, and (b) the Sn 3d region showed that the oxidation state of Sn (IV), indicating that Sn was not in the metallic form.

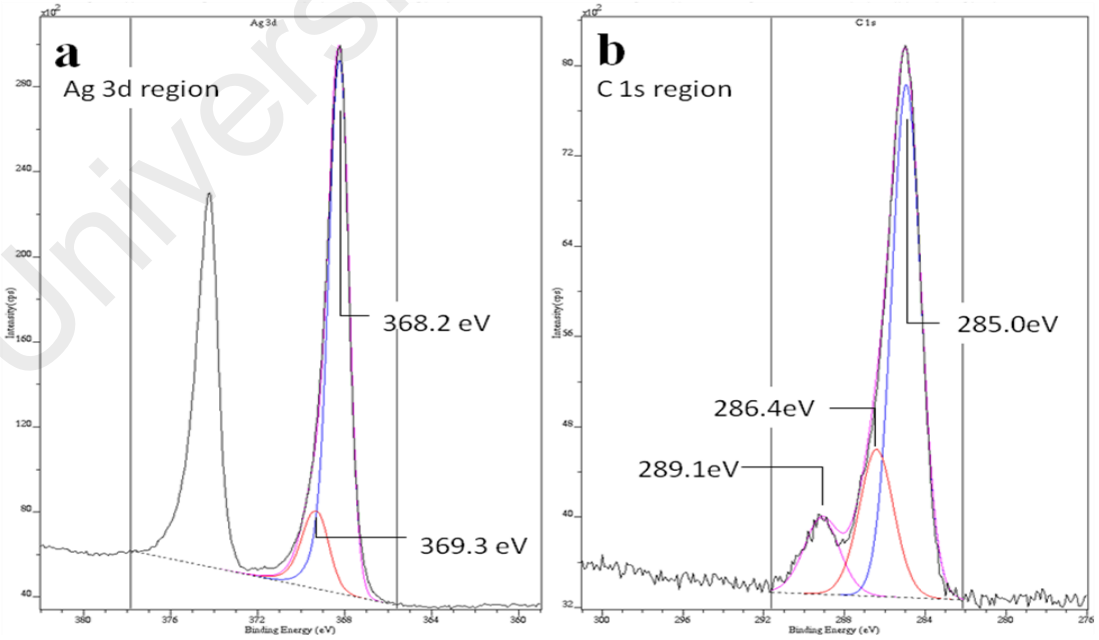


**Figure 4.11: The high-resolution XPS spectra of Ag 3d and C 1s for Ag-R.** a) The Ag 3d region showed the oxidation state of $Ag^0$ indicating the presence of metallic Ag, and b) the C 1s region represented the C-C, C-H, C-O, O=C-O bindings.

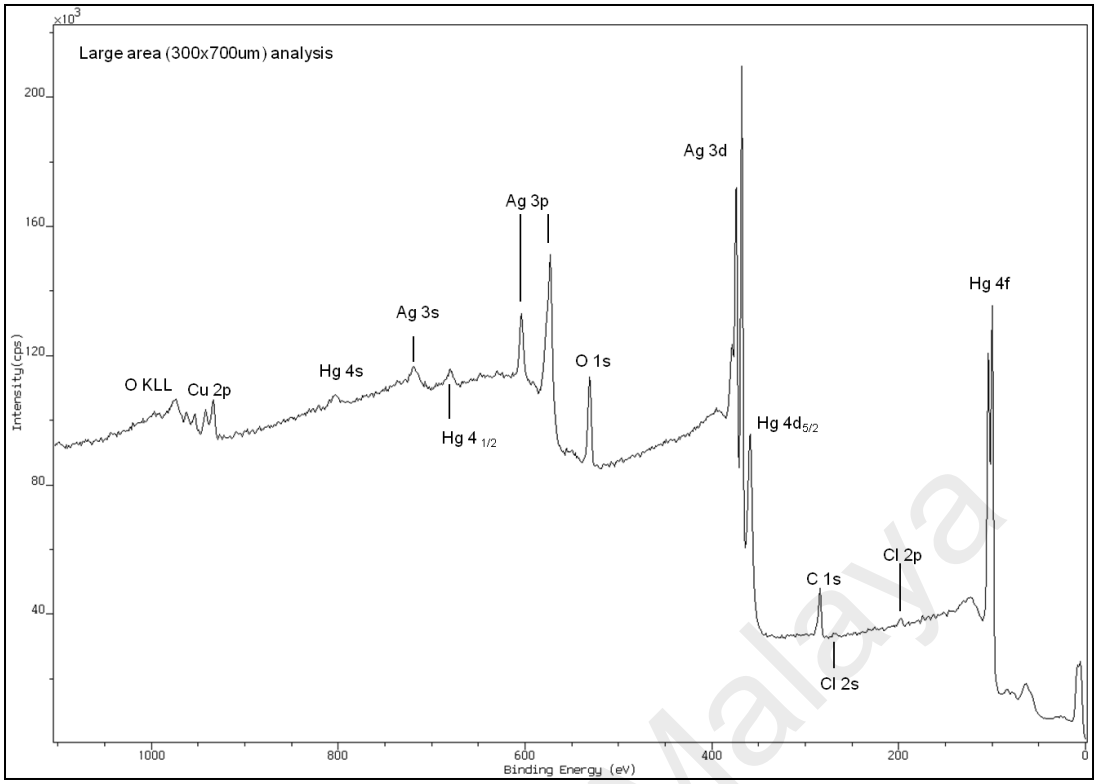


**Figure 4.12: The XPS survey spectrum of Ag-Hg.** The spectrum indicated the presence of Ag, Hg, Cu, Cl, O, and C. Cu and Cl appeared as impurities in this alloy.

**Table 4.4: The relative atomic concentrations of the Ag-Hg elements.**

| Element | Peak Quantified | Relative atomic concenteration (%) |
|---|---|---|
| **Copper** | Cu 2p | 2.68 |
| **Silver** | Ag 3p* | 29.12 |
| **Oxygen** | O 1s | 21.06 |
| **Carbon** | C 1s | 30.64 |
| **Mercury** | Hg 4f | 14.75 |
| **Chlorine** | Cl 2p | 1.75 |
| **Total** | | **100.00** |

The XPS survey spectrum of the Ag-Hg is illustrated in **Figure 4.12** and the atomic concentrations of the elements present in this alloy are detailed in **Table 4.4**. This XPS spectrum indicated the presence of elements in different configurations including Ag (3s, 3d, and 3p), Cu (2p), Hg (4s, 4d, and 4f), Cl (2s, 2p), O (1s), and C (1s). The relative

atomic percentages of Ag 3p and Hg 4f were 29.12% and 14.75%, respectively. The other elements such as Cu and Cl, which appeared in percentages less than 3%, were probably introduced during the electrochemical process applied for producing the Ag.Hg alloy.

**Figure 4.13** and **Figure 4.14** represent the high-resolution XPS peaks of Cu 2p and O 1s as well as Ag 3d and C 1s in the Ag-Hg alloy, respectively. The Cu 2p peaks in **Figure 4.13(a)** showed the binding energy value of 934.8 eV, which indicated the presence of Cu (II) oxide. The broader peaks also ascribed to the $Cu^{2+}$ state. The O 1s peak in **Figure 4.13(b)** showed similar results as previously discussed. In **Figure 4.14(a)**, the Ag 3d peak overlapped with the Hg 4d region, while the C 1s region in **Figure 4.14(b)** showed similar properties described previously for Ag-Sn and Ag-R. **Figure 4.15** shows the XPS peak of Hg 4f for the Ag-Hg alloy. The binding energies of Hg 4f were 101.8 eV (Hg $4f_{5/2}$) and 100.8 eV (Hg $4f_{7/2}$), confirming the presence of Hg bonded with Ag. In summary, this sample contained no unbounded Hg, although Cu was detected in its composition.

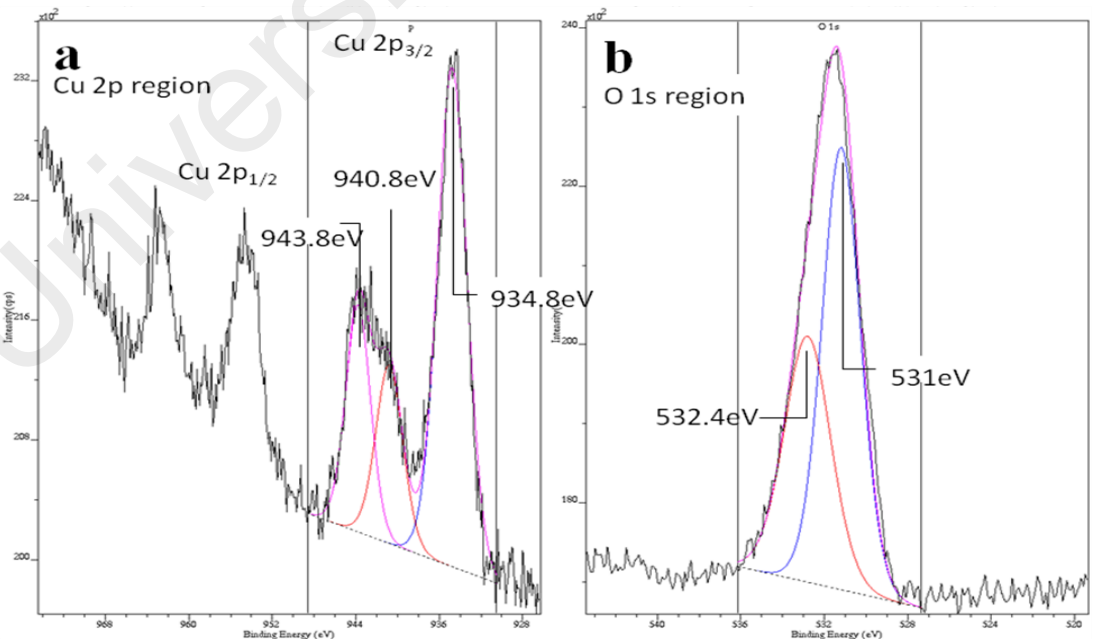


**Figure 4.13: The high-resolution XPS spectra of Cu 2p and O 1s for the Ag-Hg alloy.** a) The Cu 2p region showed the oxidation state of Cu (II), and b) the O 1s region indicated the presence of metal oxides.

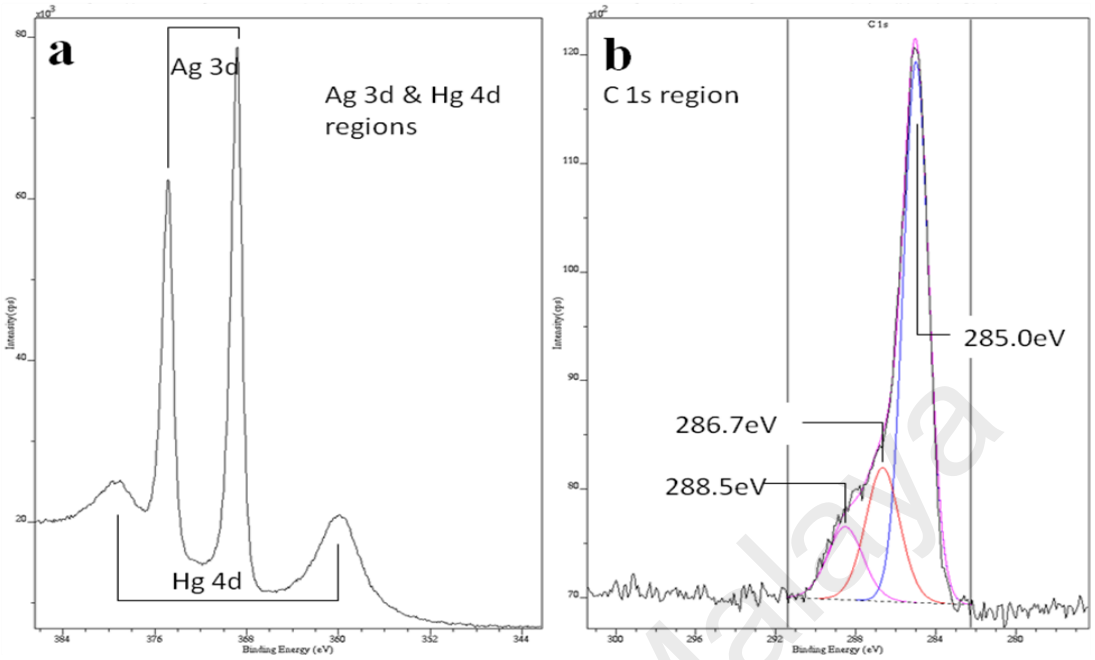


**Figure 4.14: The high-resolution XPS spectra of Ag 3d, Hg 4d, and C 1s for the Ag-Hg alloy.** a) The Ag 3d and Hg 4d regions showed the presence of bound Hg, and b) the C 1s region illustrated the existence of C-C, C-H, C-O, O=C-O bindings.

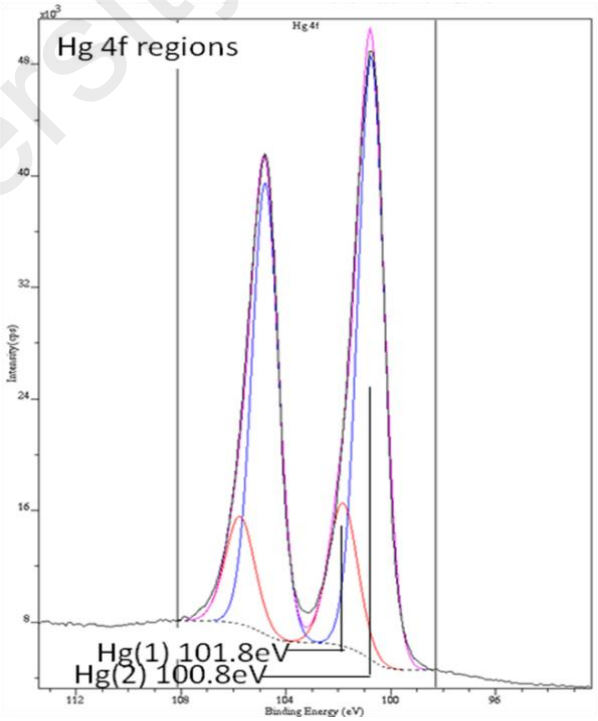


**Figure 4.15: The high-resolution XPS spectrum of Hg 4f for the Ag-Hg alloy.** The absence of unbounded Hg confirmed in the Hg 4f region.

The XPS survey spectrum of the Silverfil$^{TM}$ alloy (Ag-Hg+Ag-R) is shown in **Figure 4.16.** This XPS survey spectrum indicated the presence of Ag (3s, 3d and 3p), Cu (2p), Sn (3d, 3p), Hg (4s, 4p, 4d, 4f), Cl (2s, 2p), O (1s), and C (1s) in different configurations. The elemental concentrations for the Ag-Hg+Ag-R alloy are detailed in **Table 4.5**. The relative atomic percentage of Ag 3p and Hg 4f were respectively 23.08% and 6.35%. A number of other elements including Sn (6.63%), Cu (2.03%), and Cl (1.33%) were also detected in low percentages. As highlighted previously, these impurities could have been generated as by-products during the electrochemical production of the Ag-Hg alloy.

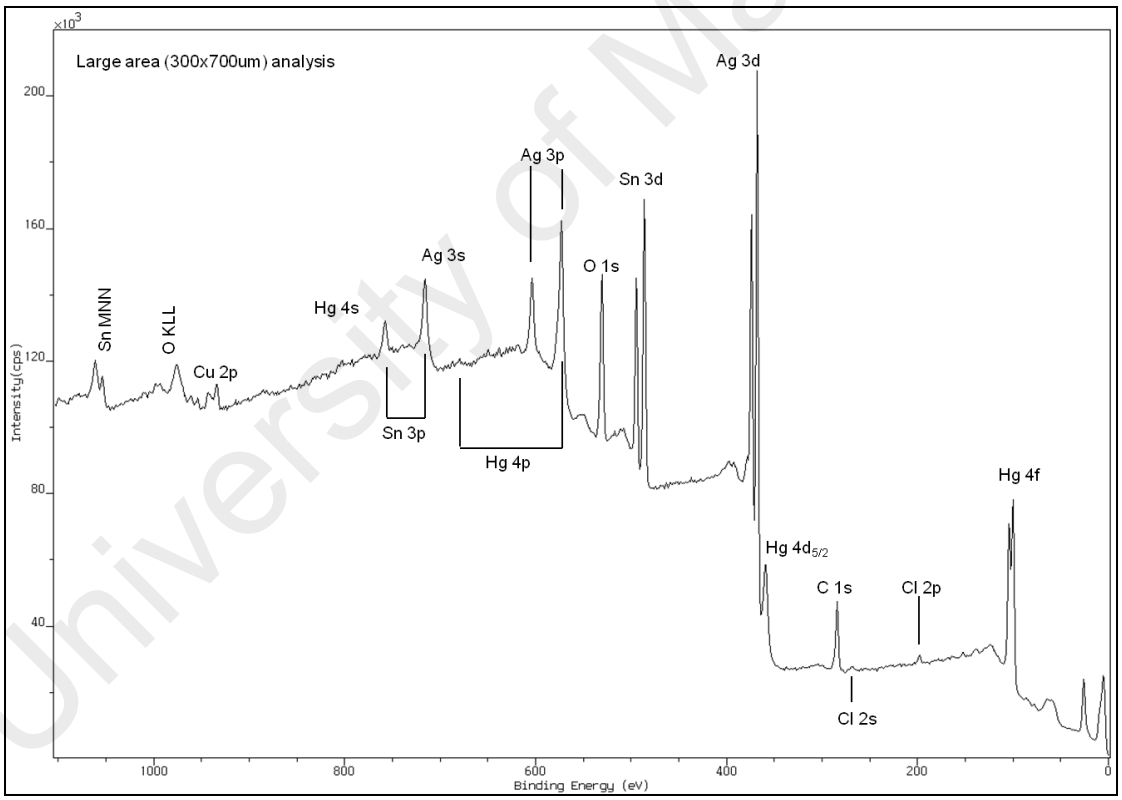


**Figure 4.16: The XPS survey spectrum of the Silverfil$^{TM}$ alloy.**

**Table 4.5: The relative atomic concentrations of the elements present in the Ag-Hg+Ag-R alloy.**

| Element | Peak Quantified | Relative atomic concenteration (%) |
|---|---|---|
| **Copper** | Cu 2p | 2.03 |
| **Silver** | Ag 3p* | 23.08 |
| **Tin** | Sn 3d | 6.63 |
| **Oxygen** | O 1s | 27.92 |
| **Carbon** | C 1s | 32.67 |
| **Mercury** | Hg 4f | 6.35 |
| **Chlorine** | Cl 2p | 1.33 |
| **Total** | | **100.01** |

**Figure 4.17** to **Figure 4.19** represent the high-resolution XPS peaks of the Ag-Hg+Ag-R alloy for Cu 2p and O 1s regions, Ag 3d and C 1s regions, and Hg 4f regions, respectively.

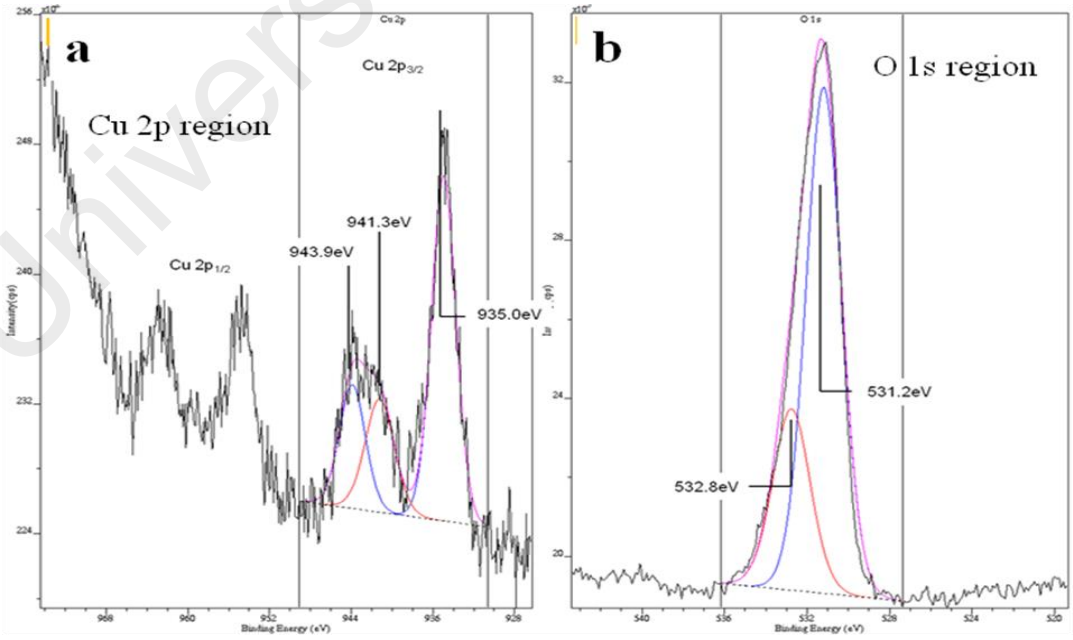


**Figure 4.17: The high-resolution XPS spectra of Cu 2p and O 1s for the Ag-Hg+Ag-R alloy.** a) The Cu 2p region showed the oxidation state of Cu (II), and (b) the O 1s region showed the presence of metal oxides.

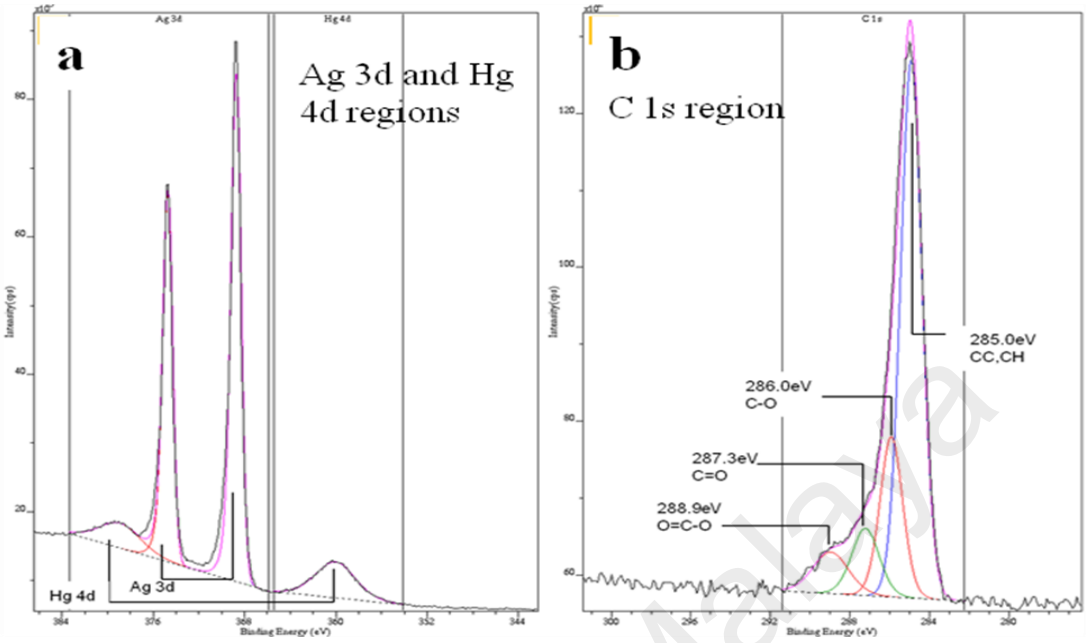


**Figure 4.18: The high-resolution XPS spectra of Ag 3d, Hg 4d, and C 1s for the Ag-Hg+Ag-R alloy.** a) The Ag 3d and Hg 4d regions showed the presence of Hg only in a bound form, and b) the C 1s region showed the C-C, C-H, C-O, and O=C-O bounds.

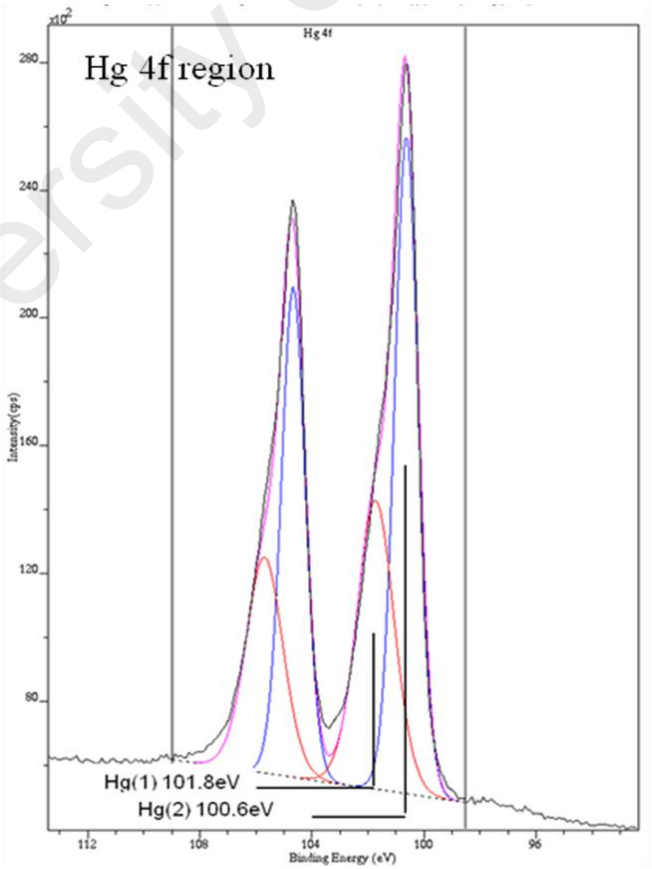


**Figure 4.19: The high-resolution XPS spectra of Hg 4f for the Ag-Hg+Ag-R alloy.** No unbound Hg was detected in this region.

## 4.2 Synthesis and Characterisation of AgNPs

### 4.2.1 The Effect of EDA Content on the Size of AgNPs

EDA is a typical chelating agent, which controls the formation and growth of Ag particles during the synthesis process (Xu et al., 2009). The influence of EDA content on the obtained sizes of the synthesised AgNPs was investigated using the DLS technique. **Figure 4.20** shows the size distribution of AgNPs synthesised using 0.05 ml, 0.10 ml, 0.20 ml, and 0.40 ml of EDA. The experimental results (**Figure 4.20(a)**) clearly demonstrated that the EDA concentration of 0.05 ml could produce the smallest Ag particles. The mean particle sizes obtained during the first (red line) and second (green line) scans were approximately 10 nm and 100 nm, respectively. During the third scan, the particles became highly agglomerated and the particle size was thus increased to 250 nm. In comparison, the EDA concentrations of 0.10 ml, 0.20 ml, and 0.40 ml produced larger particle sizes as depicted in (**Figures 4.20(b)-(d**)). In summary, the obtained DLS results indicated that the lower EDA contents generally resulted in smaller particle sizes. Therefore, sample A1 (synthesised using 0.05 ml of EDA) was chosen for further investigations.

**Figure 4.21** shows the obtained XRD pattern of sample B1. All the diffraction peaks were sharp, implying the high crystallinity of the synthesised AgNPs. Four peaks were located at 2 theta angles of 38.22°, 44.42°, 64.54°, and 77.48°, corresponding to the Miller indices of (111), (200), (220) and (311) planes of Ag with face centered cubic (FCC) crystal structure, in agreement with JCPDS 04-0783.

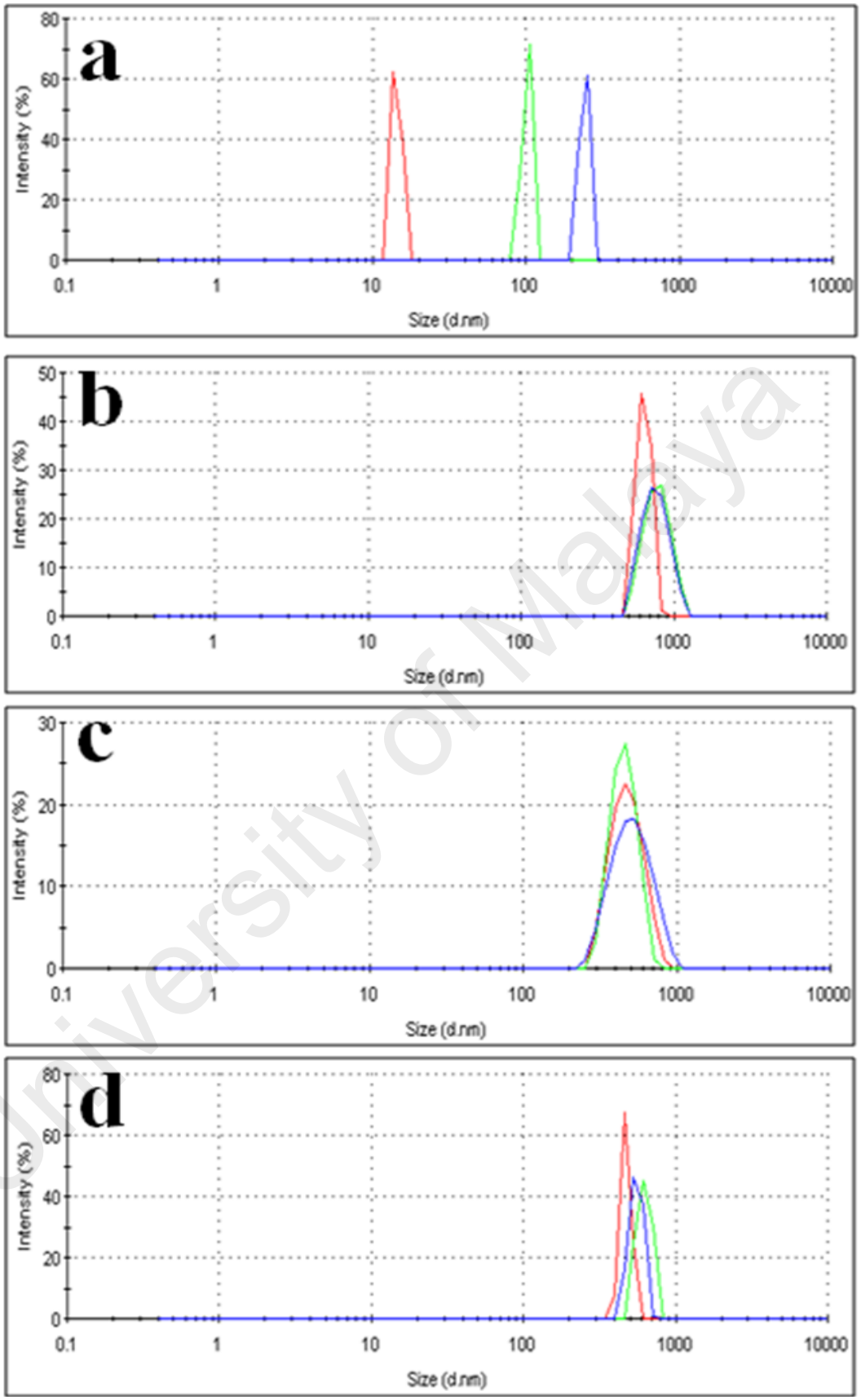


**Figure 4.20: The DLS size distribution spectra of the AgNPs synthesised using varied EDA concentrations**. a) 0.05 ml, b) 0.10 ml, c) 0.20 ml, and d) 0.40 ml EDA. The DLS measurements were repeated three times for each experimental group where the red, green, and blue lines represent the first, second, third scans.

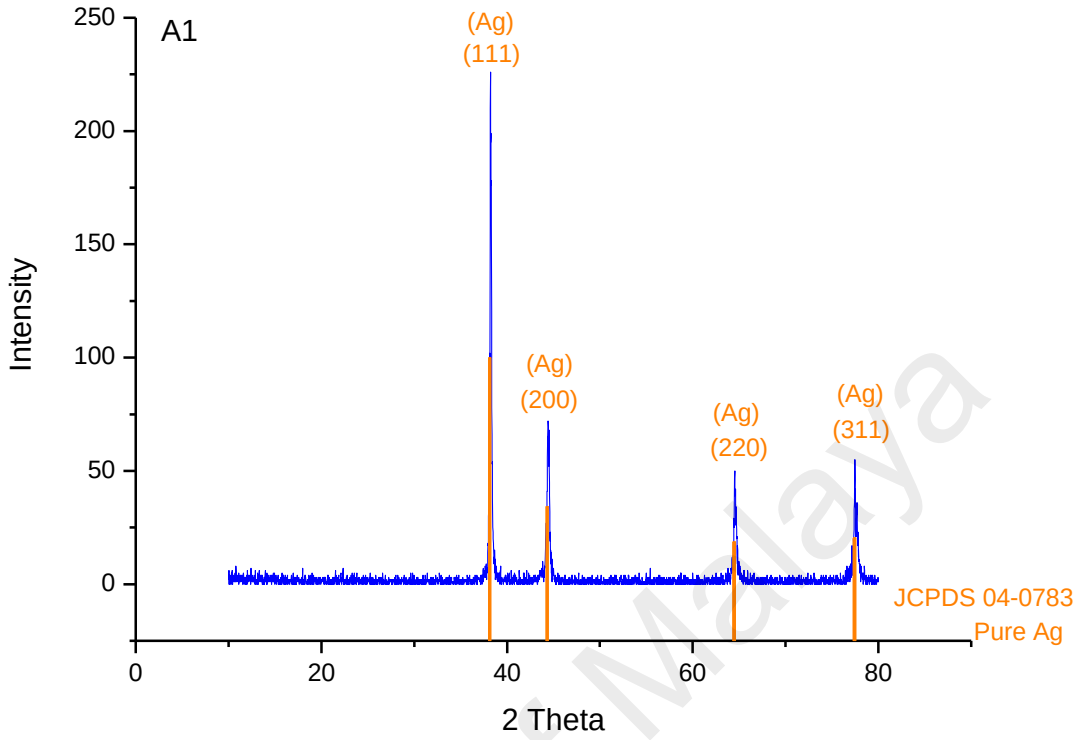


**Figure 4.21: The XRD pattern of the AgNPs synthesised using 0.05 ml of EDA.** Pure and highly crystalline AgNPs were obtained with the FCC crystal structure.

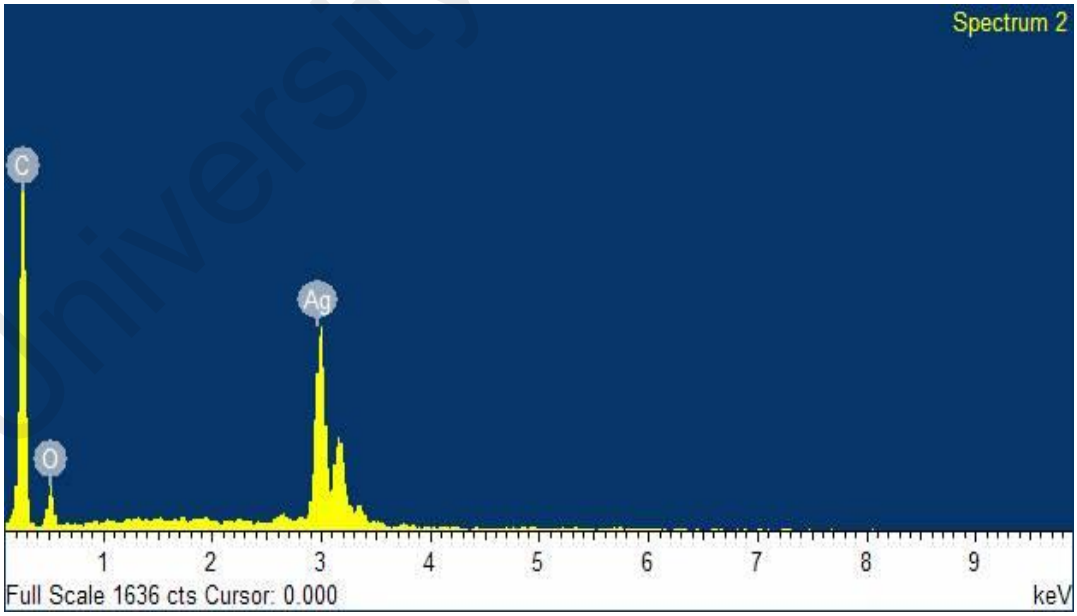


**Figure 4.22: The EDX spectrum of the AgNPs synthesised using 0.05 ml of EDA.** A strong Ag peak at approximately 3 keV was observed without detection of any impurity.

**Table 4.6: The elemental composition of the AgNPs synthesised using 0.05 ml of EDA.**

| Elements | Relative Atomic Percentage (%) |
|---|---|
| **C** | 59.47 |
| **O** | 17.72 |
| **Ag** | 22.81 |
| **Total** | 100.00 |

The EDX analysis of the AgNPs synthesised using 0.05 ml of EDA (sample A1) is shown in **Figure 4.22**. The EDX spectrum revealed a strong signal belonged to the binding energy of $Ag_L$ at around 3 keV, indicating the successful synthesis of AgNPs. Moreover, no evidence of any chemical contamination during the synthesis was detected in the elemental analysis (**Table 4.6**). It is noteworthy that the presence of other peaks such as carbon (C) and oxygen (O) was due to utilisation of carbon tapes for attachment of the samples onto the metallic sample holder.

In summary, the results obtained by the DLS, XRD, and EDX analyses confirmed that the EDA content of 0.05 ml could result in formation of AgNPs with a suitable range of particle size, high degree of crystallinity, and high purity. Therefore, this amount of EDA was utilised for synthesis of AgNPs required in further experimental steps for fabrication of the experimental nanosilver amalgam.

### 4.2.2 The Influence of $AgNO_3$ Concentration on the Particle Size and Crystallite Size of AgNPs

In this study, the effect of $AgNO_3$ concentration on the particle and crystallite sizes of synthesised AgNPs has been studied. As mentioned in Chapter 3, only the samples B5 to B9 resulted in well-triturated amalgams according to the manufacturer's feedback.

Therefore, these five samples were further subjected to detailed characterisations in order to determine the optimal AgNPs for formulation of the experimental nanosilver amalgam. The particle size profiles of the AgNPs synthesised with varying concentrations of $AgNO_3$ were obtained by SAXS using the Gaussian distribution and presented in **Figure 4.23**. These graphs clearly showed that all the Ag particles were synthesised in the nano size range.

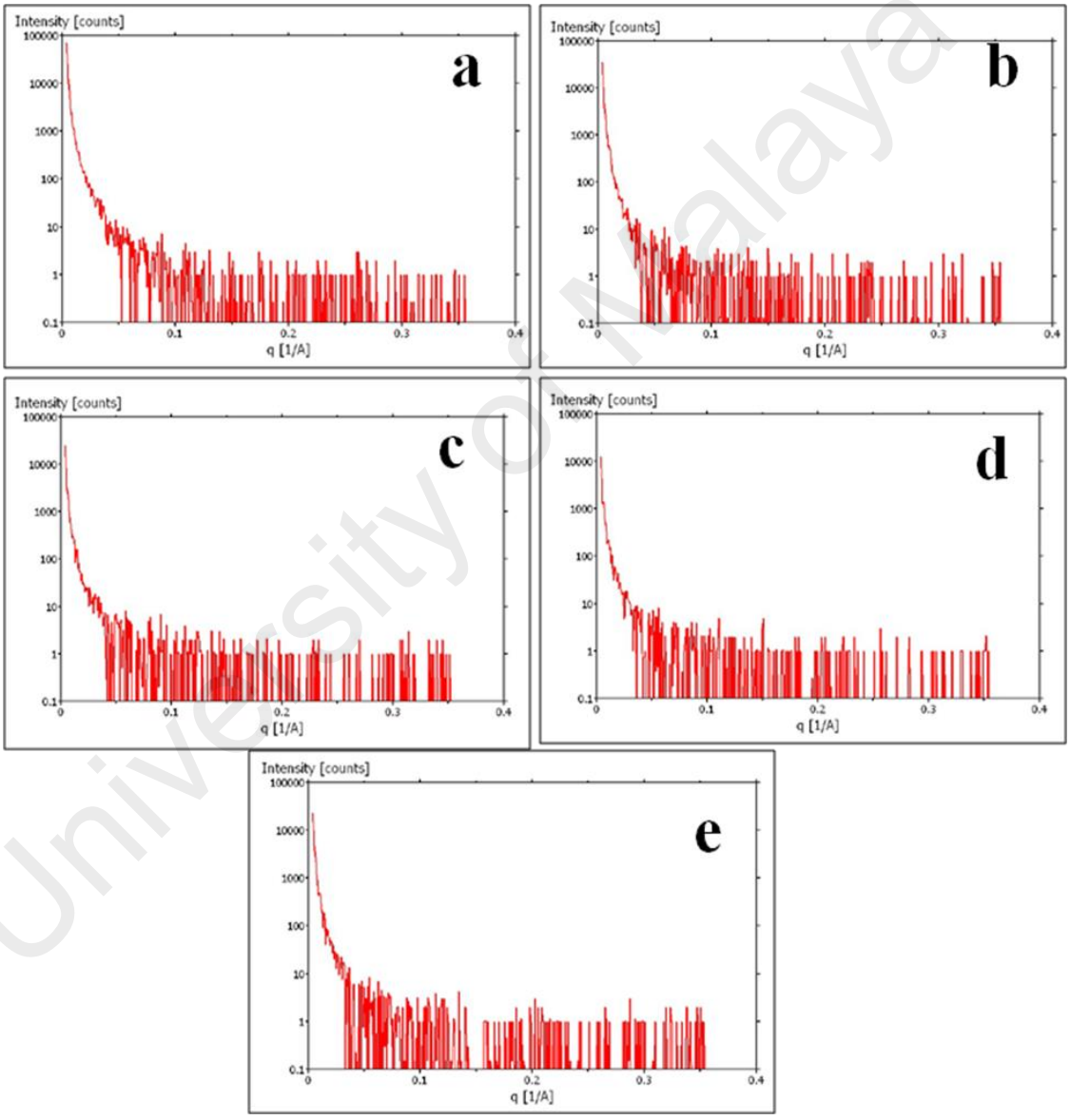


**Figure 4.23: The SAXS patterns of the AgNPs synthesised by different $AgNO_3$ concentrations.** a) B5 (0.80 M), b) B6 (1.0 M), c) B7 (1.2 M), d) B8 (1.6 M), e) B9 (2.0 M). All the graphs indicated formation of Ag particles in the nano size range.

The size distributions of the synthesised particles were obtained by analysis of the scattering profiles (**Figure 4.24**). The estimated values of the mean radius were 18.46±47.84 nm, 18.88±45.97 nm, 17.97±50.31 nm, 18.70±47.02 nm, and 18.81±46.12 nm for samples B5, B6, B7, B8, and B9 respectively. Moreover, the highest frequently observed radius value was found in sample B5 (16.4 nm), followed by B6 (14.4 nm), B7 (16.4 nm), B8 (16.0 nm), and B9 (13.2 nm). As presented in **Table 4.7**, the calculated crystallite sizes for the samples B5, B6, B7, B8, and B9 were respectively 56.29 nm, 70.36 nm, 70.36 nm, 68.66 nm, and 54.2 nm, indicating the significant influence of the $AgNO_3$ concentration on crystallite size of the obtained AgNPs.

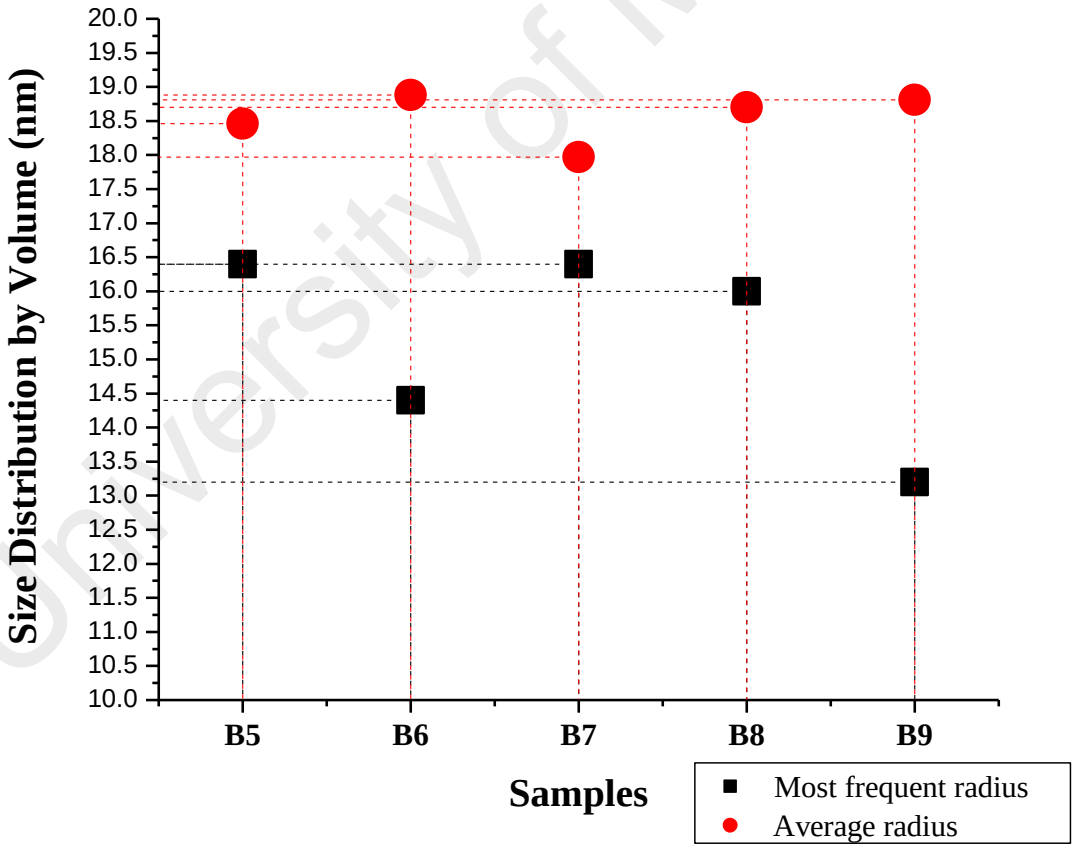


**Figure 4.24: The SAXS plot of size distribution by volume for the AgNPs synthesised using different $AgNO_3$ concentrations.**

**Table 4.7: The crystallite sizes of the AgNPs synthesised using different $AgNO_3$ concentrations.**

| Sample | Peak position (2 Theta) | FWHM* | Crystallite size (nm) |
|---|---|---|---|
| **B5 (0.8M)** | 38.0427 | 0.1560 | 56.29 |
| **B6 (1.0M)** | 38.0728 | 0.1248 | 70.36 |
| **B7 (1.2M)** | 38.0719 | 0.1248 | 70.36 |
| **B8 (1.6M)** | 38.0601 | 0.1279 | 68.66 |
| **B9 (2.0M)** | 38.117 | 0.205 | 54.20 |

*FWHM: Full width at half maximum.

The XRD analyses of the AgNPs synthesised with different concentrations of $AgNO_3$ (Appendix B) confirmed the formation of highly crystalline AgNPs with the FCC structure, similar to those discussed previously in Section 4.2.1. These obtained results were in agreement with those reported in the related literature (Gomathi et al., 2017; Jiang et al., 2005; Liu et al., 2008; Wang et al., 2005). Moreover, no trace of any oxide phase was detected in the synthesised samples.

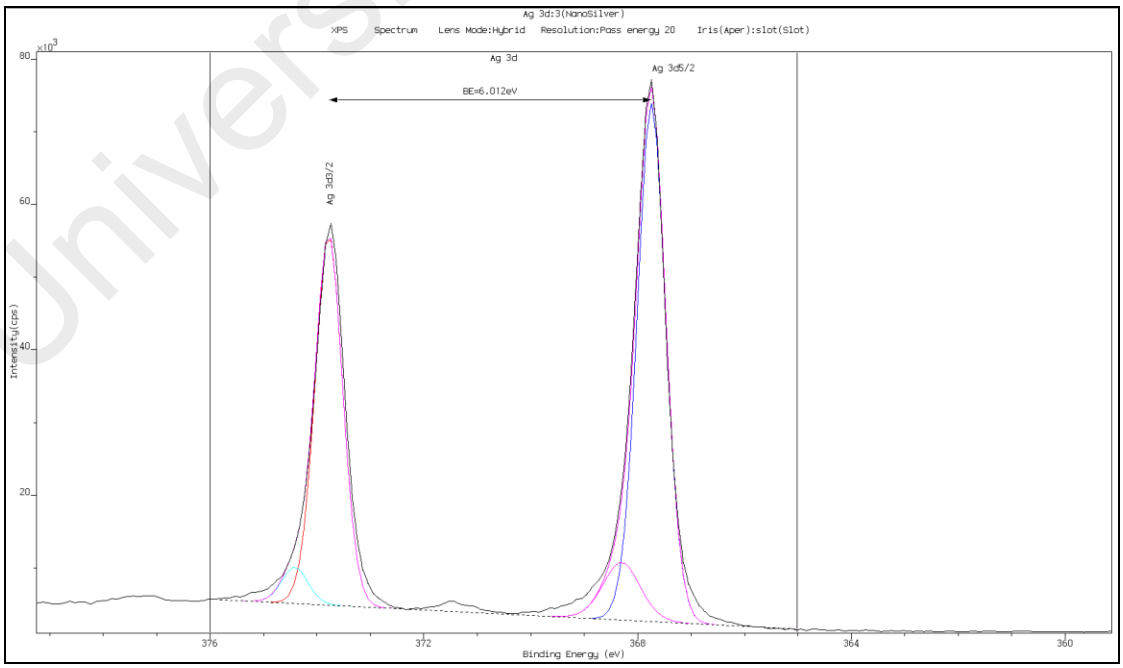


**Figure 4.25: The high-resolution XPS spectrum of Ag 3d for the AgNPs synthesised using 2M of $AgNO_3$ (Sample B9).** The binding energy of Ag 3d was assigned to the metallic state ($Ag^0$).

Based on the SAXS plot of size distribution by volume, sample B9 (AgNPs synthesised with 2M of $AgNO_3$) showed the lowest frequent radius (13.2 nm) with mean particle size of 18.81 nm. Futhermore, this sample possessed the smallest crystallite size (54.20 nm) compared to other AgNPs produced using lower concentrations of $AgNO_3$ and it was preferred by the Silverfil$^{TM}$ manufacturer due to its more fovourable handling and manipulation. Therefore, sample B9 was chosen for further analyses in this study.

**Figure 4.25** shows the high-resolution XPS peak of Ag 3d for the sample B9. The peak shows a doublet pair arised from the spin-orbital coupling of $3d_{5/2}$ and $3d_{3/2}$. The difference between the binding energies of these two peaks was 6.012 eV, confirming the presence of $Ag^0$ state. The AgNPs were not synthesised in any oxidised form as there was no evidence of components at lower binding energies.

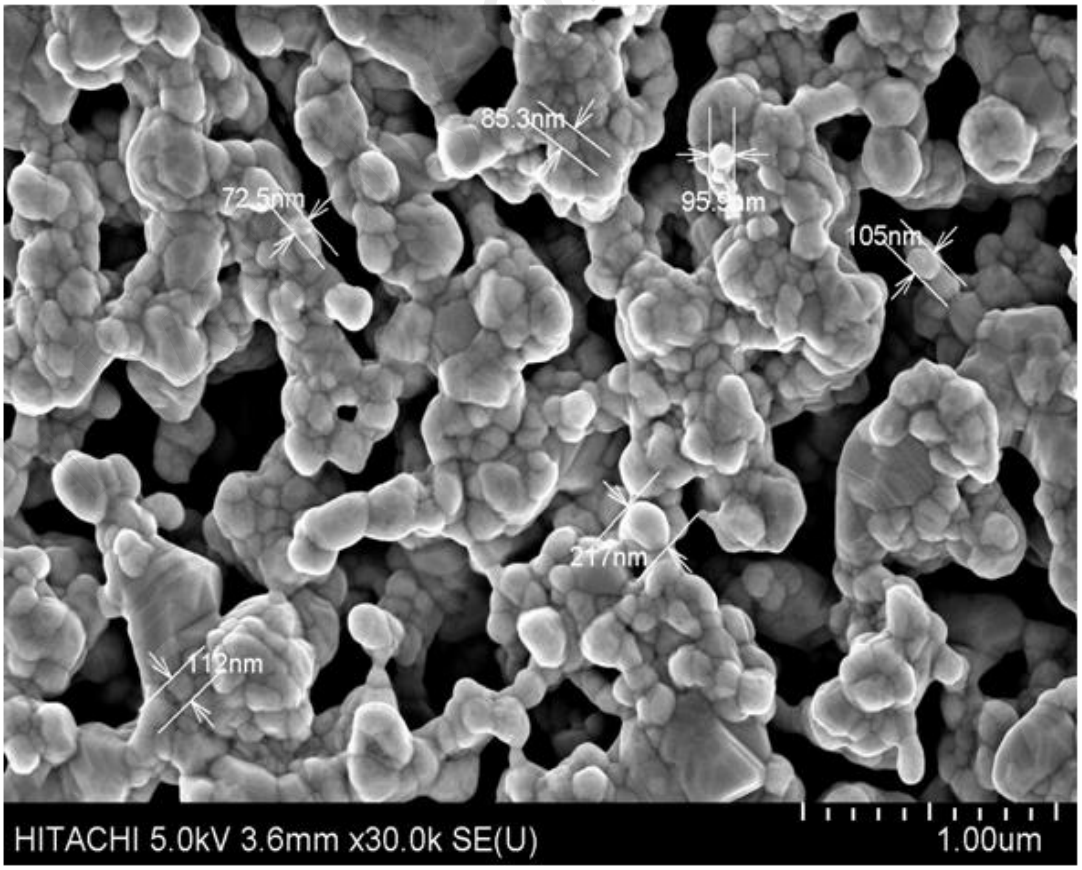


**Figure 4.26: The particle morphology of the AgNPs synthesised using a 2M $AgNO_3$ solution.** The mean particle size was approximately 141.55±52.12 nm.

**Table 4.8: The relative atomic percentages of the elements present in the AgNPs synthesised using a 2M $AgNO_3$ solution.**

| Element | Relative Atomic Percentage (%) |
|---|---|
| C | 44.8 |
| O | 14.1 |
| Ag | 42.1 |
| **Total** | **100.0** |

In general, AgNPs could be fabricated in various morphological shapes such as spheres, rod, cubes, triangles, wires, and the flower-like structure (Hong, Li, Lin, & Li, 2009; Sharma et al., 2009). The morphological investigation of sample B9 (**Figure 4.26)** revealed the formation of polygonal-shaped particles with mean size of 141.55±52.12 nm, which was larger than its crystallite size obtained by the SAX analysis. The relative atomic percentages of C, O, and Ag were respectively 44.8%, 14.1%, and 42.1% as presented in **Table 4.8**.

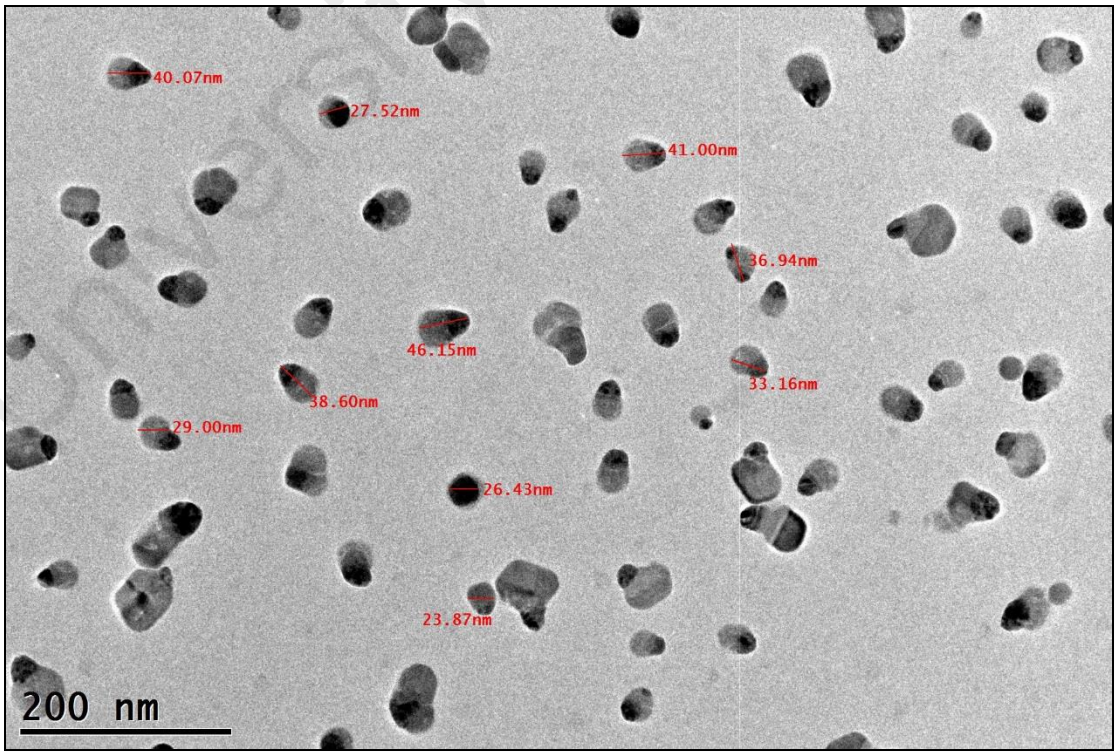


**Figure 4.27: HRTEM image of the AgNPs synthesised using a 2M $AgNO_3$ solution.** The mean particle size was approximately 34.27±7.38 nm.

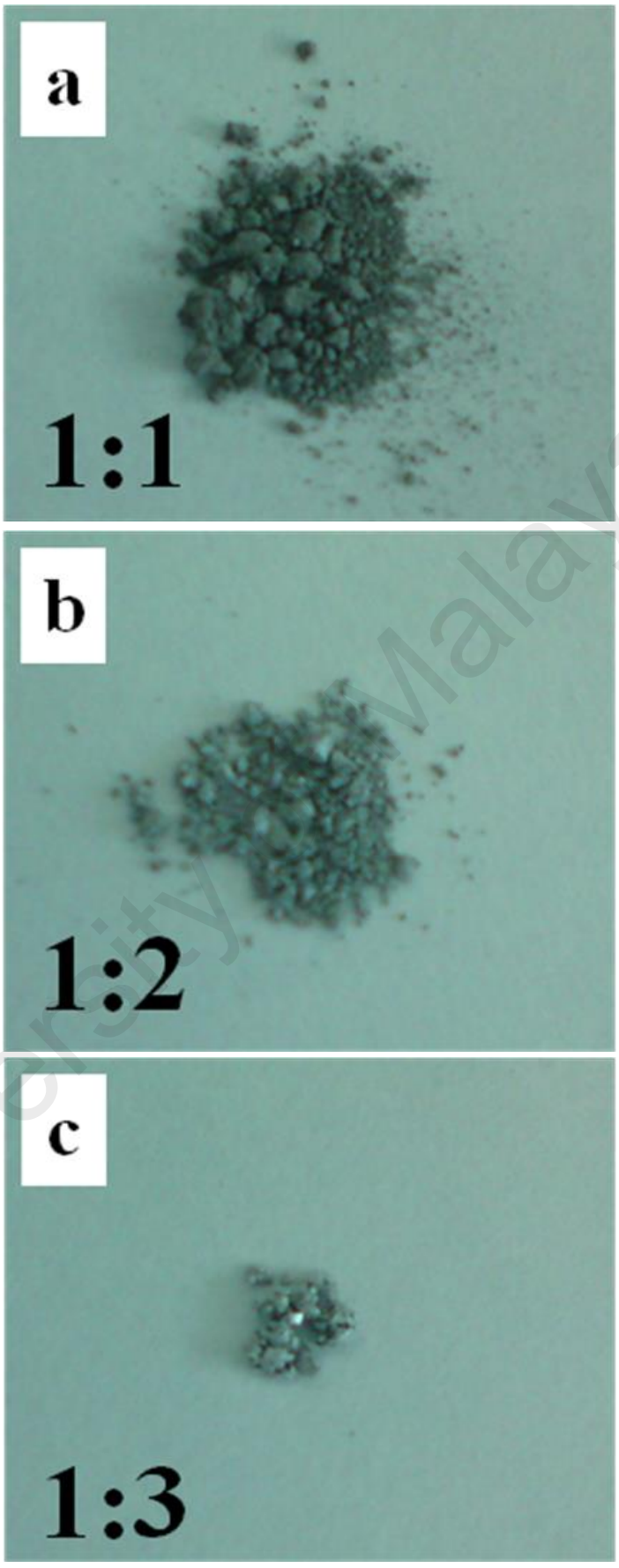


**Figure 4.28: The physical appearance of the triturated experimental nanosilver amalgams with varying AgNPs:Hg ratios where the AgNPs were synthesised using a 2M $AgNO_3$ solution.** The amalgams prepared with ratio of a) 1:1 appeared dry and powdery, b) 1:2 were dry and powdery, and c) 1:3 were well-triturated.

Investigation of the particle size and shape of sample B9 by HRTEM (**Figure 4.27**) also revealed that the particles were apparently discrete and homogeneously dispersed. The particles were mainly observed in the polygonal or spherical forms with an mean diameter of 34.27±7.38 nm.

## 4.3 Reconfirmation of the AgNPs:Hg Ratio Recommended by the Manufacturer for Formulation of the Experimental Nanosilver Amalgam

In this study, three ratios of AgNPs:Hg (1:1, 1:2, and 1:3) were examined for trituration of the experimental nanosilver amalgam to reaffirm the manufacturer's claim that the optimal AgNPs:Hg ratio was 1:3. **Figure 4.28** illustrates the physical appearance of the amalgams produced using sample B9 and triturated with differed Hg ratios. According to this figure, the AgNPs:Hg ratio of 1:3 produced a well-triturated amalgam, whereas the other studied ratios resulted in formation of dry and powdery amalgams.

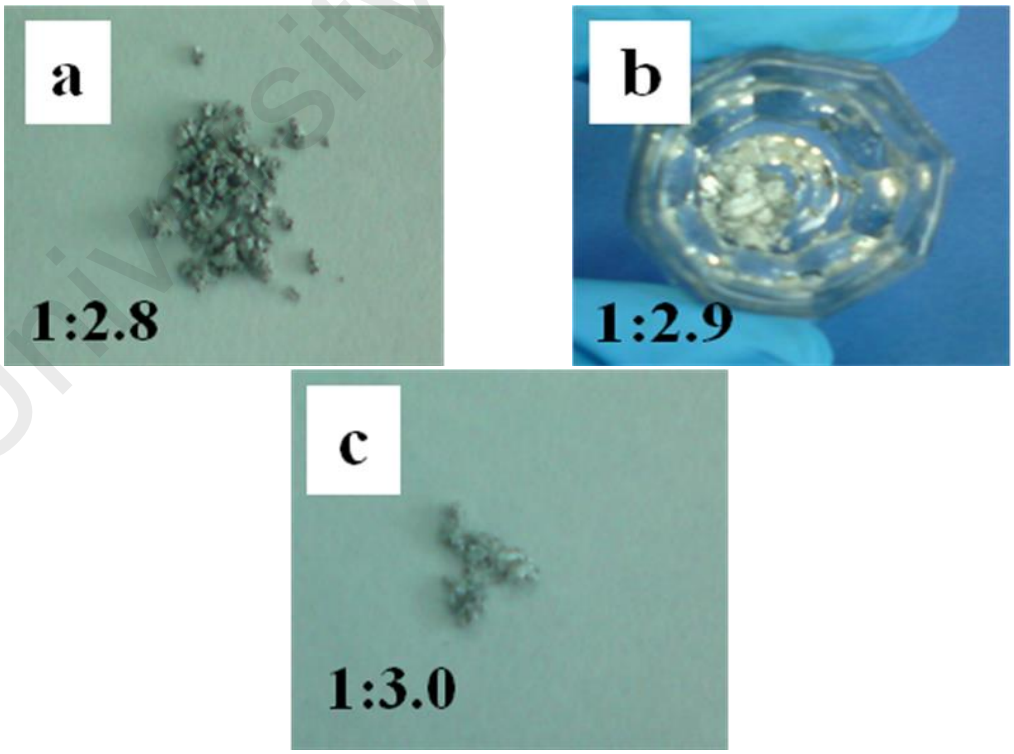


**Figure 4.29: The physical appearances of the experimental nanosilver amalgams triturated using different AgNPs:Hg ratios.** a) 1:2.8: the amalgam appeared dry and powdery, b) 1:2.9: the amalgam appeared well triturated, and c) 1:3: the amalgam appeared well triturated.

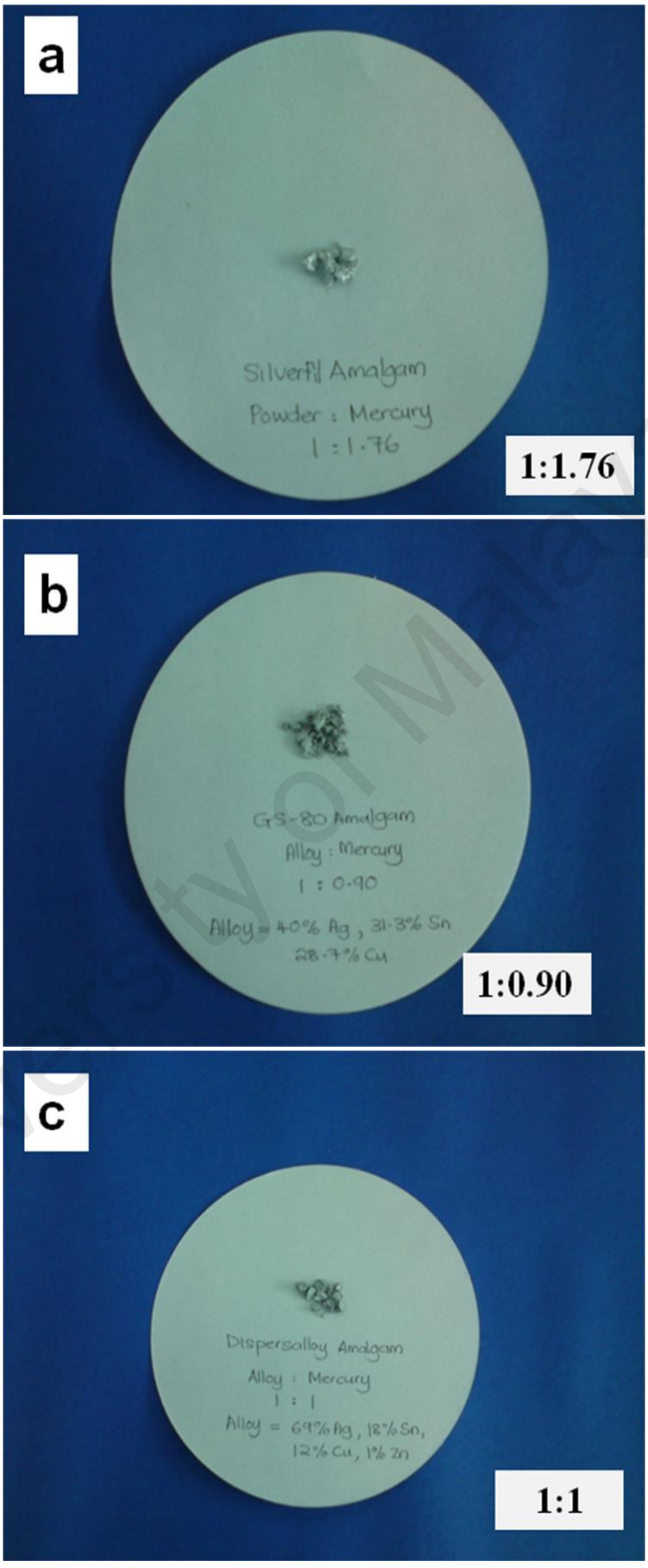


**Figure 4.30: Physical appearances of the triturated amalgams.** a) Silverfil™, b) GS80, and c) Dispersalloy.

## 4.4 Tuning of the AgNPs:Hg Ratio for Fabrication of the Optimised Experimental Nanosilver Amalgam

**Figure 4.29** illustrates the physical appearances of the triturated experimental nanosilver amalgams produced with sample B9 and three different Hg ratios. The AgNPs:Hg ratio of 1:2.9 produced a well-triturated experimental nanosilver amalgam and thus, it was considered as the optimal AgNPs:Hg ratio for formulation of the experimental nanosilver amalgam. The Silverfil™, GS80, and Dispersalloy amalgams were also prepared to compare their physical appearance (**Figure 4.30**) with that of the optimised experimental nanosilver amalgams upon trituration**.** **Figure 4.31** also shows that the optimised experimental nanosilver amalgam inserted and carved in typodont teeth could endow a better aesthetic appearance compared to the Silverfil™ amalgam.


**Figure 4.31: The optimised experimental nanosilver amalgam and Silverfil™ filled into the prepared cavities of a dental typodont.** The aesthetic appearance of the experimental nanosilver amalgam was better compared to Silverfil™.

## 4.5 Characterisation of the Optimised Experimental Nanosilver Amalgam

### 4.5.1 Comparison of the Chemical, Physical, and Morphological Properties of the Optimised Experimental Nanosilver Amalgam with Silverfil™, GS80, and Dispersalloy

The microstructure, phase structure, and chemical states of the optimised experimental nanosilver amalgam were compared with those of Silverfil™, GS80, and Dispersalloy amalgams. The mechanical properties of these amalgams including the compressive strength, diametral tensile strength, and Vickers microhardness were also compared in this study.

#### 4.5.1.1 Microstructural Comparisons

**Figure 4.32** shows that Silverfil™ was composed of the polygonal-shaped particles, whereas the GS80 and Disperalloy amalgams contained particles with irregular shapes (admixed particles).

Analysis of the particle size distributions of the metal alloys also showed that Silverfil™ possessed the widest range of particle size (146-786 nm), followed by GS80 (83-636 nm), and Dispersalloy (122-221 nm). Microstructural investigation of the unpolished optimised experimental nanosilver amalgam and Silverfil™ by the FESEM analysis (**Figure 4.33)** showed formation of the cluster matrices of Ag and Hg on their surfaces.

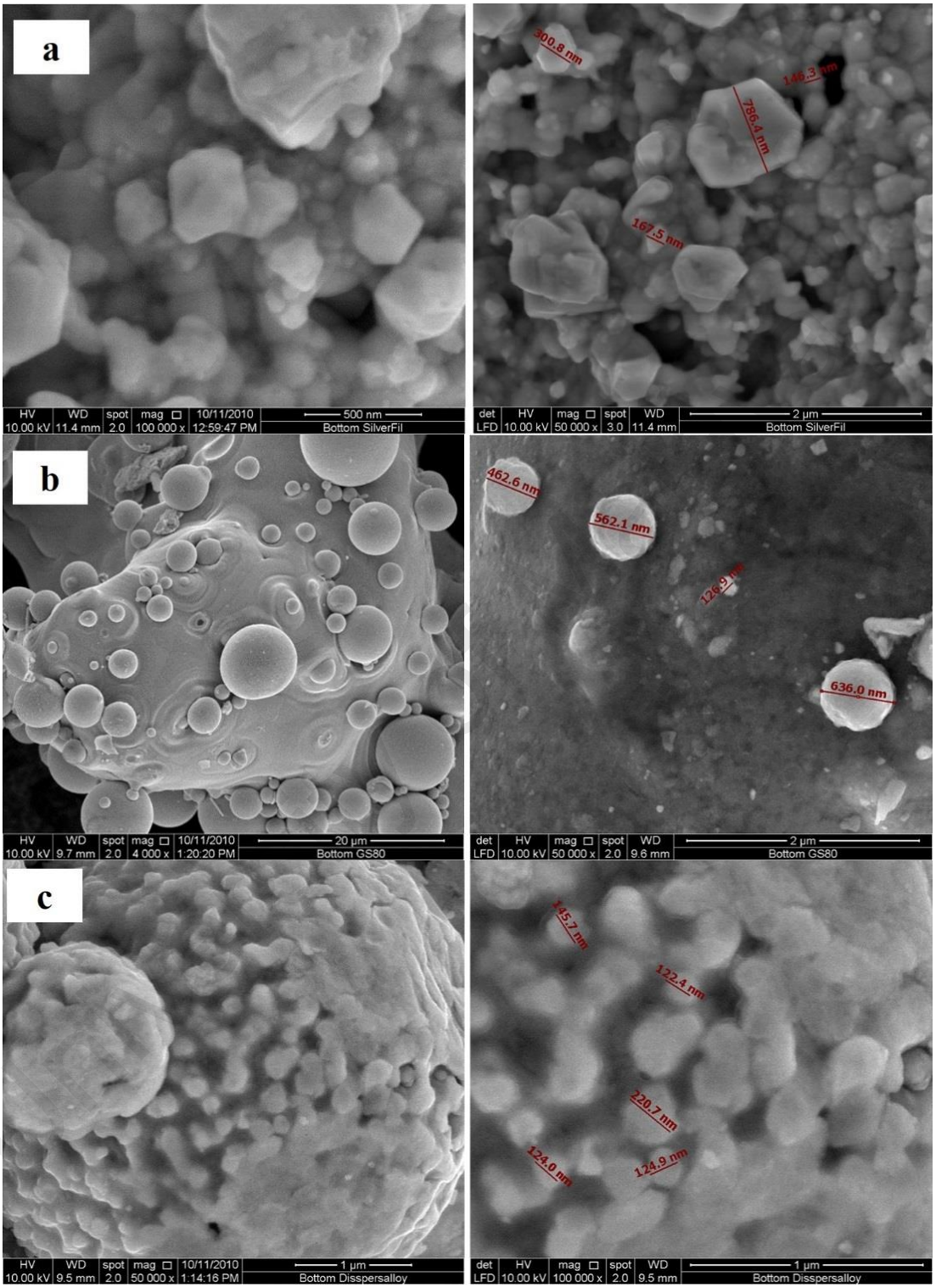


**Figure 4.32: The FESEM images from the metallic alloys of three dental amalgams.** a) Silverfil™ consisted of polygonal-shaped particles with a size range of 146-786 nm, b) GS80 was composed of irregular particle shapes ranging from 83 to 636 nm), and c) Dispersalloy contained irregular-shaped particles with a size range of 122-221 nm.

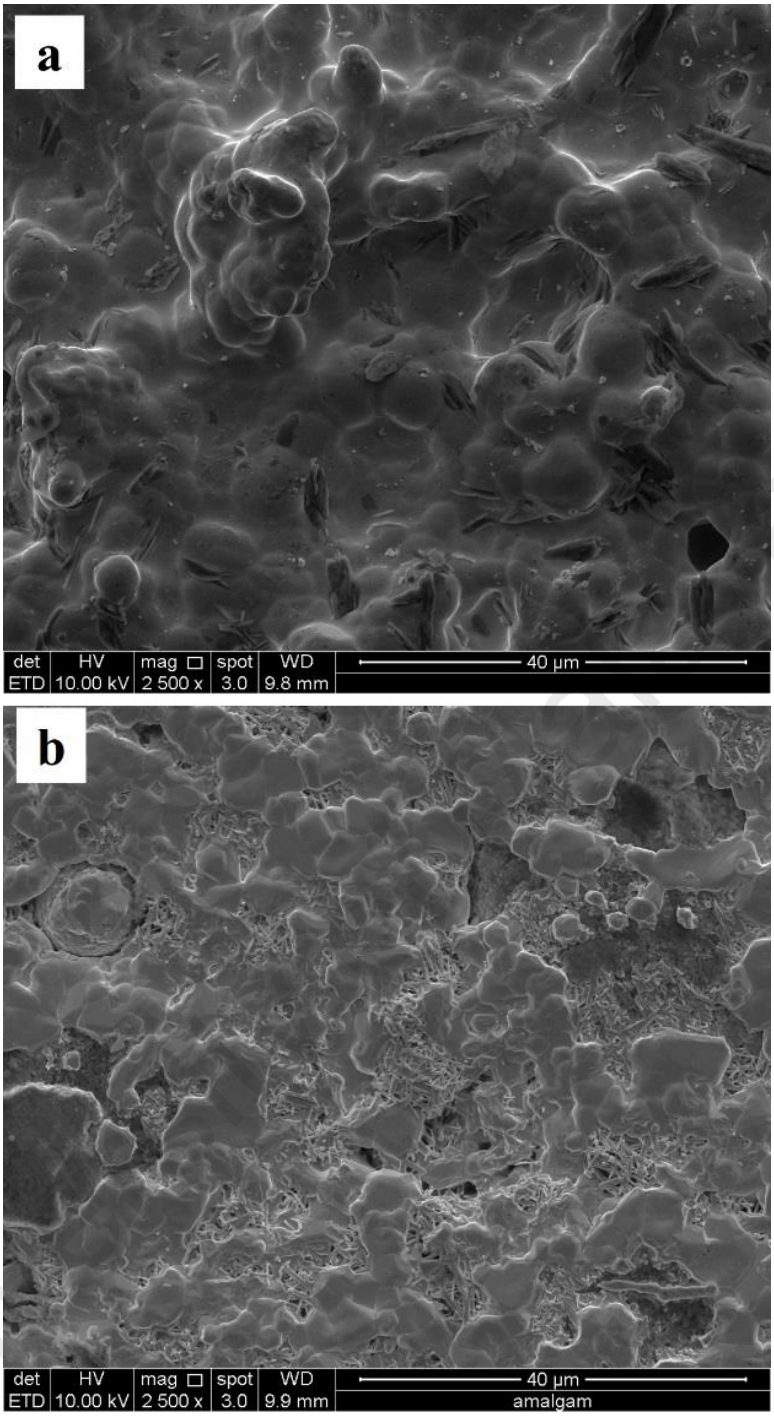


**Figure 4.33: The FESEM images from the unpolished surfaces of a) Optimised experimental nanosilver amalgam, and (b) Silverfil™.** Both the amalgams showed cluster matrices in their morphological structures (magnification 2500X).

The FESEM images of the polished and unpolished Silverfil™, GS80, and Dispersalloy amalgams are illustrated in **Figure 4.34**. The surface morphologies of the polished amalgams (**Figure 4.34(a,c,e))** showed the presence of different phases, whereas clusters of alloy with crystal matrix compounds were observed in the unpolished samples (**Figure 4.34(b,d,f))**. The observed voids in **Figure 4.34(b)** could result in higher

reactivity for absorbtion of Hg. The EDX analysis of the polished surface of the optimised experimental nanosilver amalgam indicated the absence of impurities **(Figure 4.35)**. According to the elemental analysis (**Table 4.9**), the weight percentages of Ag and Hg in this amalgam were 41.00% and 49.36%, respectively.

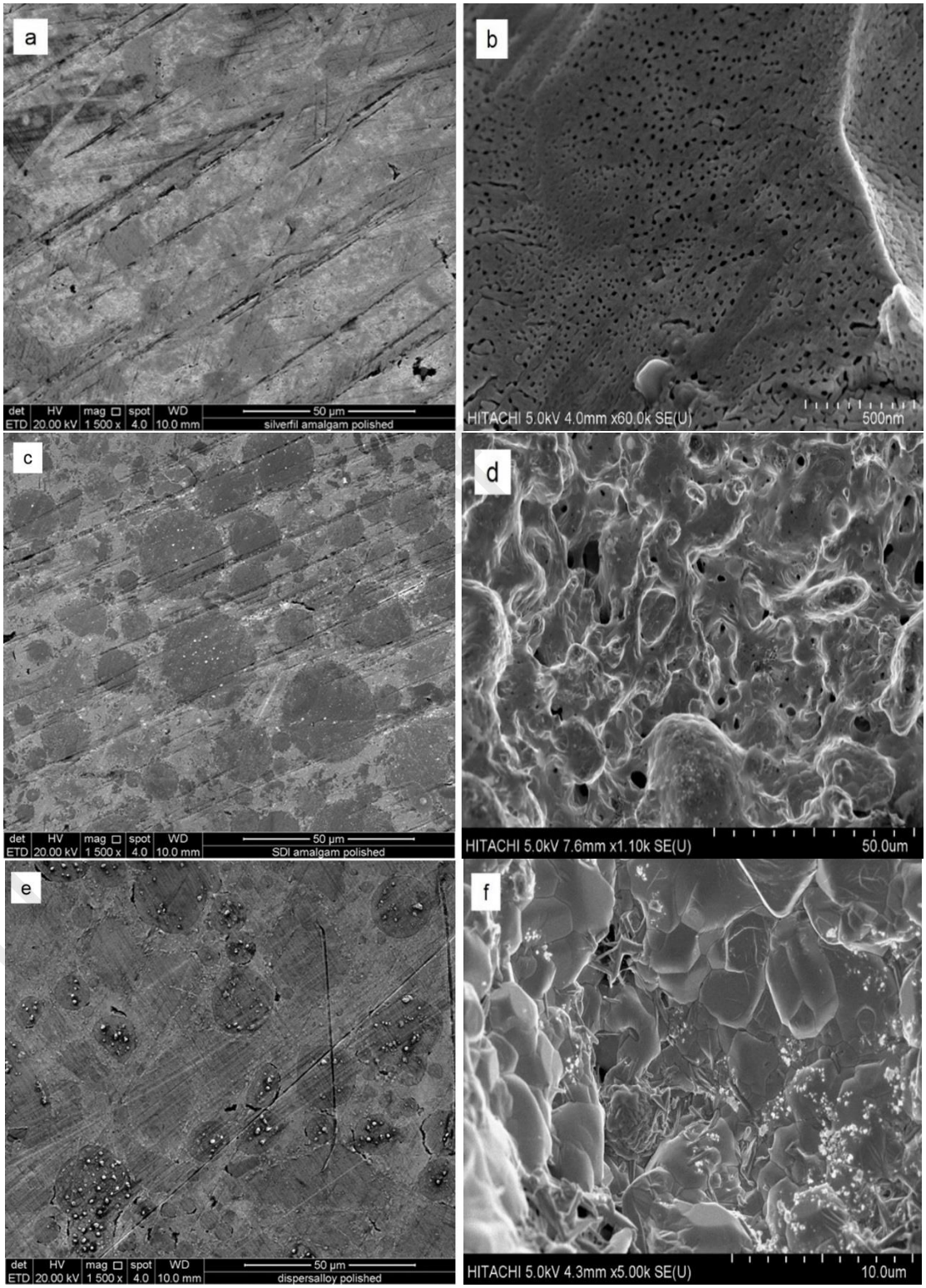


**Figure 4.34: Low-magnification FESEM images of the (a,c,e) polished, and (b,d,f) unpolished amalgams. (a,b) Silverfil™, (c,d) GS80, and (e,f) Dispersalloy.**

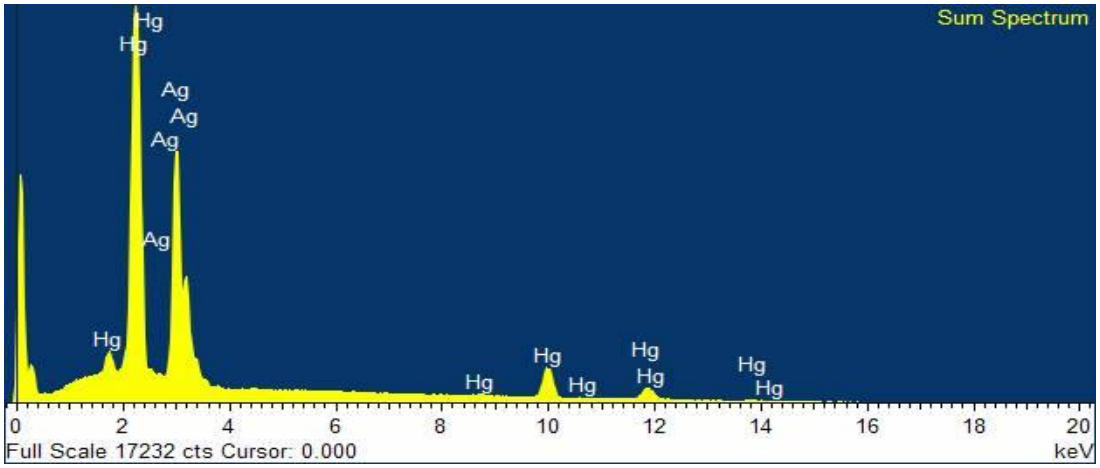


**Figure 4.35: The EDX spectrum of the optimised experimental nanosilver amalgam.** The amalgam contained no any element as impurity in it composition.

**Table 4.9: The relative atomic percentages of the elements present in the optimised experimental nanosilver amalgam.**

| Element | Relative Atomic Percentage (%) |
|---|---|
| **C** | 56.19 |
| **Ag** | 26.59 |
| **Hg** | 17.22 |
| **Totals** | 100.00 |

The EDX analysis was also carried out on polished surfaces of the other three amalgams in order to identify their elemental distribution profiles. **Figure 4.36(a)-(c)** respectively demonstrate the EDX spectra of Silverfil$^{TM}$, GS80, and Dispersalloy recorded in the spot-profile mode. The EDX analyses revealed that Silverfil$^{TM}$ contained of Ag and Hg, whereas GS80 and Dispersalloy contained of Ag, Sn, Cu, and Hg. The percentages of various elements present in the compositions of these amalgams are listed in **Table 4.10.** The relative atomic percentages of Ag 3d and Hg 4f were 17.72% and 16.69% in Silverfil$^{TM}$. On the other hand, the GS80 amalgam composed of 25.7% Ag, 22.04% Sn, 31.76% Cu, and 20.41% Hg. Dispersalloy also contained the Ag, Sn, Cu, and Hg elements with atomic percentages of 21.99%, 5.14%, 7.23%, and 9.76%, respectively.

The elemental maps of the polished surface of the optimised experimental nanosilver amalgam shown in **Figure 4.37** revealed the heterogeneous distributions of Ag and Hg atoms. The dark spots represented the silver phase while the light spots indicated the homogenous mixture of the intermetallic compound.

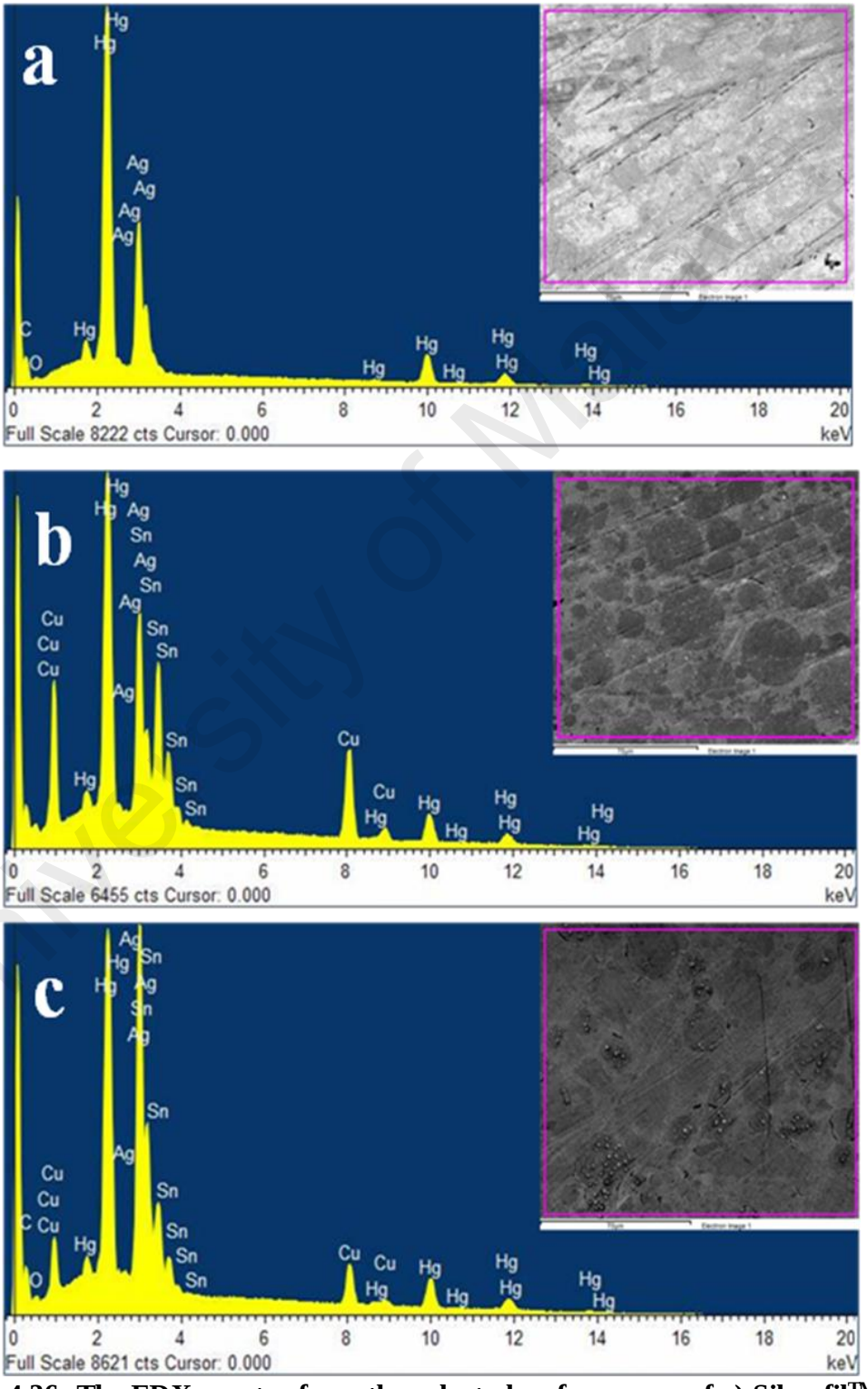


**Figure 4.36: The EDX spectra from the selected surface areas of a) Silverfil™, b) GS80, and c) Dispersalloy.**

**Table 4.10: The atomic percentages of various elements detected in the Silverfil™, GS80, and Dispersalloy amalgams by the EDX analysis.**

| Amalgams | Relative Atomic Percentage (%) | | | | | | |
|---|---|---|---|---|---|---|---|
| | C | O | Ag | Sn | Cu | Hg | Total |
| **Silverfil™** | 55.00 | 10.59 | 17.72 | - | - | 16.69 | 100 |
| **GS80** | - | - | 25.79 | 22.04 | 31.76 | 20.41 | 100 |
| **Dispersalloy** | 42.92 | 12.96 | 21.99 | 5.14 | 7.23 | 9.76 | 100 |

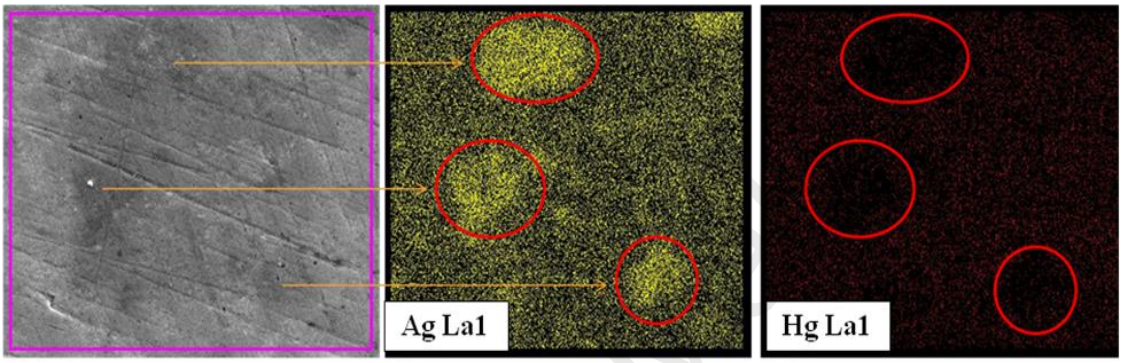


**Figure 4.37: The elemental mapping of Ag and Hg in the optimised experimental nanosilver amalgam.**

**Figure 4.38** to **Figure 4.40** also illustrate the elemental mappings of the varied elements present in the Silverfil™, GS80, and Dispersalloy amalgams. **Figure 4.38** shows that Silverfil™ consisted of two elements including Ag and Hg, which were homogeneously distributed in the Ag-Hg matrix system. The elemental mappings of GS80 (**Figure 4.39**) also showed a homogeneous distribution of all the elements within its matrix. It was observed that a mixture of Cu-Sn (η; $Cu_6Sn_5$) and Ag-Sn (γ; $Ag_3Sn$) phases was formed in GS80. The Ag-Cu eutectic particles were also surrounded with the η phase in this amalgam. A similar elemental distribution was found in Dispersalloy where the Cu, Ag, and Sn atoms were distributed homogeneously (**Figure 4.40**). It was found that a mixture of γ, η ($Cu_6Sn_5$ and CuSn), and Ag-Hg ($\gamma_1$; $Ag_2Hg_3$) phases was present in the Dispersalloy amalgam.

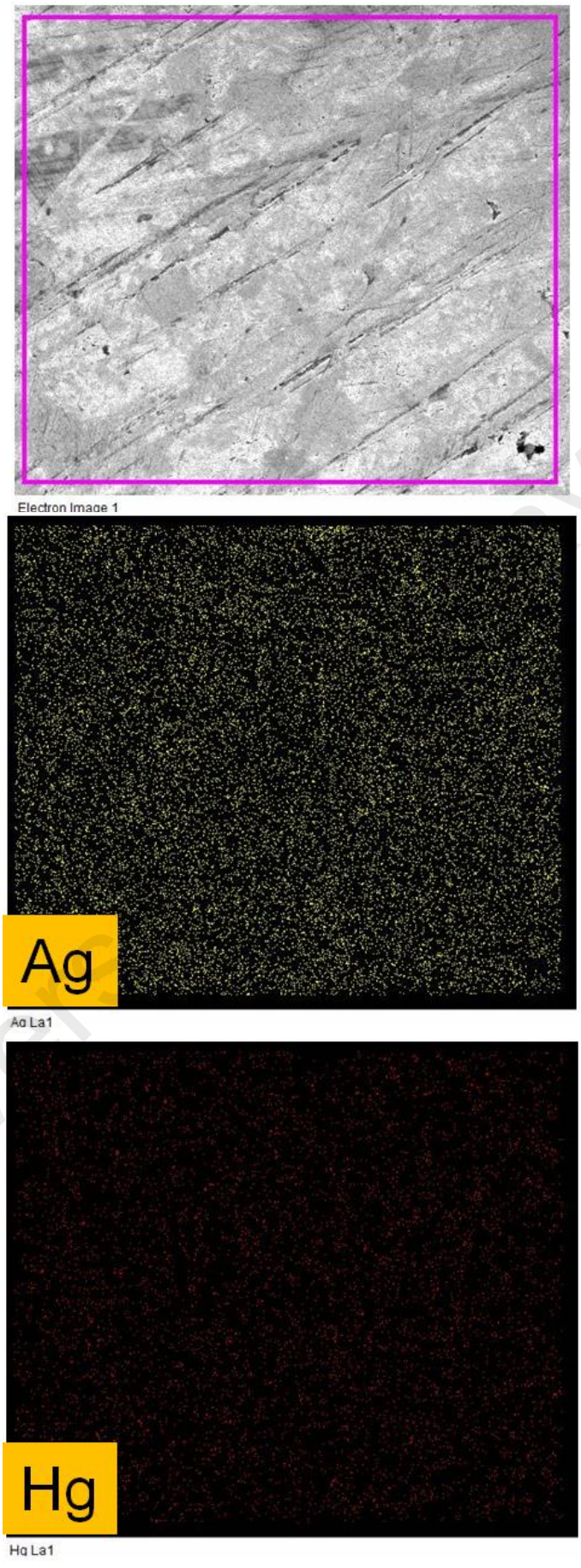


**Figure 4.38: The EDX mappings of the Ag and Hg elements in Silverfil™.** The maps showed homogeneous distributions of the Ag and Hg atoms in the matrix.

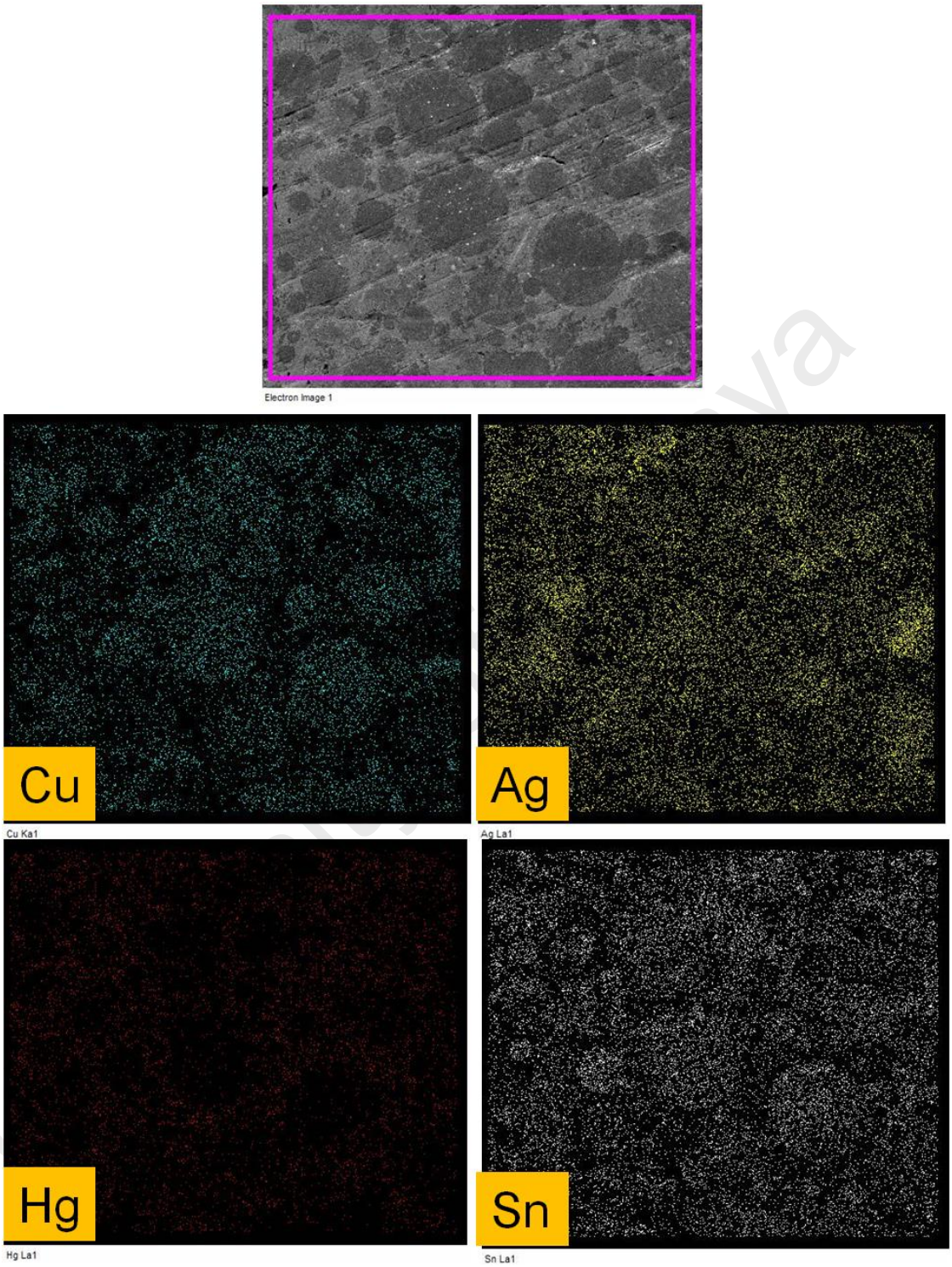


**Figure 4.39: The EDX elemental mapping analysis of the GS80 amalgam.** The maps showed homogeneous distributions of the Cu, Ag, Hg, and Sn atoms in this amalgam.

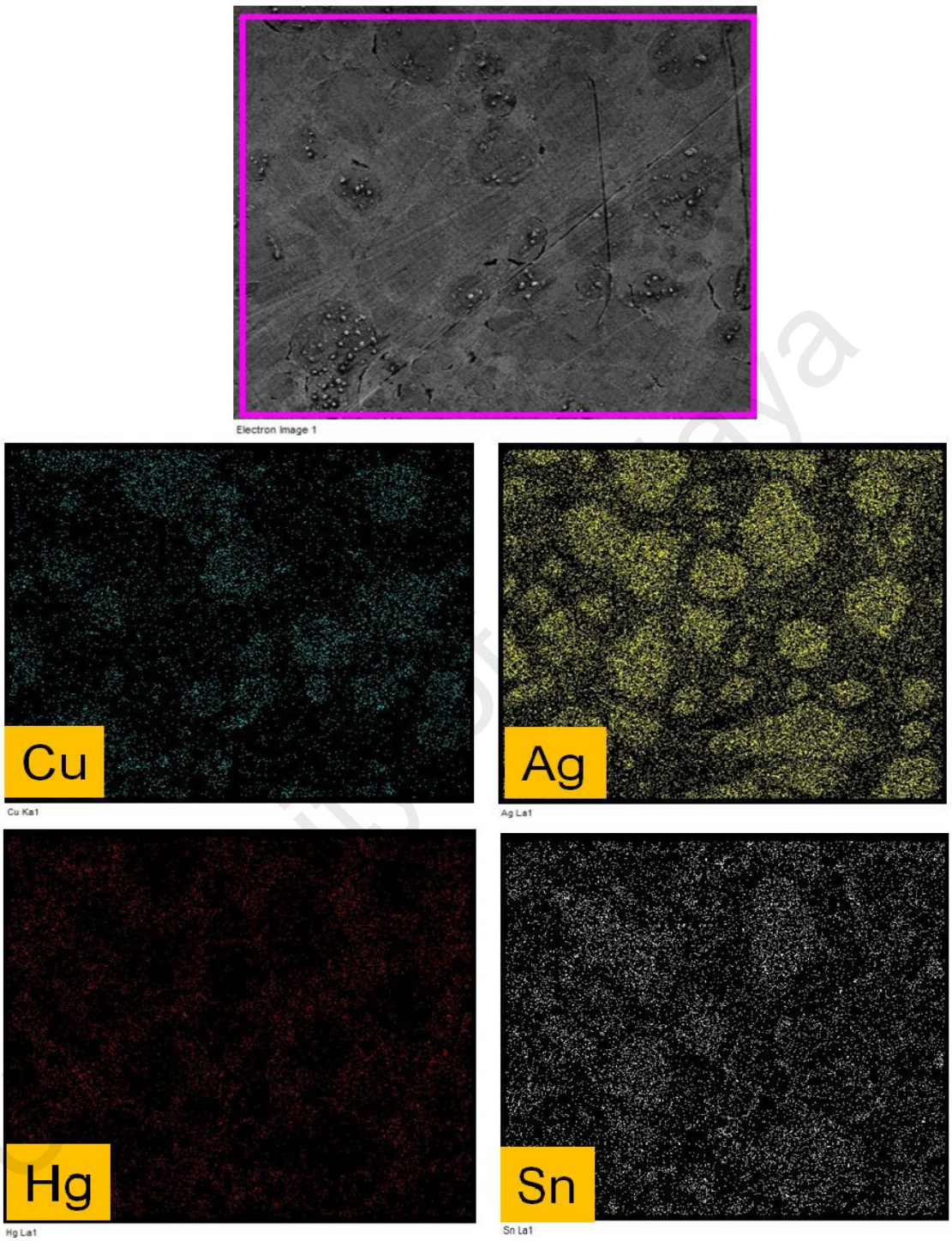


**Figure 4.40: The EDX elemental mapping analysis of the Dispersalloy amalgam.** Homogeneous distributions of the Cu, Ag, Sn, and Hg atoms were confirmed in these maps.

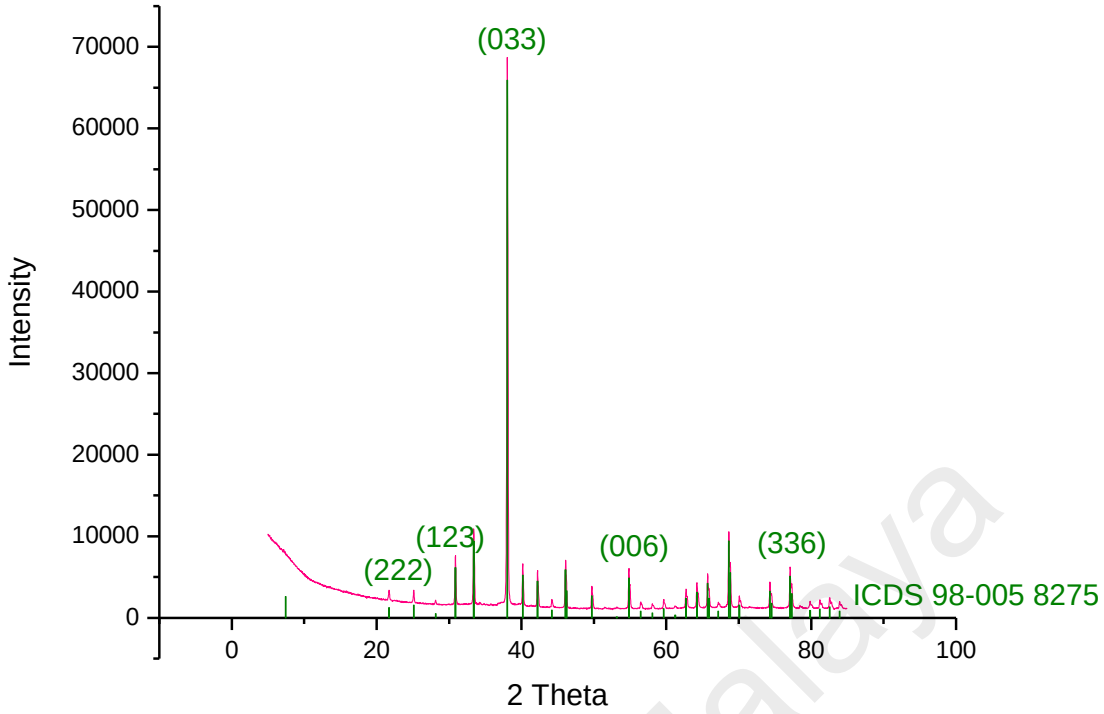


**Figure 4.41: The XRD diffraction pattern of the optimised experimental nanosilver amalgam.**

#### 4.5.1.2 Phase Comparisons

The XRD diffraction pattern of the optimised experimental nanosilver amalgam presented in **Figure 4.41** revealed that the intermetallic structure of $Ag_2Hg_3$ was highly crystalline with isometric (cubic) structure and the unit cell of 10.05 Å. The miller index values reported that the chemical composition of the optimised experimental nanosilver amalgam was similar to gamma moschellandsbergite ($Ag_2Hg_3$), a natural mineral (ICDS file No. 98-005 8275), inferring that the optimised experimental nanosilver amalgam could provide a stability similar to that of $Ag_2Hg_3$.

The XRD pattern of Silverfil™ (**Figure 4.42**) also showed its presence in the crystalline phase. Similar to the optimised experimental nanosilver amalgam, all the diffraction peaks of the Silverfil™ were well corresponded to the cubic structure of gamma moschellandsbergite (JCPDS11-0067). Therefore, Silverfil™ is also produced with a high stability due to its high fraction of the stable compound ($Ag_2Hg_3$).

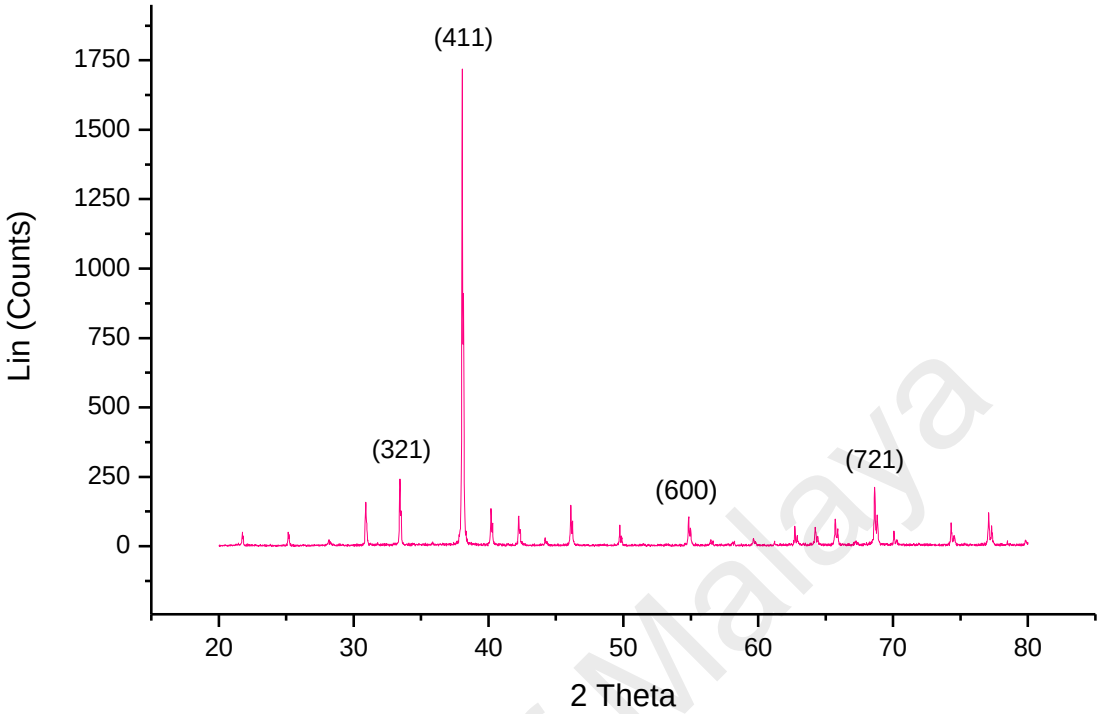


**Figure 4.42: The XRD diffraction pattern of Silverfil™.**

The XRD patterns of GS80 and Dispersalloy shown in **Figure 4.43** also revealed their highly crystalline structure. For GS80 (**Figure 4.43(a)**), the major peaks could be readily indexed by the values reported in JCPDS 71-0529, indicating the presence of $Ag_2Hg_{3.02}$. The peaks with lower intensities mostly matched the reference peaks of pure Hg (JCPDS 74-0039) with the hexagonal crystal structure. The peak observed at 43.36° also corresponded to pure Cu with the FCC crystalline structure (JCPDS 89-2838). The main diffraction peaks of Dispersalloy (**Figure 4.43(b)**) matched the reference peaks of Ag-Hg according to JCPDS34-0624, while the broader peak at 43.3° matched the value reported for pure Cu with the FCC crystalline structure (JCPDS 89-2838).

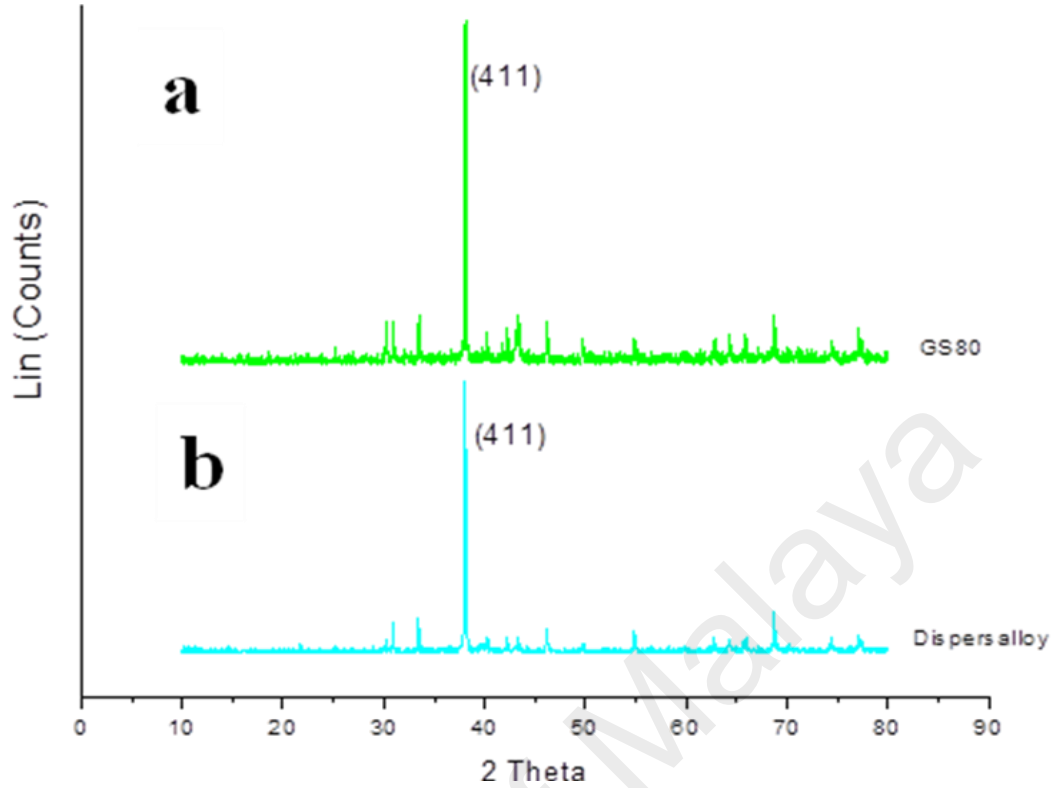


**Figure 4.43: The XRD diffraction patterns of a) GS80, and b) Dispersalloy.**

#### 4.5.1.3 Chemical States of Hg in Different Amalgams

To study the chemical states of Hg, the optimised experimental nanosilver amalgam was analysed by the XPS technique. The relative atomic percentages of the elements detected in the optimised experimental nanosilver amalgam are given in **Table 4.11.**

**Table 4.11: The relative atomic concentrations of the elements present in the optimised experimental nanosilver amalgam.**

| Element | Peak Quantified | Relative atomic concenteration (%) |
|---|---|---|
| **Silver** | Ag 3d | 6.02 |
| **Oxygen** | O 1s | 25.03 |
| **Carbon** | C 1s | 64.86 |
| **Mercury** | Hg 4f | 4.09 |
| **Total** | | **100.00** |

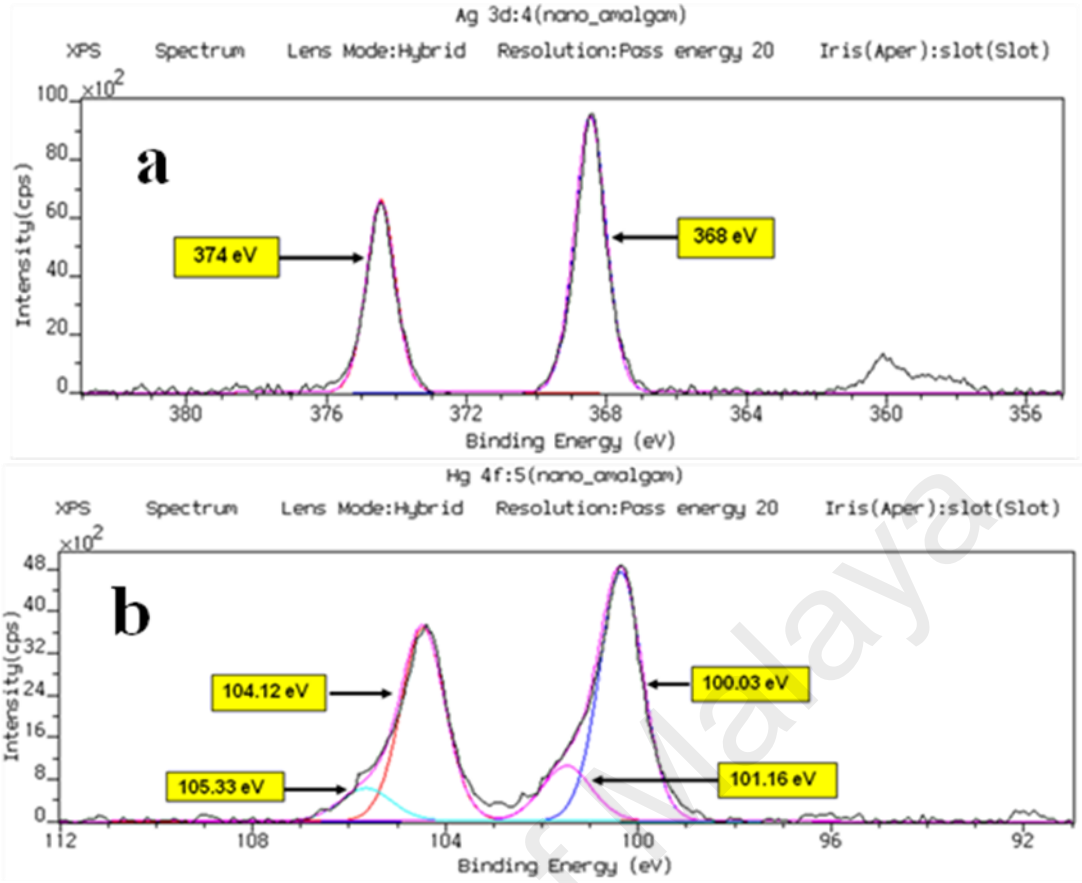


**Figure 4.44: The XPS spectra of the optimised experimental nanosilver amalgam.** a) The Ag 3d region showed the metallic state ($Ag^0$), and b) the Hg 4f region showed oxide state (bound Hg).

The XPS spectrum of the optimised experimental nanosilver amalgam is shown in **Figure 4.44**. The Ag 3d peak in **Figure 4.44(a)** showed a doublet pair arised due to the spin-orbital coupling of $3d_{5/2}$ and $3d_{3/2}$. The binding energies of the Ag $3d_{5/2}$ and Ag $3d_{3/2}$ peaks were respectively 368.0 eV and 374.0 eV, where the energy difference of 6.0 eV between these two peaks confirmed the formation of $Ag^0$.

On the other hand, the Hg 4f peak in **Figure 4.44(b)** showed the binding energies of 101.1 eV and 104.2 eV for Hg $4f_{5/2}$ and Hg $4f_{7/2}$, corresponding to the Hg alloy. Therefore, no unbound Hg was detected in the XPS spectrum of the optimised experimental nanosilver amalgam. A higher surface area to volume ratio derived from the decreased size of Ag particles could be the reason for an enhanced interaction between the Ag and Hg atoms. Therefore, the Hg becomes supersaturated with Ag and nucleation of $\gamma_1$

crystals occurs (Okabe et al., 1996). The XPS peaks of C 1s and O 1s also respectively showed the binding energies of 285 eV and 531 eV, as previously discussed.

The XPS survey spectrum of Silverfil™ is represented in **Figure 4.45** with the expected photoelectron peaks of O 1s, C 1s, Sn 3d, Ag 3d, and Hg 4f. The relative atomic percentages of the constituting elements of Silverfil™ were 24.19%, 47.85%, 13.18%, 10.17%, and 4.60% for O, C, Sn, Ag, and Hg (**Table 4.12**).

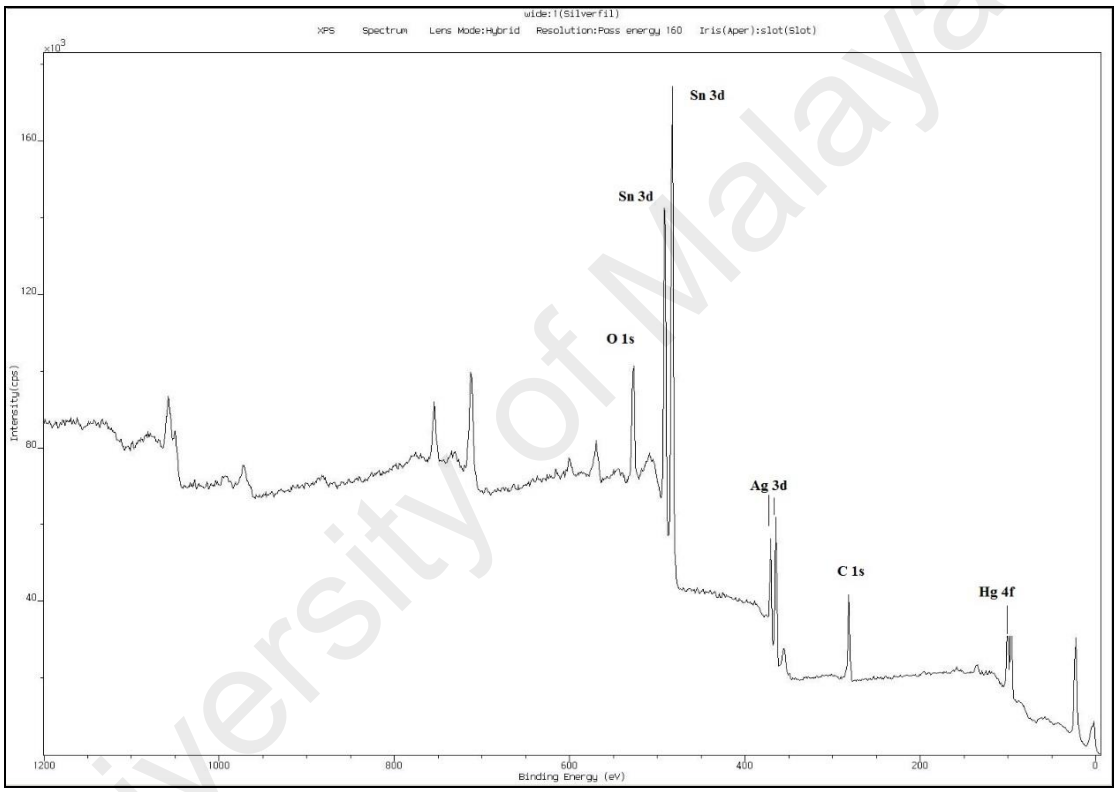


**Figure 4.45: The XPS survey spectrum of Silverfil™.** The spectrum indicated the presence of Ag, Sn, Hg, O, and C.

**Table 4.12: The relative atomic concentrations of the elements present in Silverfil™, GS80, and Dispersalloy.**

| Amalgams/ Elements | Relative Atomic Concentration (%) | | | | | | | |
|---|---|---|---|---|---|---|---|---|
| | C 1s | O 1s | Ag 3d | Sn 3d | Zn 2p | Cu 2p | Hg 4f | Total |
| **Silverfil™** | 47.86 | 24.19 | 10.17 | 13.18 | - | - | 4.60 | 100 |
| **GS80** | 50.17 | 26.20 | 4.06 | 12.71 | 1.84 | 0.66 | 4.36 | 100 |
| **Dispersalloy** | 59.87 | 22.84 | 2.76 | 3.75 | 8.4 | - | 2.38 | 100 |

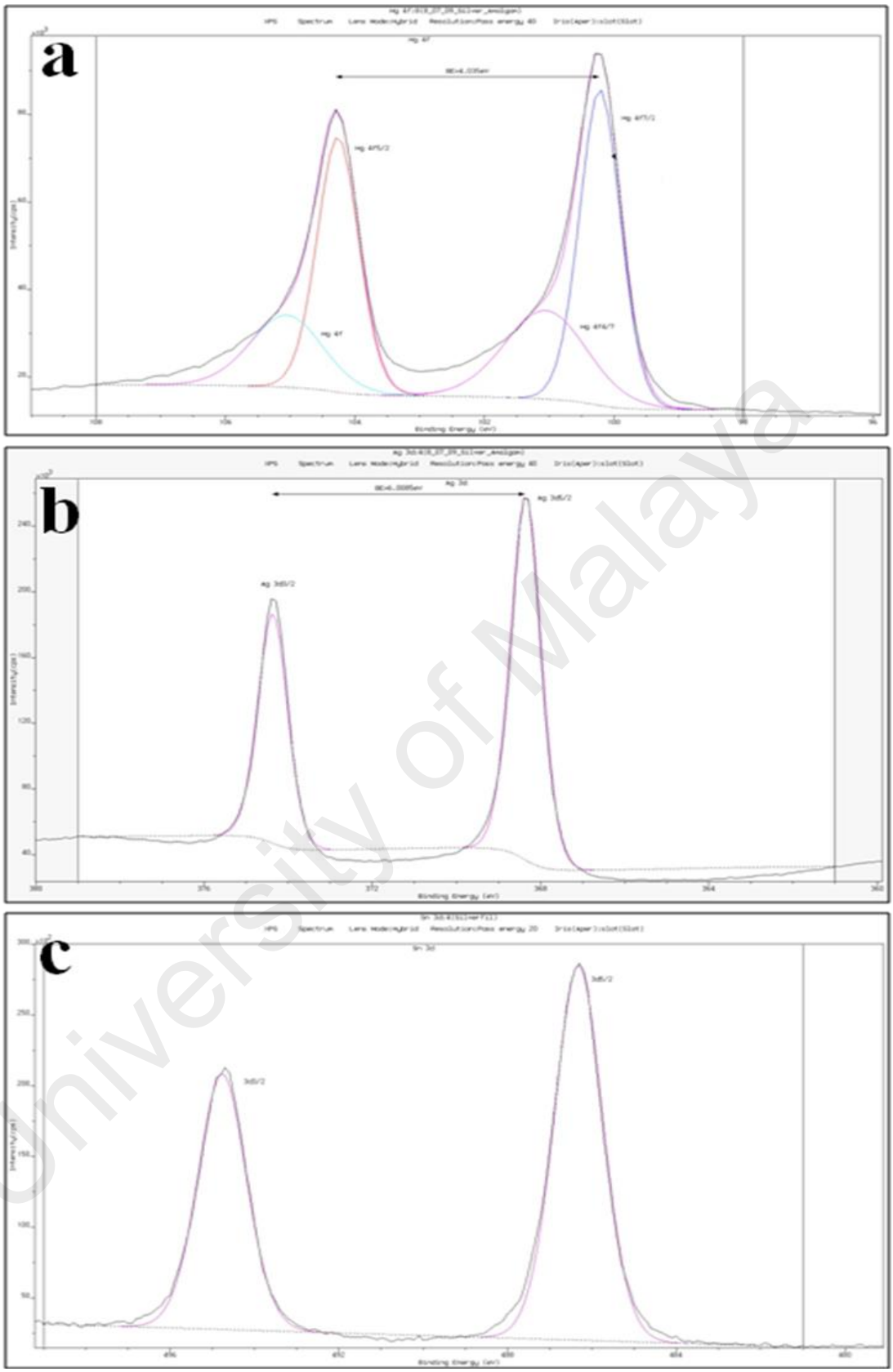


**Figure 4.46: The high-resolution XPS spectra of the Ag 3d, Hg 4f, and Sn 3d regions for Silverfil™.** a) The Ag 3d region showed the presence of metallic $Ag^0$, b) the Hg 4f region confirmed that Hg was totally in bound state, and c) the Sn 3d region indicated that Sn was present in the oxide state.

The high-resolution XPS peaks of Ag 3d, Hg 4f, and Sn 3d belonged to Silverfil$^{TM}$ are illustrated in **Figure 4.46**. The XPS peak of Ag 3d of Silverfil$^{TM}$ (**Figure 4.46(a)**) showed a doublet pair, which arised from the spin-orbital coupling of $3d_{5/2}$ and $3d_{3/2}$ (Wanger et al., 1992). The binding energies for the Ag $3d_{5/2}$ and Ag $3d_{3/2}$ peaks were 368.0 eV and 374.0 eV, respectively with a 6.0 eV difference between both binding energies, which confirmed the formation of metallic silver ($Ag^0$). On the other hand, a 4.03 eV difference between the binding energy values of the Hg $4f_{5/2}$ (104.2 eV) and Hg $4f_{7/2}$ (100.2 eV) peaks confirmed the presence of Hg in the alloyed state (**Figure 4.46(b)**). The XPS peak of Sn 3d (**Figure 4.46(c)**) also showed the presence of Sn $3d_{5/2}$ and Sn $3d_{3/2}$ doublet. After curve fitting, two peaks were obtained at 486.2 eV and 494.2 eV, which corresponded to Sn (II) and Sn (IV). Observation of the Sn peaks in the XPS spectrum of Silverfil$^{TM}$ indicated that Sn entered as impurity in the early preparation processes. The higher relative atomic percentage of Sn in Silverfil$^{TM}$ compared to GS80 and Dispersalloy (**Table 4.12**) might influence the Hg release upon amalgamation. The diffusion and release rates of the Hg atoms are inversely proportional to the thickness of oxide layer (Marek, 1997).

The survey scan spectrum of GS80 shown in **Figure 4.47** demonstrated the photoelectron peaks of O 1s, C 1s, Sn 3d, Cu 2p, Ag 3d, Zn 2p, and Hg 4f with relative atomic concentrations of 26.20%, 50.17%, 12.71%, 0.66%, 4.06%, 1.84%, and 4.36%, respectively (**Table 4.12**). Investigation of the survey scan spectrum of Dispersalloy (**Figure 4.48**) also revealed the existence of similar photoelectron peaks other than Cu, which was not detected in the Dispersalloy composition. However, the relative atomic percentages (**Table 4.12**) of the Dispersalloy elements were different than those measured for GS80. The highest relative atomic percentage was observed for C 1s (59.87%), followed by O 1s (22.86%), Zn 2p (8.4%), Sn 3d (3.75%), Ag 3d (2.76%), and Hg 4f (2.38%).

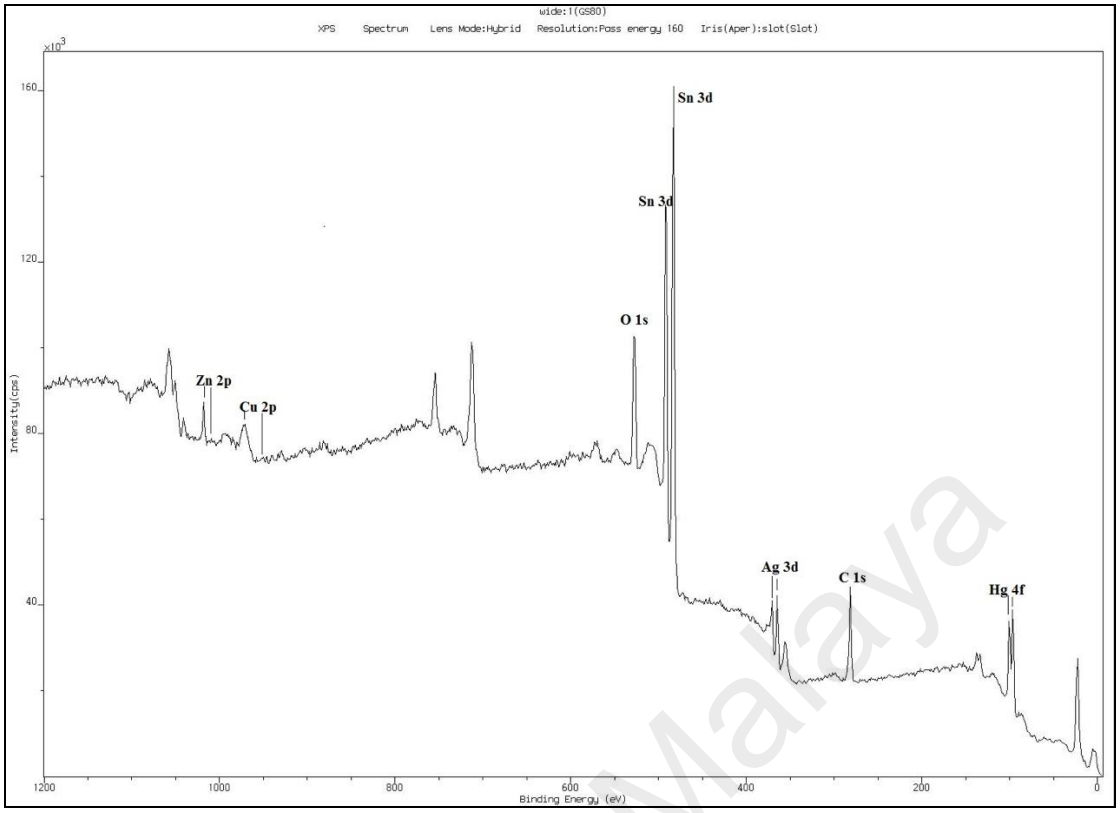


**Figure 4.47: The XPS survey spectrum of GS80.** The spectrum indicated the presence of Ag, Sn, Hg, Zn, Cu, O, and C.

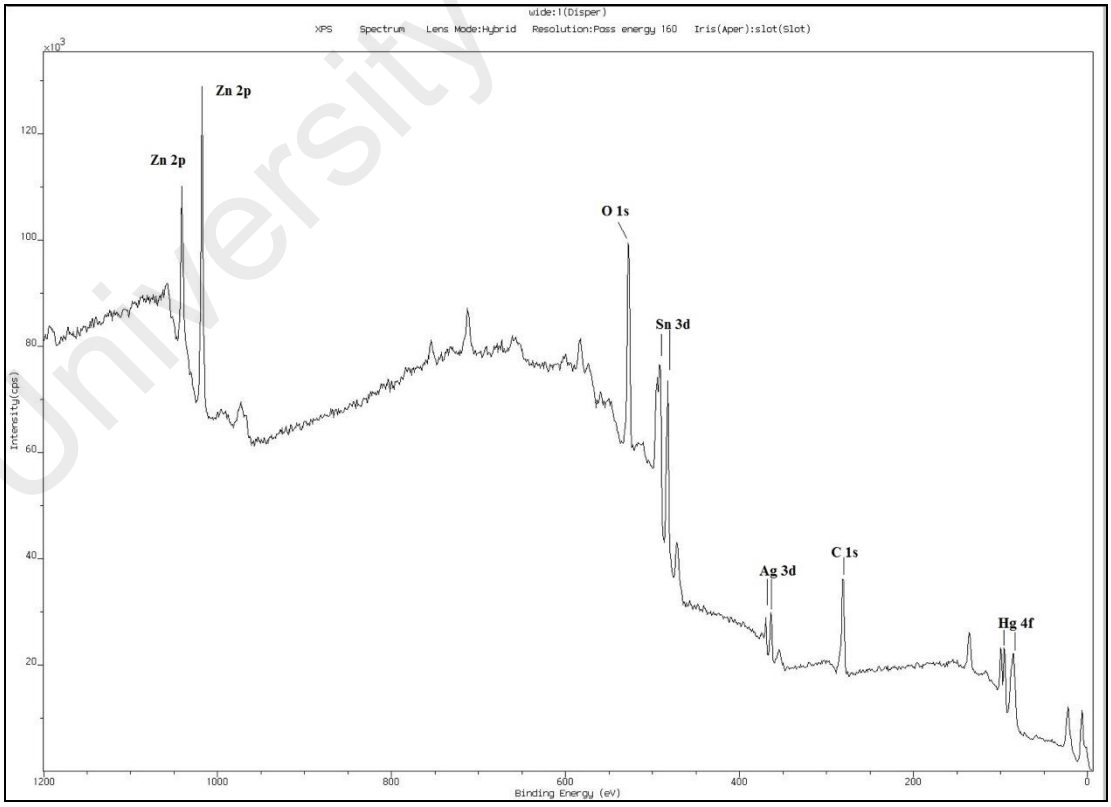


**Figure 4.48: The XPS survey spectrum of Dispersalloy.** The spectrum indicated the presence of Ag, Sn, Hg, Zn, O, and C.

### 4.5.2 Comparison of the Compressive Strength, Diametral Tensile Strength, and Vickers Microhardness of the Optimised Experimental Nanosilver Amalgam with Silverfil™, GS80, and Dispersalloy.

The optimised experimental nanosilver amalgam was also compared with Silverfil™ and two other commercial amalgams in terms of its compressive strength, diametral tensile strength, and Vickers microhardness. **Figure 4.49** illustrates the compressive strength values of the studied amalgams measured after 24 hours and 7 days of incubation in distilled water at 37±1°C. The compressive strength of the optimised experimental nanosilver amalgam after storage for 24 hours (380.62±37.10 MPa) was significantly higher than Dispersalloy (190.68±44.18 MPa) ($P<0.05$). However, ANOVA and Bonferroni post hoc tests showed no significant differences when the optimised experimental nanosilver amalgam was compared with Silverfil™ and GS80. After 7 days of storage, the compressive strength of the optimised experimental nanosilver amalgam (234.99±174.45 MPa) became significantly lower compared to Silverfil™ (349.83±14.14 MPa), and significantly higher than GS80 (80.93±35.06 MPa).

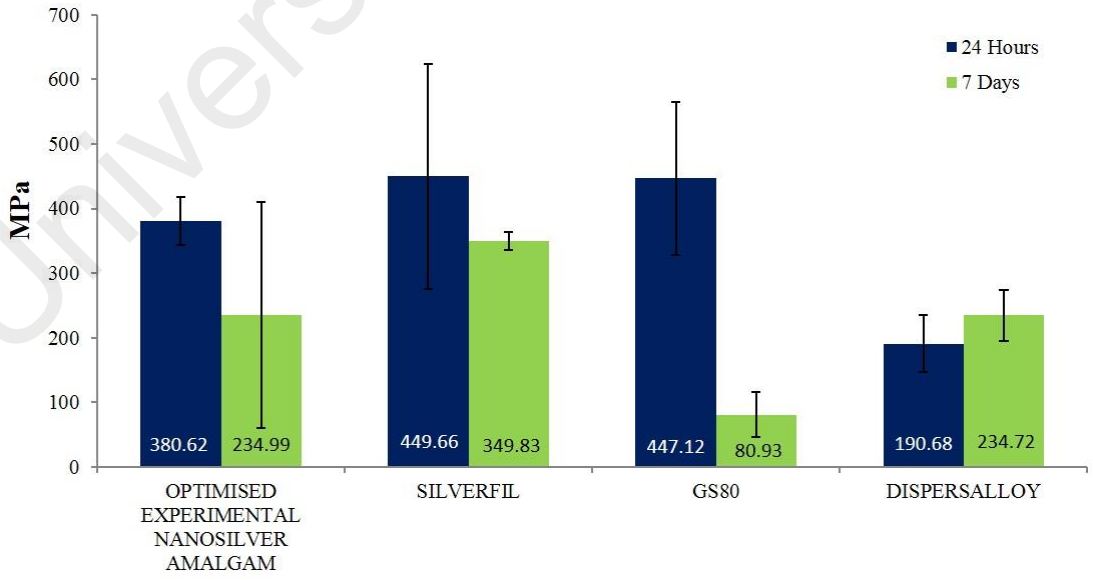


**Figure 4.49: The values of compressive strength for the optimised experimental nanosilver amalgam, Silverfil™, GS80, and Dispersalloy after 24 hours and 7 days storage in distilled water at 37±1°C.** Silverfil™ showed the highest compressive strengths after both the storage periods.

The diametral tensile strength values measured after 24 hours and 7 days are also demonstrated in **Figure 4.50.** The value of diametral tensile strength measured after 24 hours for the optimised experimental nanosilver amalgam was 128.77±63.59 MPa, which was significantly higher than Silverfil™ (72.71±10.23 MPa), GS80 (39.32±7.79 MPa), and Dispersalloy (41.66±7.78 MPa), respectively ($P<0.05$). Similar results were also obtained for the diametral tensile strength values determined after 7 days, where the optimised experimental nanosilver amalgam showed a significantly higher diametral tensile strength (157.88±49.95 MPa) compared to GS80 (33.18±5.05 MPa) and Dispersalloy (38.64±2.85 MPa) ($P<0.05$). However, no significant difference was observed between the diametral tensile strength values of the optimised experimental nanosilver amalgam and Silverfil™ at this storage period.

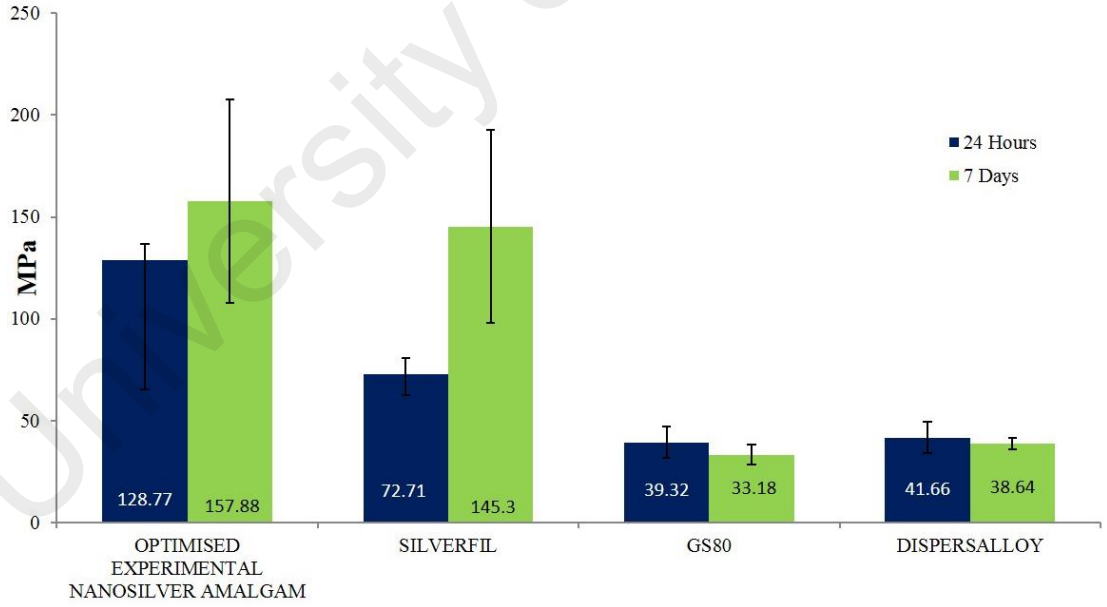


**Figure 4.50: The values of diametral tensile strength for the optimised experimental nanosilver amalgam, Silverfil™, GS80, and Dispersalloy after incubation in distilled water for 24 hours and 7 days at 37±1°C.** The optimised experimental nanosilver amalgam showed the highest values after both the storage periods.

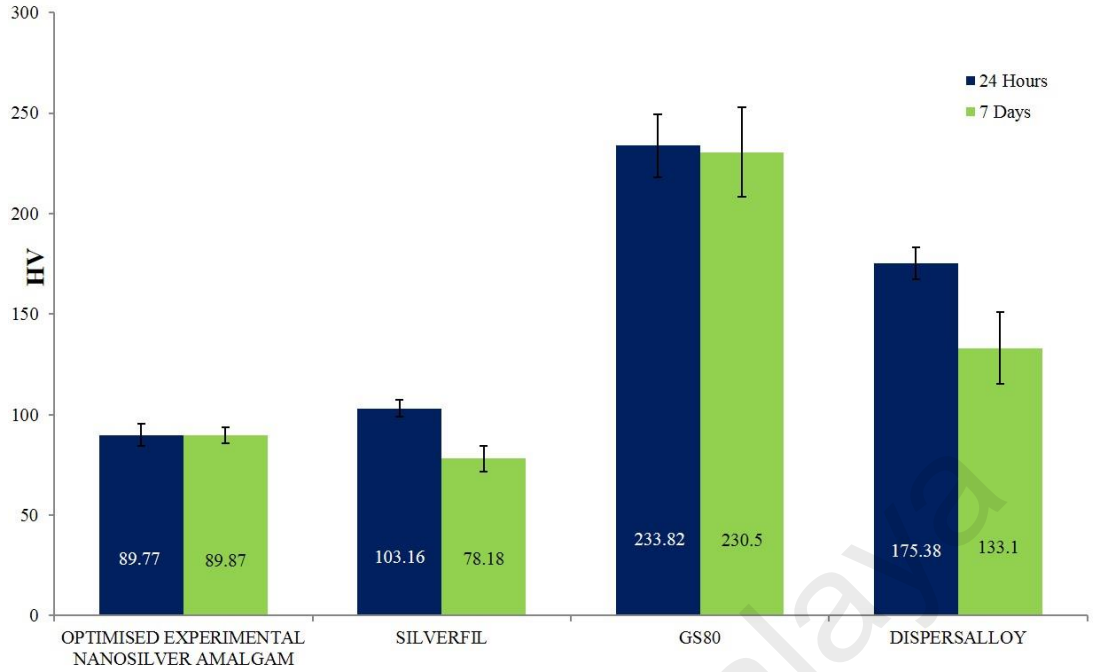


**Figure 4.51: The Vickers microhardness values for the optimised experimental nanosilver amalgam, Silverfil™, GS80, and Dispersalloy tested after 24 hours and 7 days of storage in distilled water at 37±1°C.** GS80 exhibited the highest microhardness values for both the studied periods.

The Vickers microhardness values measured after 24 hours and 7 days of incubation in distilled water at 37±1°C are shown in **Figure 4.51**. The ANOVA and Bonferroni post hoc tests showed that the Vickers microhardness of the optimised experimental nanosilver amalgam measured after 24 hours (89.77±5.55 HV) was significantly lower ($P<0.05$) compared to Silverfil™ (103.16±4.39 HV), GS80 (233.82±15.68 HV), and Dispersalloy (175.38±8.02 HV). Similarly after 7 days, the Vickers microhardness of the optimised experimental nanosilver amalgam (89.87±3.91 HV) was significantly lower compared to those of GS80 (230.50±22.35HV) and Dispersalloy (133.10±17.75 HV). However, no statistically significant difference was observed between the Vickers microhardness values of the optimised experimental nanosilver amalgam and Silverfil™.

In conclusion, the synthesised AgNPs were mainly in spherical form with the mean particle diameter of 34.27±7.38 nm and crystallite size of 54.20 nm. The AgNPs:Hg ratio of 1:2.9 was selected as the optimal ratio for preparation of the optimised experimental

nanosilver amalgam. The optimised experimental nanosilver amalgam showed a similar morphology to the commercially available Silverfil™ and contained no unbound (non-reacted) Hg in its composition. The phase structures of both Silverfil™ and the optimised experimental nanosilver amalgam were similar to the natural moschellandsbergite ($Ag_2Hg_3$) mineral. Compared to Silverfil™, GS80, and Dispersalloy, the optimised experimental nanosilver amalgam showed the highest value of diametral tensile strength after 24 hours and 7 days of incubation in distilled water at 37°C.

# CHAPTER 5: DISCUSSION

## 5.1 Silverfil™ Starting Materials

The starting materials of Silverfil™ including Ag-Sn, Ag-R, Ag-Hg, and Ag-Hg+Ag-R were supplied by the manufacturer. For the Ag-Sn alloy, the elemental mapping analyses confirmed homogeneous distribution of both Ag and Hg in the matrix. The interaction between Ag and Sn generally forms two intermetallic compounds of ε-$Ag_3Sn$ and ζ-$Ag_4Sn$ (Wang et al., 2015). However, the ε-$Ag_3Sn$ phase with an orthorhombic structure, space group of Pmmn (a=5.96800, b=4.78020, and c=5.18430), and the mean crystallite size of 37.66 nm was only observed in the XRD analyses and ζ-$Ag_4Sn$ was not identified. According to Kriegner (2016), both intermetallic compounds cannot be accurately determined within the accuracy level of the XRD analysis. However, the oxidation state of Sn observed in the XPS analyses was Sn (IV), suggesting the existence of ζ-$Ag_4Sn$ in the alloy. Therefore, it was concluded that the Ag-Sn alloy contained both $Ag_3Sn$ and $Ag_4Sn$ phases, while the former was dominant in the alloy composition.

In the Step 2 of the process applied for Silverfil™ manufacturing, Ag-Sn undergoes a replacement reaction with HCl to produce Ag-R. The Ag-R compositions obtained by the EDX and XRD analyses were markedly different from that obtained using the XPS technique, where XPS detected the presence of Sn with atomic percentage of 20.20%. The elements detected other than Ag were considered as extra elements or impurities. The presence of Sn as an impurity was possibly due to the incomplete reaction during the Step 1 of Silverfil™ manufacturing process, where Ag-Sn was derived. Therefore, the manufacturer could probably use higher HCl quantities to overcome the limited reactability of Ag-Sn. Equations (5.1a) and (5.1b) represent the reactions occurred in Step 2 of the manufacturing process. In this reaction, Ag (I) is reduced to $Ag^0$ with binding

energy of 368.2 eV, as detected in the XPS analyses. Hence, the manufacturer's claim on formation of Ag-R as a pure phase containing solely the Ag element was rejected.

$$Ag_4Sn + 4HCl \rightarrow 4Ag + SnCl_4 + 2H_2 \quad \textbf{(5.1a)}$$

$$Ag_3Sn + 4HCl \rightarrow 3Ag + SnCl_3 + 2H_2 \quad \textbf{(5.1b)}$$

In Step 3, the manufacturer produced Ag-Hg by precipitating $AgNO_3$ and $Hg(NO_3)_2$ solutions using a metallic copper rod. During this process, the metallic copper dissolves to form copper nitrate ($Cu(NO_3)_2$), while both the Ag and Hg ions in the solution precipitated to form the Ag-Hg alloy termed as "pre-amalgamated" sample by the manufacturer. According to the XRD investigations carried out by the manufacturer, this alloy resembles paraschachnerite, a mineral in nature with chemical formula of $Ag_3Hg_2$, and no other compound was reported as impurity in the alloy composition. However, in this study, the XRD analyses showed the presence of both $Ag_2Hg_3$ and $Ag_3Hg_2$ phases, where the peaks mostly matched those of $Ag_2Hg_3$ in the standard databases. It is important to note that a higher accuracy of the XPS analysis compared to the EDX technique led to detection of low concentrated elements such as Cu and Cl with atomic percentages of 2.68% and 1.75%, which were not identified in the EDX investigations. These elements had probably entered as contaminations from the metallic copper rod used during the precipitation reaction. Therefore, a proper washing is recommended to the manufacturer for thorough removal of the contaminations and producing pure Ag-Hg alloys. Most importantly, the XPS analysis clearly showed the absence of unbound Hg in this starting material.

In regard to the fourth starting material composed of Ag-Hg+Ag-R, the XPS analyses detected the presence of Sn, Cu, and Cl with atomic concentrations of 6.63%, 2.03%, and 1.33%, respectively, although these elements were not observed in the EDX analysis. These impurities were most likely introduced during the Step 1 to Step 3 of the manufacturing process. In addition, The XRD results showed the presence of $Ag_3Sn$ phase in this starting material.

The XPS analysis detected the presence of all the impurities in Silverfil™ starting materials, which indicated that this analytical technique is more sensitive and accurate compared to EDX. The significant differences between the results obtained by XPS and EDX analyses have been reported to be due to a number of factors such as different capabilities, limitations, depths of analysis, and fundamental physical principles (Gorzalski et al., 2017). The XPS technique generally examines the chemical composition of the surface region and it is capable to detect the trace elements, while EDX and XRD examine the 'bulk' concentration of the elements present in the samples (Murdock et al., 2008). Furthermore, XPS is more sensitive for the elements with high atomic numbers and most elements existing 1-3 nm below the sample surface are detectable with atomic percentages of approximately 0.1% (Embong, 2011; Krishnan et al., 2011). However, the detection limits for EDX are typically 0.1% by weight in a depth of 1-2 μm. In particular, the main advantages of XPS over EDX is its ability to resolve the binding energy differences and thus detect the binding conditions of the elements of interest. However, the samples for XPS analysis must be solid and vacuum compatible. The advantage of EDX analysis is its ability to be coupled with FESEM, enabling selection of the specific regions of interest for quantitative elemental analyses. The manufacturer had analysed the Silverfil™ starting materials using EDX and XRD, thus failed to identify the impurities, which were present in low concentrations.

In accordance to the first objective of this study, the Silverfil™ starting materials were characterised to determine the atomic percentages of their constituting elements and identify the impurities in their compositions. This is imperative as in any dental amalgam, the composition of each metal in the alloy could affect their properties, reaction mechanism, and microstructure in parallel to other parameters such as particle size and shape (Chen et al., 1999; Mitchell et al., 1996).

The percentages of Sn (6.63%) and Cu (2.03%) as impurities in the Silverfil™ starting materials can be considered high, which could result in higher compressive and diametral tensile strengths in Silverfil™ for both testing periods of 24 hours and 7 days compared to the control amalgams. According to Mahler (1997), Cu in the alloy can affect the strength and flow of the set amalgam. In fact, the Cu concentration is one of the main criteria for classification of dental amalgams. When the Cu concentrations is less than 6 wt.%, the alloy is known as "low-Cu", whereas the "high-Cu" alloys contain above 6 wt.% Cu in their composition (Solanki, 2017). Although the percentage of Cu identified in the Silverfil™ starting materials was almost 30% of its maximum limit in the low-Cu alloys, it could still show an effect on the mechanical strength and will be discussed in the following section.

Cu and Sn also play important roles in initiation and propagation of corrosion in the dental amalgams (Upadhyay et al., 2006). Sn in the forms of either SnO or $SnO_2$ is reported as a major corrosion product in the conventional amalgams (Lin et al., 1983). However, the corrosion studies were out of this research scope. In addition, incorporation of Sn in the alloy could generate dimensional changes in the set amalgam. A study showed that the Sn contents more than 30% induce amalgam shrinkage, while reducing the Sn concentration to below 25% results in amalgam expansion (Waterstrat, 1990). Therefore,

the Sn concentration of approximately 25% was recommended in order to minimise the dimensional changes in the amalgam alloys.

In this study, the XPS results confirmed the absence of unbound Hg in the set Silverfil™ amalgam. The presence of Sn as impurity in the Silverfil™ composition might also contribute to inhibit the Hg release from the Ag-Hg phase. According to Mahler et al. (1994), the amount of Sn in the γ1 phase could significantly influence the amalgam potential for emission of Hg vapour. It was also found that the γ1 phase becomes saturated during trituration of the amalgam alloys with Hg; however, increase of the Sn concentration led to reduced Hg contents in the set amalgam over time. Therefore, it was concluded that the Hg content was inversely proportional to the Sn concentration. This statement was supported by Jensen (1989), who showed that the lattice constant of γ1 was reduced with time. In another study, Hanawa et al (1987) identified the presence of Sn oxide through XPS analysis and reported its role in Hg inhibition on the amalgam surface. Therefore, the present study also concluded that the Sn element introduced as impurity in the Silverfil™ composition could cause improved Hg suppression in this amalgam.

## 5.2 Synthesis and Characterisation of AgNPs

Synthesis of AgNPs via the chemical reduction route is of particular interest, which produces nanoparticles with a relatively high stability and colloidal dispersion in water or organic solvents (Sharma et al., 2009). As discussed in Chapter 2, the chemical reduction method provides an excellent control over the reaction and the obtained product thus possesses a desired morphological shape with narrow size distribution. The following equations are the chemical reactions occurred for precipitation of AgNPs (Liu et al., 2008).

$$Ag^{+} + (CH_2NH_2)_2 \rightarrow [Ag\ (CH_2NH_2)_2]^{+} \quad \textbf{(5.2a)}$$

$$4\ [Ag\ (CH_2NH_2)_2]^{+} + 5N_2H_4 \rightarrow 4Ag \downarrow + 4\ N_2H_4^{+} + N_2 + 4(CH_2NH_2)_2 \quad \textbf{(5.2b)}$$

In the current study, $AgNO_3$ was used as the Ag precursor to facilitate formation of AgNPs during the synthesis process. The pH value of the reaction mixture was also adjusted to approximately 10 as acidic condition shows detrimental effect on precipitation of the spherical AgNPs, leading to formation of flaky, dendritic, or non-uniform shapes (Guo et al., 2010). The synthesis was carried out by incorporation of EDA as a potential surface capping agent to provide a high control over size of the precipitated nanoparticles. EDA also acts as a ligand for directing the structure of the molecular coordination during the reaction process. On the other hand, this capping agent controls desorption of $Ag^{+}$ cations from the complex compound and thus regulates formation and growth of the Ag nuclei.

In order to reduce the $Ag^{+}$ ions of the complex compound into the metallic Ag ($Ag^{0}$) as presented in Equation 5.2b, a reducing agent is required to donate a sufficient amount of electrons to the complex compound (Zhou et al., 2015). By utilisation of strong reducing agents such as borohydride, small monodispersed particles could be produced, though generation of larger particles is difficult. Conversely, the weaker reducing agents such as citrates provide slower reduction rates, while the size distribution of the produced particles is far from narrow (Sharma et al., 2009). Therefore in this study, hydrazine hydrate was used as the reducing agent to produce nanoparticles with improved controllability over their size distribution. During the chemical reduction, four electrons are donated by hydrazine hydrate to reduce the $Ag^{+}$ ions into the metallic $Ag^{0}$ form. According to the visual observations in this study, when the colourless hydrazine hydrate was in contact with $AgNO_3$ solution, its colour changed into yellowish brown, which was in agreement with the previous studies (Mendis et al., 2016). As a result, formation of Ag

was primarily identified through visible observation of the solution colour. Upon formation of the AgNPs, the solution turned into colourless, followed by appearance of grey clusters. These clusters elucidated formation of the colloidal Ag particles in the solution. Metallic Ag is inert and becomes ionised when reacts with moisture, thus the ionised Ag is highly reactive (Rai et al., 2009).

In order to minimise agglomeration of AgNPs during their formation and precipitation, CTAB, a quaternary ammonium surfactant was also incorporated as a dispersing agent in the reaction mixture (Liu et al., 2008). Generally, the dispersion agents absorb on the solid-liquid interface and form a layer of molecular membrane to hinder inter-contact between the particles (Songping et al., 2005). Upon addition of CTAB, no any colour change was observed in the solution. In the reaction 5.2a, incorporation of identical molar ratios of the $Ag^+$ cations and EDA resulted in formation of the complex compound of $[Ag(CH_2NH_2)_2]^+$. The EDA precursor could control desorption of $Ag^+$ ions from the complex compound, thus regulating formation and growth of the Ag nuclei.

The crucial influences of particles size, size distribution, and shape on various chemical and physical characteristics of the nanoparticles necessitates proper regulation of these parameters during the synthesis of AgNPs, These morphological features in turn are strongly influenced by the preparation method, experimental conditions, interaction kinetics of the metal ions with the reducing agents, surface capping agents, and the adsorption mechanism of the stabilising agent on the nanoparticles surfaces (Khan et al., 2011; Sharma et al., 2009). In this work, the effects of EDA concentration on the particle size, and size distribution of the obtained AgNPs were investigated (Prathna et al., 2011). It was observed that the EDA concentrations as low as 0.05 ml could endow AgNPs with lowest mean particle sizes and narrowest size distribution, while increased amounts of EDA incorporated in the reaction mixture led to larger particles and wider size distributions.

The effect of $AgNO_3$ concentration on the particle size of AgNPs was also investigated in this study, where the amounts of other compounds (i.e. EDA, CTAB, and $N_2H_4.H_2O$) were remained constant. It was observed that the higher concentrations of $AgNO_3$ produced smaller AgNPs, consistent with previous reports (Korbekandi et al., 2012; Prathna et al., 2011; Sobczak Kupiec et al., 2011). In fact, increased $AgNO_3$ concentrations lead to faster nucleation of the Ag particles, thus forming relatively smaller AgNPs with high specific surface areas (Sobczak Kupiec et al., 2011). In addition, the collision frequency of the precipitated particles is significantly incremented with increase of the $AgNO_3$ concentration. Thus, the particles easily aggregate into large agglomerates at high $AgNO_3$ concentrations (Sobczak Kupiec et al., 2011). A similar observation was observed by Korbekandi et al., (2012) where increased $AgNO_3$ concentrations resulted in deposition of smaller nanoparticle sizes.

## 5.3 Formulation of the Experimental Nanosilver Amalgam Based on the Silverfil™ Concept

The under-triturated amalgams often show increased expansion and flow with reduced mechanical strength, whereas the over-triturated specimens tend to shrink, directly proportional to the over-trituration level. Therefore, an accurate trituration must prevent shrinkage, maximise the mechanical strength, and decrease the amalgam flow.

Among three selected ratios of AgNPs:Hg (1:1, 1:2, and 1:3 ) investigated by the manufacturer, the ratio of 1:3 was found to provide the best triturated amalgam. In order to reaffirm this claim, these three AgNPs:Hg ratios were re-evaluated in this study in terms of their ability to produce a well-triturated amalgam. The specimens prepared with the AgNPs:Hg ratio of 1:1 were under-triturated, dry, and crumbly, which opposed the recommended ratios of 1:1 and 1:0.9 for Dispersalloy and GS80, respectively. A similar

result was obtained for the AgNPs: Hg ratio of 1:2 (a higher ratio compared to 1:1.76 for Silverfil™). This could be due to the high surface area and surface energy of the synthesised AgNPs, which necessitate addition of higher amounts of Hg. According to Berthoud's method, smaller particle sizes increase the surface area to volume ratio of the alloy and therefore increase the dissolution rate of Hg (Okabe et al., 1996). Theoretically, the surface area of AgNPs can be calculated using the following equation (Wani et al., 2011; Wani et al., 2010):

$$S.A = \frac{6000}{D\rho} \quad \textbf{(5.3)}$$

Where, S.A, D, and ρ are the surface area ($m^2.g^{-1}$), particle size (nm), and the theoretical density of Ag, respectively. In this equation, the AgNPs are assumed in spherical shape with smooth surfaces and constant particle sizes (Wani et al., 2011; Wani et al., 2010). Based on Equation (5.3), the AgNPs synthesised in this study provided the surface area of 16.69 $m^2.g^{-1}$, which was 2 folds higher than that produced by Ag-R (9.81 $m^2.g^{-1}$).

When the AgNPs:Hg ratio was increased to 1:3, well-triturated amalgams with a satin-like appearance were produced (Hatrick et al., 2015). Thus, we concurred with the manufacturer that the AgNPs:Hg ratio of 1:3 was the most suitable ratio for manipulation and handling of the experimental nanosilver amalgam. Among all the samples, the AgNPs synthesised using 2M $AgNO_3$ (sample B9) showed the most favourable handling and manipulation, most likely due to its smaller particle size and narrower range of size distribution. Although the AgNPs:Hg ratio required for preparation of the experimental nanosilver amalgam was higher compared to Silverfil™, GS80, and Dispersalloy, the possibility of further lowering the Hg content was studied by evaluation of three ratios of 1:2.8, 1:2.9, and 1:3.0. Based on the physical appearances, the AgNPs:Hg ratio of 1:2.9

was selected as the optimal ratio to produce well-triturated experimental nanosilver amalgams.

It is important to note that Silverfil™ contains pre-amalgamated Ag-Hg beside the Ag-R in its alloy composition, whereas the experimental nanosilver amalgam was produced using solely pure AgNPs. This difference between the formulations of Silverfil™ and the experimental nanosilver amalgam alloys was one of the main limitations of the present study as the formulation and preparation method of the pre-amagamated sample were not disclosed by the manufacturer.

The nanoparticles have recieved a great attention for various applications in dentistry. For instance, nanoparticles has been intergated into the dental tubules to seal their opening and thus reduce the nerves exposure in order to help treating the dental hypersensitivity (Dabbagh et al., 2014; Priyadarsini et al., 2018). Li et al. (2008) also reported that the hydroxyapatite nanoparticles could retard auxiliary erosive demineralisation through their robousted adsorption into the enamel cavities originated from acidic erosion. In particular, AgNPs have been used in several areas of dentistry such as restorative dentistry, imlantology, endodontics, and dental prostheses with the aim to increase the oral health related quality of life (Priyadarsini et al., 2018). The current study also recommended utilisation of AgNPs in formulation of dental amalgams, eventhough these restorative materials are approching their phase down era.

## 5.4 Characterisation of the Optimised Nanosilver Amalgam

The microstructure, phase structure, chemical states, and selected mechanical characteristics of the optimised nanosilver amalgam were compared with those of Silverfil™, GS80, and Dispersalloy. Both GS80 and Dispersalloy selected as control

amalgams in this study were high-copper amalgams, which show better mechanical properties compared to the low-copper counterparts (Solanki, 2017). GS80 was selected as representative of the ternary alloys with spherical and lathe-cut particles. This amalgam consisted of 40 wt.% Ag, 31.3 wt.% Sn, and 28.7 wt.% Cu. On the other hand, Dispersalloy was selected as representative of the quaternary Ag-Sn-Cu-Zn alloys with lathe-cut particles and Ag/Cu eutectic spheres. Dispersalloy contained 69 wt.% Ag, 18 wt.% Sn, 12 wt.% Cu, and 1 wt.% Zn. Comparison of the chemical compositions of these two amalgams indicated higher concentrations of Cu and Sn in GS80 compared to Dispersalloy, which theoretically result in higher mechanical properties such as hardness and compressive strength in GS80. Silverfil$^{TM}$, on the other hand contained only Ag-R and pre-amalgamated Ag-Hg in its composition as claimed by the manufacturer. However, our detailed characterisations revealed that Silverfil$^{TM}$ also contained Cu and Sn with atomic percentages of 2.03% and 6.63%, respectively.

A highly-crystalline optimised experimental nanosilver amalgam was synthesised in this study with a similar XRD pattern to Silverfil$^{TM}$, where all the peaks matched the crystallographic structure of moschellandsbergite ($Ag_2Hg_3$), a natural mineral with a high stability. Moreover, no any secondary phase was observed in the XRD patterns of these amalgams. Although GS80 and Dispersalloy also showed similar peaks to moschellandsbergite, additional Ag-Sn and $Cu_6Sn_5$ phases were however identified in GS80 and Dispersalloy, respectively.

In term of morphology, both Silverfil$^{TM}$ and the optimised experimental nanosilver amalgam possessed alloy clusters with crystal matrix compounds. In contrast to GS80 and Dispersalloy, the surfaces of Silverfil$^{TM}$ and the experimental nanosilver amalgam showed many inhomogeneous zones. The majority of crystals were quite large and mostly formed as aggregations. In accordance with the previous reports (Churnjitapirom et al.,

2015), the GS80 particles were observed in either spherical, oval, or droplet shapes, On the other hand, Dispersalloy contained clusters of spherical particles stacked on each other.

The rate of Hg release from the amalgam is significantly relied on its alloy composition. For instance, the Hg release decreases when the Sn concentration is increased in the γ1 phase. In fact, Sn content of the γ1 phase is a major determinant of Hg vapour release (Ferracane et al., 1995). It is also reported that incorporation of In could result in decreased rates of Hg release after trituration (Okabe et al., 1994). Moreover, formation of the tin oxide and zinc oxide layers on the amalgam surface could also reduce the Hg release (Ferracane et al., 1992). In contrast, development of indium oxide layer on the amalgam surface had no effect on suppressing the Hg release (Uo et al., 2003). However, in spite of the presence of various elements in GS80 and Dispersalloy such as Cu, Sn and Zn (for Dispersalloy only), these amalgams still contain unbound Hg, as confirmed by different characterisation techniques in this study.

The binding energies of the optimised experimental nanosilver amalgam suggested that Ag was in the metallic state, while Hg was mainly in the oxides state. Therefore, it can be concluded that no unbound mercury ($Hg^0$) existed in the optimised experimental nanosilver amalgam upon setting. For Silverfil™, the XPS analysis detected the presence of Sn, which probably introduced as contamination during the fabrication procedure. The binding energy of Silverfil™ showed that both Hg and Sn were in oxide states, whereas Ag was mainly present in the metallic state. Therefore, the absence of unbound Hg in the Silverfil™ formulation was confirmed in this study. The presence of impurities such as Sn in the Silverfil™ formulation may also play a role in suppression of the Hg vapour release. In contrast, the binding energies of Hg in both GS80 and Dispersalloy were less than 100 eV, representing the presence of unbound Hg in the metallic state **(Appendix**

**C)**. All the binding energies of elements in the amalgams were comparable with the published binding energy data (Wanger et al., 1992).

In terms of the mechanical characteristics, the experimental results showed that the diametral tensile strength, compressive strength, and Vickers microhardness values measured 24 hours and 7 days were significantly different among the tested amalgam groups. The compressive strength is an important factor which must be considered for selection of a filling material as a high compressive strength is necessary to resist the masticatory and parafunctional forces (Cho et al., 1999). In general, the compressive strengths of about 380 MPa and 414 MPa are obtained for the low-copper and high-copper amalgams, respectively (Thomas, 2013). The compressive strength of the optimised experimental nanosilver amalgam after storage in distilled water at 37°C for 24 hours (380.62±37.10 MPa) was significantly higher than Dispersalloy (190.68±44.18MPa). However, the ANOVA and Bonferroni post hoc tests showed no significant difference when the optimised experimental nanosilver amalgam was compared with Silverfil$^{TM}$ and GS80. The compressive strength values measured for Silverfil$^{TM}$ and GS80 were in agreement with those reported in previous works. However, the compressive strength of Dispersalloy measured in this study (190.68±44.18 MPa for 24 hours and 234.72±39.11 MPa for 7 days) was far different from the previously published values (Osborne et al., 1995). Osborne & Summitt (1995) evaluated the mechanical properties and clinical performance of the Gallium restorative materials and found that the compressive strength of Dispersalloy was 414±27.5 MPa after 24 hours and 459.9±22.3 MPa after 7 days of testing. In another study, a compressive strength of 361 MPa was reported for Dispersalloy after 24 hours (Lin et al., 2011). A possible reason for obtaining lower values of compressive strength for Dispersalloy in this study is the slower rates of amalgamation reactions in the lathe-cut amalgams compared to the spherical powder and admixed amalgams (Mante et al., 1998). Therefore, some specimens may not become well-packed

and the generated voids in the amalgam structure lead to lower values of compressive strength. In addition, an excessive expansion due to the prolonged incubation in water may also contribute to the decreased mechanical strength of Dispersalloy. The compressive strength of GS80 was higher compared to Dispersalloy after 24 hours of incubation in distilled water, probably due to their elemental differences such as higher Cu and Sn concentrations in GS80, which theoretically result in higher compressive strength of this amalgam (Solanki, 2017). As for Silverfil™, the presence of Cu as impurity might the reason of its higher compressive strength values for both incubation periods compared to the optimised experimental nanosilver amalgam.

After 7 days of storage, the compressive strength of the optimised experimental nanosilver amalgam (234.99±174.45 MPa) was significantly lower compared to Silverfil™ (349.83±14.14 MPa), and significantly higher than GS80 (80.93±35.06 MPa). This is probably due to the increased aggregation of nanoparticles derived from their high surface energy, which results in larger particles with poor dispersion in the amalgam matrix. The aggregated nanoparticles also create weak zones in the form of voids, leading to degraded mechanical properties of the optimised experimental nanosilver amalgam. However, ANOVA and Bonferroni post tests showed no significant difference when the optimised experimental nanosilver amalgam was compared to Silverfil™ and GS80. These results were in agreement with the previous studies, which reported that the addition of nanoparticles showed no significant effect on compressive strength of the resulting amalgams (Stencel et al., 2018; Yoshida et al., 1999).

Diametral tensile testing is the most popular method for evaluating tensile strength of the brittle materials, which evades some inherent difficulties encountered in the direct and flexural tensile testings. The values of diametral tensile strength for different types of commercially available dental amalgam are generally in the range of 43 MPa to 58 MPa

(Sakaguchi et al., 2018). In this study, the mean diametral tensile strength measured after 24 hours for the optimised experimental nanosilver amalgam was significantly higher (128.77±63.59 MPa) compared to the other tested amalgams. After 7 days of storage in distilled water at 37°C, the optimised experimental nanosilver amalgam again showed a significantly higher diametral tensile strength (157.88±49.95 MPa) compared to GS80 (33.18±5.05 MPa) and Dispersalloy (38.64±2.85 MPa) ($P<0.05$). However, no significant difference was observed between the optimised experimental nanosilver amalgam and Silverfil™ when diametral tensile strength was measured after 7 days. This result may indicate that the mechanical properties of the optimised experimental nanosilver amalgam were comparable to those of Silverfil™. The values of diametral tensile strength obtained for the control amalgams at varied incubation periods are comparable to those reported in a number of previous studies. According to Osborne & Summitt (1995), the diametral tensile strength of Dispersalloy after 24 hours and 7 days were respectively 48.3±7.6 MPa and 50.4±7.8. On the other hand, Bhattacharya et al. (2017) reported that the diametral tensile strength values of GS80 were 23.7±0.368 MPa and 33.9±3.03 MPa after 24 hours and 7 days. In conclusion, the mean diametral tensile strength values of all the amalgams tested in this study were above the satisfactory value of 30 MPa.

It is noteworthy that the diametral tensile strength of the optimised experimental nanosilver amalgam became 75%-78% greater than that of control amalgams after 7 days. This could be related to a post-hardening process, which may occur after the setting time in the single phase matrices (Radakrishnan, 2008). This statement was also applicable for Silverfil™, where the diametral tensile strength of this amalgam was increased by 50% after 7 days compared to the incubation period of 24 hours.

Measurement of the Vickers microhardness values of the four studied dental amalgams and their comparative analysis by ANOVA and Bonferroni post hoc tests

indicated a lower hardness of the optimised experimental nanosilver amalgam after 24 hours compared to Silverfil™, GS80, and Dispersalloy. The obtained microhardness values were probably proportional to the Cu contents of the amalgams, where GS80 (containing 28.7% Cu) showed the highest microhardness value, followed by Dispersalloy (12% Cu), Silverfil™ (Cu as impurity), and the optimised experimental nanosilver amalgam (0% Cu). Similarly after 7 days of storage, GS80 presented the highest Vickers microhardness, followed by Dispersalloy. However, the optimised experimental nanosilver amalgam became slightly harder than Silverfil™ after 7 days, most likely due to its better post-hardening, as described previously.

Previous studies showed that incorporation of nano-sized materials led to higher microhardness values compared to their conventional formulations (Beun et al., 2007). However, the present study showed no considerable enhancement in the microhardness value after introduction of AgNPs into the amalgam composition, probably due to an inhomogeneous distribution of nanoparticles and formation of agglomerates on the amalgam surface.

# CHAPTER 6: CONCLUSION

Dental amalgam has been widely used for direct restorations, endodontic retrograde root fillings, and core fabrication due to its cost effectiveness, durability, resistance to chewing force, and easy handling during operations. Furthermore, dentists often favour amalgam for restoration of the more challenging cases. However, WHO in cooperation with United Nations Environment Programme (UNEP) has recognised the necessity of a global phase-down of Hg in accordance to the Minamata Treaty in 2013, which was also signed by Malaysia in 2014. While WHO has recommended to replace amalgam with other restorative materials, these alternatives are often excessively expensive in the middle- and low-income countries and thus, amalgam is still the preferred dental restorative material in large parts of the world. In fact, it has been recognised that the developing countries are currently making efforts to phase down the usage of dental amalgam, rather than to phase out this restorative material.

In the early 2000's, Silverfil™ was introduced commercially in Malaysia as an amalgam free of unbound mercury. However, a large size variation in the particle sizes of the starting materials was the main challenge in fabrication of Silverfil™, resulting in low control over its physico-mechaical properties. To address this problem, this study introduced nano-sized Ag particles in the manufacturing process of Silverfil™. It was found that the AgNPs could significantly affect the physico-mechanical properties of the resulted dental amalgam. With incooperation of AgNPs into the amalgam formulation, Hg was completely absorbed during trituration due to the higher surface area and surface energy endowed by the nanoparticles, resulting in complete removal of the unbound Hg upon amalgam setting.

## 6.1 Limitations of the Study

1. In Step 1 of the amalgam preparation, Hg was weighed under a fume cupboard to prevent exposure to its vapours. However this approach could not provide sufficient safety as Hg easily evaporates at room temperature, even under the fume cupboard.

2. In opposite to Silverfil™, the AgNPs were not triturated with pre-amalgamated Ag-Hg due to manufacturer's reluctance to reveal the Silverfil™ composition.

3. The focus of the current study was only on characterisation of the elemental composition, microstrutural properties, phase structures, oxidation states of the elements, and selected mechanical tests such as compressive strength, diametral tensile strength, and Vickers microhardness.

## 6.2 Conclusions

1. The first aim of this study was to characterise the starting materials of Silverfil™ including Ag-Sn, Ag-R, Ag-Hg, and Ag-Hg+Ag-R, which were all supplied by the Silverfil™ manufacturer.

2. Although the manufacturer claimed that all the Silverfil™ starting materials were pure, a number of impurities such as Sn and Cu were identified in this study, which might significantly affect the amalgam strength and its unbound Hg content.

3. The Ag-R component was similar to 'normal' Ag in terms of the phase identification and oxidation states. Therefore, the 'reactive silver' is only a term used by the manufacturer. In fact, the metallic Ag becomes highly reactive when converted to the ionised state.

4. The manufacturer was mainly concerned about the inconsistency in size of the Ag-R particles. This problem could be addressed through introduction of Ag nanoparticles with a narrow distribution of particle size into the amalgam formulation. Therefore, the second part of this study focused on synthesis of pure crystalline polygon-shaped AgNPs.

5. The third aim of this study was to formulate the experimental nanosilver amalgam based on the Silverfil™ concept. The AgNPs synthesised using a 2M $AgNO_3$ solution were determined as the optimal type of AgNPs for formulation of the experimental nanosilver amalgam. The AgNPs:Hg ratio of 1:2.9 provided the minimal Hg content, which could result in well-triturated amalgams. The chemical investigations also showed no unbound mercury present in both the optimised experimental nanosilver amalgam and Silverfil™.

6. The last aim of this study was to characterise and compare the physical and mechanical properties of the optimised experimental nanosilver amalgam with those of Silverfil™, GS80, and Dispersalloy. The morphological investigations

depicted formation of clusters in the optimised experimental nanosilver amalgam with lower agglomeration compared to Silverfil™, GS80, and Dispersalloy.

7. The chemical investigations confirmed the presence of Ag-bounded Hg and absence of unbound mercury ($Hg^0$) in the optimised experimental nanosilver amalgam and Silverfil™. However, $Hg^0$ was detected in both GS80 and Dispersalloy using the XPS analysis.

8. The optimised experimental nanosilver amalgam provided a higher diametral tensile strength compared to Silverfil™, GS80, and Dispersalloy, 24 hours and 7 days after amalgamation. In contrast, the optimised experimental nanosilver amalgam exhibited the lowest Vickers microhardness after amalgamation.

9. In overall, the obtained results rejected the null hypothesis of this study in favour of the alternative hypothesis that AgNPs significantly affect the physico-mechanical properties of dental amalgams.

### 6.3 Recommendations to the Manufacturer

1. As Sn and Cu were detected as impurities in the Silverfil™ starting materials, the manufacturer is recommended to reassess the fabrication process and utilise a proper washing method to remove the impurities.

2. The manufacturer only used XRD and EDX for chemical characterisations of the starting materials, which often fail to identify the trace elements in the alloy composition. Therefore, the manufacturer is recommanded to also use more sensitive analytical approaches such as XPS for chemical investigations of the starting materials in order to ensure absence of any impurity in their formulations.

3. The Step 1 in preparation of Silverfil$^{TM}$, which involves the production of 'reactive silver', can be eliminated as the obtained product shows similar chemical and structural properties with those of 'normal' Ag.

4. The manufacturer is recommended to apply a mixture of AgNPs and the pre-amalgamated alloy and further evaluate the properties of the obtained amalgam.

**5.** The optimised experimental nanosilver amalgam contains a relatively higher Hg compared to Silverfil$^{TM}$, which could be reduced when AgNPs is alloyed with other metallic elements.

### 6.4 Recommendations for Further Research

1. Further studies are required to investigate the toxicity level of AgNPs included in formulations of Silverfil$^{TM}$ and the optimised experimental nanosilver amalgam

2. It is recommended to investigate the effect of Cu nanoparticles on surface hardness of the experimental nanosilver amalgam.

## REFERENCES


Abraham, J. E., Svare, C. W., & Frank, C. W. (1984). The effect of dental amalgam restorations on blood mercury levels. *Journal of Dental Research, 63*(1), 71-73.

Abramovitz, I., Beyth, N., Weinberg, G., Borenstein, A., Polak, D., Kesler-Shvero, D., & Houri-Haddad, Y. (2012). In vitro biocompatibility of endodontic sealers incorporating antibacterial nanoparticles. *Journal of Nanomaterials, 2012*, 1-12.

Abu Kassim, N. H., Yahya, N. A., Radzi, Z., Basirun, W. J., & Ghani, A. A. (2007). *Silverfil: Its physical characterization*. Paper presented at the 3rd International Conference on Biomedical Engineering 2006, Kuala Lumpur, Malaysia.

Acciari, H., Codaro, E., & Guastaldi, A. C. (1998). A comparative study of the corrosion of high copper dental amalgams. *Materials Letters, 36*(1-4), 148-151.

Acciari, H., Guastaldi, A., & Brett, C. (2005). Corrosion of the component phases presents in high copper dental amalgams. Application of electrochemical impedance spectroscopy and electrochemical noise analysis. *Corrosion Science, 47*(3), 635-647.

Agnihotri, S., Mukherji, S., & Mukherji, S. (2014). Size-controlled silver nanoparticles synthesized over the range 5–100 nm using the same protocol and their antibacterial efficacy. *Royal Society of Chemistry Advance, 4*(8), 3974-3983.

Ahmed, S., Ahmad, M., Swami, B. L., & Ikram, S. (2016). A review on plants extract mediated synthesis of silver nanoparticles for antimicrobial applications: A green expertise. *Journal of Advanced Research, 7*(1), 17-28.

Ajitha, B., Divya, A., Harish, G. S., & Sreedhara Reddy, P. (2013). The influence of silver precursor concentration on size of silver nanoparticles grown by soft chemical route. *Research Journal of Physical Science, 1*(7), 11-14.

Al-Saleh, I. (2011). Mercury (Hg) burden in children: The impact of dental amalgam. *Science of the Total Environment, 409*(16), 3003-3015.

Al-Thabaiti, S. A., Al-Nowaiser, F. M., Obaid, A. Y., Al-Youbi, A. O., & Khan, Z. (2008). Formation and characterization of surfactant stabilized silver nanoparticles: a kinetic study. *Colloids and Surfaces B: Biointerfaces, 67*(2), 230-237.

Alqadi, M., Noqtah, O. A., Alzoubi, F., Alzouby, J., & Aljarrah, K. (2014). pH effect on the aggregation of silver nanoparticles synthesized by chemical reduction. *Materials Science-Poland, 32*(1), 107-111.

Amany, A., El-Rab, S. F. G., & Gad, F. (2012). Effect of reducing and protecting agents on size of silver nanoparticles and their anti-bacterial activity. *Der Pharma Chemica, 4*(1), 53-65.

Angelescu, D. G., Vasilescu, M., Anastasescu, M., Baratoiu, R., Donescu, D., & Teodorescu, V. S. (2012). Synthesis and association of Ag (0) nanoparticles in

aqueous Pluronic F127 triblock copolymer solutions. *Colloids Surfaces A: Physicochemical Engineering Aspects, 394*, 57-66.

Anusavice, K. J., Shen, C., & Rawls, H. R. (2013). *Phillips' science of dental materials* (12th ed.). Missouri: Elsevier Saunders.

Barregard, L., Trachtenberg, F., & McKinlay, S. (2007). Renal effects of dental amalgam in children: the New England children's amalgam trial. *Environmental Health Perspectives, 116*(3), 394-399.

Bates, M. N. (2006). Mercury amalgam dental fillings: an epidemiologic assessment. *International Journal of Hygiene Environmental Health Perspectives, 209*(4), 309-316.

Berdouses, E., Vaidyanathan, T. K., Dastane, A., Weisel, C., Houpt, M., & Shey, Z. (1995). Mercury release from dental amalgams: an in vitro study under controlled chewing and brushing in an artificial mouth. *Journal of Dental Research, 74*(5), 1185-1193.

Berglund, A., Pohl, L., Olsson, S., & Bergman, M. (1988). Determination of the rate of release of intra-oral mercury vapor from amalgam. *Journal of Dental Research, 67*(9), 1235-1242.

Bernardo, M., Luis, H., Martin, M. D., Leroux, B. G., Rue, T., Leitão, J., & DeRouen, T. A. (2007). Survival and reasons for failure of amalgam versus composite posterior restorations placed in a randomized clinical trial. *The Journal of the American Dental Association, 138*(6), 775-783.

Bernhoft, R. A. (2012). Mercury toxicity and treatment: A review of the literature. *Journal of Environmental and Public Health, 2012*, 460508.

Berry, T. G., Nicholson, J., & Troendle, K. (1994). Almost two centuries with amalgam: Where are we today? *The Journal of the American Dental Association, 125*(4), 392-399.

Beun, S., Glorieux, T., Devaux, J., Vreven, J., & Leloup, G. (2007). Characterization of nanofilled compared to universal and microfilled composites. *Dental Materials, 23*(1), 51-59.

Bharti, R., Wadhwani, K. K., Tikku, A. P., & Chandra, A. (2010). Dental amalgam: An update. *Journal of Conservative Dentistry, 13*(4), 204-208.

Bhattacharya, A., Vaidya, S., Tomer, A. K., & Raina, A. (2017). GIC at it's best–A review on ceramic reinforced GIC. *International Journal of Applied Dental Sciences, 3*(4), 405-408.

Biswas, A., Bayer, I. S., Biris, A. S., Wang, T., Dervishi, E., & Faupel, F. (2012). Advances in top–down and bottom–up surface nanofabrication: Techniques, applications & future prospects. *Advances in Colloid and Interface Science, 170*(1-2), 2-27.

Björkman, L., Sandborgh-Englund, G., & Ekstrand, J. (1997). Mercury in saliva and feces after removal of amalgam fillings. *Toxicology and Applied Pharmacology, 144*(1), 156-162.

Bogle, K. A., Dhole, S. D., & Bhoraskar, V. N. (2006). Silver nanoparticles: Synthesis and size control by electron irradiation. *Nanotechnology, 17*(13), 3204.

Bracho-Troconis, C., Colon, P., Bartout, J. D., & Bienvenu, Y. (2000). Influence of thermal treatments on Ag Sn Cu powders in order to reduce mercury contents in dental amalgam. *Journal of Materials Science: Materials in Medicine, 11*(1), 1-9.

Brunthaler, A., König, F., Lucas, T., Sperr, W., & Schedle, A. (2003). Longevity of direct resin composite restorations in posterior teeth: A review. *Clinical Oral Investigations, 7*(2), 63-70.

Cenci, M. S., Piva, E., Potrich, F., Formolo, E., Demarco, F. F., & Powers, J. M. (2004). Microleakage in bonded amalgam restorations using different adhesive materials. *Brazilian Dental Journal, 15*(1), 13-18.

Chandki, R., Kala, M., Kumar, K. N., Brigit, B., Banthia, P., & Banthia, R. (2012). 'Nanodentistry': Exploring the beauty of miniature. *Journal of Clinical and Experimental Dentistry, 4*(2), 119-124.

Chaudhuri, R. G., & Paria, S. (2010). Synthesis of sulfur nanoparticles in aqueous surfactant solutions. *Journal of Colloid and Interface Science, 343*(2), 439-446.

Chen, D., Qiao, X., Qiu, X., & Chen, J. (2009). Synthesis and electrical properties of uniform silver nanoparticles for electronic applications. *Journal of Materials Science, 44*(4), 1076-1081.

Chen, K., Ju, C., & Chern Lin, J. (1999). Effect of particle configuration on structure and properties of dispersed Pd-containing dental amalgam. *Biomaterials, 20*(19), 1851-1866.

Cheng, L., Weir, M. D., Xu, H. H., Antonucci, J. M., Kraigsley, A. M., Lin, N. J., Lin-Gibson, S., & Zhou, X. (2012a). Antibacterial amorphous calcium phosphate nanocomposites with a quaternary ammonium dimethacrylate and silver nanoparticles. *Dental Materials, 28*(5), 561-572.

Cheng, L., Weir, M. D., Xu, H. H., Antonucci, J. M., Lin, N. J., Lin-Gibson, S., Xu, S. M., & Zhou, X. (2012b). Effect of amorphous calcium phosphate and silver nanocomposites on dental plaque microcosm biofilms. *Journal of Biomedical Materials Research Part B: Applied Biomaterials, 100*(5), 1378-1386.

Chitra, K., & Annadurai, G. (2014). Antibacterial activity of pH-dependent biosynthesized silver nanoparticles against clinical pathogen. *BioMed Research International, 2014*, 725165.

Cho, G. C., Kaneko, L. M., Donovan, T. E., & White, S. N. (1999). Diametral and compressive strength of dental core materials. *The Journal of Prosthetic Dentistry, 82*(3), 272-276.

Churnjitapirom, P., Teanchai, C., & Sacharoen, A. (2015). Surface hardness of Thai spherical amalgam product. *Mahidol Dental Journal, 35*, 31-36.

Çınar, Ç., Ulusu, T., Özçelik, B., Karamüftüoğlu, N., & Yücel, H. (2009). Antibacterial effect of silver-zeolite containing root-canal filling material. *Journal of Biomedical Materials Research Part B: Applied Biomaterials, 90*(2), 592-595.

Colon, P., Pradelle-Plasse, N., & Galland, J. (2003). Evaluation of the long-term corrosion behavior of dental amalgams: influence of palladium addition and particle morphology. *Dental Materials, 19*(3), 232-239.

Corrêa, J. M., Mori, M., Sanches, H. L., Cruz, A. D. d., Poiate, E., & Poiate, I. A. V. P. (2015). Silver nanoparticles in dental biomaterials. *International Journal of Biomaterials, 2015*, 485275.

Correa, M. B., Peres, M. A., Peres, K. G., Horta, B. L., Barros, A. D., & Demarco, F. F. (2012). Amalgam or composite resin? Factors influencing the choice of restorative material. *Journal of Dentistry, 40*(9), 703-710.

Dabbagh, A., Abu Kasim, N. H., Bakri, M. M., Wakily, H., Ramasindarum, C., & Abdullah, B. J. J. (2014). Polyethylene-glycol coated maghemite nanoparticles for treatment of dental hypersensitivity. *Materials Letters, 121*, 89-92.

Darroudi, M., Ahmad, M., Zamiri, R., Zak, A. K., Abdullah, A. H., & Ibrahim, N. A. (2011). Time-dependent effect in green synthesis of silver nanoparticles. *International Journal of Nanomedicine, 6*, 677.

De Amorim, R. G., Leal, S. C., Mulder, J., Creugers, N. H. J., & Frencken, J. E. (2014). Amalgam and ART restorations in children: A controlled clinical trial. *Clinical Oral Investigations, 18*(1), 117-124.

De Souza, G. M. (2015). Nanoparticles in restorative materials. In A. Kishen (Ed.), *Nanotechnology in endodontics* (pp. 139-171). Canada: Springer.

Dong, X., Ji, X., Wu, H., Zhao, L., Li, J., & Yang, W. (2009). Shape control of silver nanoparticles by stepwise citrate reduction. *The Journal of Physical Chemistry C, 113*(16), 6573-6576.

Durner, J., Stojanovic, M., Urcan, E., Hickel, R., & Reichl, F. X. (2011). Influence of silver nano-particles on monomer elution from light-cured composites. *Dental Materials, 27*(7), 631-636.

Dutton, D. J., Fyie, K., Faris, P., Brunel, L., & Emery, J. C. H. (2013). The association between amalgam dental surfaces and urinary mercury levels in a sample of Albertans, a prevalence study. *Journal of Occupational Medicine and Toxicology, 8*, 22.

Dye, B. A., Schober, S. E., Dillon, C. F., Jones, R. L., Fryar, C., McDowell, M., & Sinks, T. H. (2005). Urinary mercury concentrations associated with dental restorations in adult women aged 16–49 years: United States, 1999–2000. *Occupational and Environmental Medicine, 62*(6), 368-375.

El-Nour, K. M. A., Eftaiha, A. a., Al-Warthan, A., & Ammar, R. A. A. (2010). Synthesis and applications of silver nanoparticles. *Arabian Journal of Chemistry, 3*(3), 135-140.

Embong, Z. (2011). XPS, AES and Laser Raman Spectroscopy: A fingerprint for a materials surface characterisation. *Jurnal Sains Nuklear Malaysia, 23*(2), 26-45.

Engqvist, A., Colmsjö, A., & Skare, I. (1998). Speciation of mercury excreted in feces from individuals with amalgam fillings. *Archives of Environmental Health: An International Journal, 53*(3), 205-213.

Ernst, C. P., Brandenbusch, M., Meyer, G., Canbek, K., Gottschalk, F., & Willershausen, B. (2006). Two-year clinical performance of a nanofiller vs a fine-particle hybrid resin composite. *Clinical Oral Investigations, 10*(2), 119-125.

Fakour, H., Esmaili Sari, A., & Zayeri, F. (2010). Scalp hair and saliva as biomarkers in determination of mercury levels in Iranian women: Amalgam as a determinant of exposure. *Journal of Hazardous Materials, 177*(1-3), 109-113.

Ferracane, J. L., Adey, J. D., Nakajima, H., & Okabe, T. (1995). Mercury vaporization from amalgams with varied alloy compositions. *Journal of Dental Research, 74*(7), 1414-1417.

Ferracane, J. L., Hanawa, T., & Okabe, T. (1992). Effectiveness of oxide films in reducing mercury release from amalgams. *Journal of Dental Research, 71*(5), 1151-1155.

Flores, C. Y., Diaz, C., Rubert, A., Benítez, G. A., Moreno, M. S., de Mele, M. A. F. L., Salvarezza, R. C., Schilardi, P. L., & Vericat, C. (2010). Spontaneous adsorption of silver nanoparticles on Ti/TiO2 surfaces. Antibacterial effect on *Pseudomonas aeruginosa*. *Journal of Colloid and Interface Science, 350*(2), 402-408.

Franci, G., Falanga, A., Galdiero, S., Palomba, L., Rai, M., Morelli, G., & Galdiero, M. (2015). Silver nanoparticles as potential antibacterial agents. *Molecules, 20*(5), 8856-8874.

Ganss, C., Gottwald, B., Traenckner, I., Kupfer, J., Eis, D., Mönch, J., Gieler, U., & Klimek, J. (2000). Relation between mercury concentrations in saliva, blood, and urine in subjects with amalgam restorations. *Clinical Oral Investigations, 4*(4), 206-211.

Gen, M. (2017). Hardness testing Part 1. from http://www.twi-global.com/technical-knowledge/job-knowledge/hardness-testing-part-1-074/

Gerhardsson, L., & Lundh, T. (2010). Metal concentrations in blood and hair in pregnant females in southern Sweden. *Journal of Environmental Health, 72*(6), 37-42.

Gomathi, M., Rajkumar, P. V., Prakasam, A., & Ravichandran, K. (2017). Green synthesis of silver nanoparticles using *Datura stramonium* leaf extract and assessment of their antibacterial activity. *Resource-Efficient Technologies, 3*(3), 280-284.

Gorzalski, A. S., Donley, C., & Coronell, O. (2017). Elemental composition of membrane foulant layers using EDS, XPS, and RBS. *Journal of Membrane Science, 522*, 31-44.

Gottlieb, E. W., Retief, D. H., & Bradley, E. L. (1985). Microleakage of conventional and high-copper amalgam restorations. *Journal of Prosthetic Dentistry, 53*(3), 355-361.

Guo, G., Gan, W., Luo, J., Xiang, F., Zhang, J., Zhou, H., & Liu, H. (2010). Preparation and dispersive mechanism of highly dispersive ultrafine silver powder. *Applied Surface Science, 256*(22), 6683-6687.

Hanawa, T., Takahashi, H., Ota, M., Pinizzotto, R. F., Ferracane, J. L., & Okabe, T. (1987). Surface characterization of amalgams using X-ray photoelectron spectroscopy. *Journal of Dental Research, 66*(9), 1470-1478.

Hansen, G., Victor, R., Engeldinger, E., & Schweitzer, C. (2004). Evaluation of the mercury exposure of dental amalgam patients by the Mercury Triple Test. *Occupational and Environmental Medicine, 61*(6), 535-540.

Hasheminethad, S. A., Zebarjad, S. M., & Sajjadi, S. A. (2012). Effect of copper content on compressive strength and microstructure of dental amalgams. *Engineering, 4*(3), 155-159.

Hassan, A., Omar, S. A., & Ariffin, Z. (2010). An in vitro genotoxicity study of silver amalgam on Ames test. *The Indonesian Journal of Dental Research, 1*(1), 55-60.

Hatrick, C. D., & Eakle, W. S. (2015). *Dental Materials-E-Book: Clinical applications for dental assistants and dental hygienists* (3rd ed.). USA: Elsevier Health Sciences.

Huang, H., & Yang, Y. (2008). Preparation of silver nanoparticles in inorganic clay suspensions. *Composites Science and Technology, 68*(14), 2948-2953.

Huey, C. M. (2010). Update on dental nanocomposites. *Journal of Dental Research, 89*(6), 549-560.

International Organization for Standardization. (2015). Dentistry -Dental amalgam-ISO 24234:2015(en) (pp. 19).

Iqbal, P., Preece, J. A., & Mendes, P. M. (2012). Nanotechnology: The "Top-Down" and "Bottom-Up" approaches. In P. A. Gale (Ed.), Supramolecular Chemistry: From Molecules to Nanomaterials. USA: John Wiley & Sons, Ltd.

Iravani, S., Korbekandi, H., Mirmohammadi, S. V., & Zolfaghari, B. (2014). Synthesis of silver nanoparticles: chemical, physical and biological methods. *Research in Pharmaceutical Sciences, 9*(6), 385-346.

Jaafar, N. A., Ariffin, Z., & Alam, M. K. (2013). In vitro study of antibacterial properties of dental restorative materials towards Staphylococcus aureus and Enterococcus faecalis. *International Medical Journal, 20*(4), 490-492.

Janardhanan, R., Karuppaiah, M., Hebalkar, N., & Rao, T. N. (2009). Synthesis and surface chemistry of nano silver particles. *Polyhedron, 28*(12), 2522-2530.

Jensen, S. J. (1989). Decrease of γ1 lattice constant with time in dental silver amalgam. *European Journal of Oral Sciences, 97*(5), 465-469.

Jiang, G. H., Wang, L., Chen, T., Yu, H. J., & Wang, J. j. (2005). Preparation and characterization of dendritic silver nanoparticles. *Journal of Materials Science, 40*(7), 1681-1683.

Jiang, X. C., Chen, W. M., Chen, C. Y., Xiong, S. X., & Yu, A. B. (2011). Role of temperature in the growth of silver nanoparticles through a synergetic reduction approach. *Nanoscale Research Letter, 6*(1), 1-9.

Kasacka, I., & Łapińska, J. (2010). Salivary cells in patients with dental amalgam and composite resin material restorations—A morphological investigation. *Polish Journal of Environmental Studies, 19*(6), 1223-1227.

Kaur, P., & Luthra, R. (2016). Silver nanoparticles in dentistry: An emerging trend. *SRM Journal of Research in Dental Sciences, 7*(3), 162-165.

Khan, Z., Al-Thabaiti, S. A., Obaid, A. Y., & Al-Youbi, A. O. (2011). Preparation and characterization of silver nanoparticles by chemical reduction method. *Colloids and Surfaces B: Biointerfaces, 82*(2), 513-517.

Khurshid, Z., Zafar, M., Qasim, S., Shahab, S., Naseem, M., & AbuReqaiba, A. (2015). Advances in nanotechnology for restorative dentistry. *Materials, 8*(2), 717-731.

Killian, C. M., & Croll, T. P. (2010). Nano-ionomer tooth repair in pediatric dentistry. *Pediatric dentistry, 32*(7), 530-535.

Kim, H. S., Ryu, J. H., Jose, B., Lee, B. G., Ahn, B. S., & Kang, Y. S. (2001). Formation of silver nanoparticles induced by poly (2, 6-dimethyl-1, 4-phenylene oxide). *Langmuir, 17*(19), 5817-5820.

Korbekandi, H., Iravani, S., & Abbasi, S. (2012). Optimization of biological synthesis of silver nanoparticles using *Lactobacillus casei* subsp. *casei*. *Journal of Chemical Technology and Biotechnology, 87*(7), 932-937.

Kotakadi, V. S., Rao, Y. S., Gaddam, S. A., Prasad, T. N. V. K. V., Reddy, A. V., & Gopal, D. V. R. S. (2013). Simple and rapid biosynthesis of stable silver nanoparticles using dried leaves of *Catharanthus roseus*. Linn. G. Donn and its anti microbial activity. *Colloids and Surfaces B: Biointerfaces, 105*, 194-198.

Kriegner, D., Sytnyk, M., Groiss, H., Yarema, M., Grafeneder, W., Walter, P., Dippel, A. C., Meffert, M., Gerthsen, D., & Stangl, J. (2016). Galvanic exchange in colloidal metal/metal-oxide core/shell nanocrystals. *The Journal of Physical Chemistry C, 120*(35), 19848-19855.

Krishnan, R. V., Mittal, V. K., Babu, R., Senapati, A., Bera, S., & Nagarajan, K. (2011). Heat capacity measurements and XPS studies on uranium–lanthanum mixed oxides. *Journal of Alloys and Compounds, 509*(7), 3229-3237.

Lee, S. W., Chang, S. H., Lai, Y. S., Lin, C. C., Tsai, C. M., Lee, Y. C., Chen, J. C., & Huang, C. L. (2014). Effect of temperature on the growth of silver nanoparticles using plasmon-mediated method under the irradiation of green LEDs. *Materials, 7*(12), 7781-7798.

Letzel, H., Van't Hof, M. A., Marshall, G. W., & Marshall, S. J. (1997). The influence of the amalgam alloy on the survival of amalgam restorations: a secondary analysis of multiple controlled clinical trials. *Journal of Dental Research, 76*(11), 1787-1798.

Li, L., Pan, H., Tao, J., Xu, X., Mao, C., Gu, X., & Tang, R. (2008). Repair of enamel by using hydroxyapatite nanoparticles as the building blocks. *Journal of Materials Chemistry, 18*(34), 4079-4084.

Liguo, Y., & Yanhua, Z. (2010). Preparation of nano-silver flake by chemical reduction method. *Rare Metal Materials and Engineering, 39*(3), 401-404.

Lin, J. H. C., Chen, F. Y. Y., Chiang, H. J., & Ju, C. P. (2011). Effect of ball milling on structures and properties of dispersed-type dental amalgam. *Dental Materials, 27*(4), 65-79.

Lin, J. H. C., Marshall, G. W., & Marshall, S. J. (1983). Microstructures of Cu-rich amalgams after corrosion. *Journal of Dental Research, 62*(2), 112-115.

Liu, J., Yang, X., & Tian, X. (2008). Preparation of silver/hydroxyapatite nanocomposite spheres. *Powder Technology, 184*(1), 21-24.

Liu, Y., Chen, S., Zhong, L., & Wu, G. (2009). Preparation of high-stable silver nanoparticle dispersion by using sodium alginate as a stabilizer under gamma radiation. *Radiation Physics and Chemistry, 78*(4), 251-255.

Logeswari, P., Silambarasan, S., & Abraham, J. (2015). Synthesis of silver nanoparticles using plants extract and analysis of their antimicrobial property. *Journal of Saudi Chemical Society, 19*(3), 311-317.

López Miranda, A., López Valdivieso, A., & Viramontes Gamboa, G. (2012). Silver nanoparticles synthesis in aqueous solutions using sulfite as reducing agent and sodium dodecyl sulfate as stabilizer. *Journal of Nanoparticle Research, 14*(9), 1101.

Lotfi, M., Vosoughhosseini, S., Ranjkesh, B., Khani, S., Saghiri, M., & Zand, V. (2011). Antimicrobial efficacy of nanosilver, sodium hypochlorite and chlorhexidine gluconate against *Enterococcus faecalis*. *African Journal of Biotechnology, 10*(35), 6799-6803.

Lu, X., Zhang, B., Wang, Y., Zhou, X., Weng, J., Qu, S., Feng, B., Watari, F., Ding, Y., & Leng, Y. (2010). Nano-Ag-loaded hydroxyapatite coatings on titanium surfaces by electrochemical deposition. *Journal of the Royal Society Interface, 8*(57), 529-539.

Lu, Y. C., & Chou, K. S. (2008). A simple and effective route for the synthesis of nano-silver colloidal dispersions. *Journal of the Chinese Institute of Chemical Engineers, 39*(6), 673-678.

Mahler, D. (1997). The high-copper dental amalgam alloys. *Journal of Dental Research, 76*(1), 537-541.

Mahler, D., Adey, J. D., & Fleming, M. A. (1994). Hg emission from dental amalgam as related to the amount of Sn in the Ag-Hg (γ1) phase. *Journal of Dental Research, 73*(10), 1663-1668.

Mahler, D., Engle, J. H., & Adey, J. D. (1990). Effect of Pd on the clinical performance of amalgam. *Journal of Dental Research, 69*(11), 1759-1761.

Mahler, D., Marantz, R. L., & Engle, J. H. (1980). A predictive model for the clinical marginal fracture of amalgam. *Journal of Dental Research, 59*(8), 1420-1427.

Malik Masudi, S., & Sukminingrum, N. (2015, 30 August – 3 September). *Microleakage in Open-Sandwich Class II Dental Restorations.* Paper presented at the European Conference on Biomaterials, Krakow, Poland

Manappallil, J. J. (2015). *Basic dental materials* (4th ed.): Jaypee Brothers Medical Publishers (P) Ltd.

Manhart, J., Chen, H. Y., Hamm, G., & Hickel, R. (2004). Review of the clinical survival of direct and indirect restorations in posterior teeth of the permanent dentition. *Operative Dentistry, 29*(5), 481-508.

Mante, F. K., Lin, J. H. C., Mante, M. O., & Greener, E. H. (1998). The effect of noble metals on the mechanical properties of dispersed phase dental amalgam. *Journal of Oral Rehabilitation, 25*(4), 279-284.

Marek, M. (1997). The effect of tin in the Ag-Hg phase of dental amalgam on dissolution of mercury. *Dental Materials, 13*(5-6), 353-359.

Marquez, J. A., Murr, L. E., & Agüero, V. (2000). A study of alternative metal particle structures and mixtures for dental amalgams based on mercury additions. *Journal of Materials Science: Materials in Medicine, 11*(8), 469-479.

Maserejian, N. N., Trachtenberg, F. L., Assmann, S. F., & Barregard, L. (2007). Dental amalgam exposure and urinary mercury levels in children: The New England children's amalgam trial. *Environmental Health Perspectives, 116*(2), 256-262.

Melchart, D., Köhler, W., Linde, K., Zilker, T., Kremers, L., Saller, R., & Halbach, S. (2008). Biomonitoring of mercury in patients with complaints attributed to dental amalgam, healthy amalgam bearers, and amalgam-free subjects: A diagnostic study. *Clinical Toxicology, 46*(2), 133-140.

Mendis, P., De Silva, R. M., De Silva, K. M. N., Wijenayaka, L. A., Jayawardana, K., & Yan, M. (2016). Nanosilver rainbow: a rapid and facile method to tune different colours of nanosilver through the controlled synthesis of stable spherical silver nanoparticles. *RSC Advances, 6*(54), 48792-48799.

Mitchell, R. J., & Okabe, T. (1996). Setting reactions in dental amalgam Part 1. Phases and microstructures between one hour and one week. *Critical Reviews in Oral Biology and Medicine, 7*(1), 12-22.

Mitsiadis, T. A., Woloszyk, A., & Jiménez Rojo, L. (2012). Nanodentistry: Combining nanostructured materials and stem cells for dental tissue regeneration. *Nanomedicine, 7*(11), 1743-1753.

Mjör, I. A., & Jokstad, A. (1993). Five-year study of Class II restorations in permanent teeth using amalgam, glass polyalkenoate (ionomer) cermet and resin-based composite materials. *Journal of Dentistry, 21*(6), 338-343.

Mohd Azmi, F., Ariffin, Z., & Khursheed Alam, M. (2013). *In vitro study of antibacterial properties of dental restorative materials towards Streptococcus sobrinus and Lactobacillus salivarius.* University Science Malaysia. Retrieved from https://docs.wixstatic.com/ugd/43ee11_279e359da1bf4b10b5ed91c838fc0f2f.pdf

Monteiro, D. R., Gorup, L. F., Takamiya, A. S., de Camargo, E. R., Filho, A. C. R., & Barbosa, D. B. (2012). Silver distribution and release from an antimicrobial denture base resin containing silver colloidal nanoparticles. *Journal of Prosthodontics: Implant, Esthetic and Reconstructive Dentistry, 21*(1), 7-15.

Morsy, S. M. I. (2014). Role of surfactants in nanotechnology and their applications. *International Journal of Current Microbiology and Applied Science, 3*(5), 237-260.

Moszner, N., & Klapdohr, S. (2004). Nanotechnology for dental composites. *International Journal of Nanotechnology, 1*(1), 130-156.

Murdock, R. C., Braydich-Stolle, L., Schrand, A. M., Schlager, J. J., & Hussain, S. M. (2008). Characterization of nanomaterial dispersion in solution prior to in vitro exposure using dynamic light scattering technique. *Toxicological Sciences, 101*(2), 239-253.

Nam, K. Y. (2011). In vitro antimicrobial effect of the tissue conditioner containing silver nanoparticles. *The Journal of Advanced Prosthodontics, 3*(1), 20-24.

Natsuki, J., Natsuki, T., & Hashimoto, Y. (2015). A review of silver nanoparticles: Synthesis methods, properties and applications. *International Journal of Materials Science and Applications, 4*(5), 325-332.

Neme, A. L., Wagner, W. C., & O'Brien, W. J. (1999). Effects of palladium addition on emission of mercury vapor from dental amalgam. *Dental Materials, 15*(6), 382-389.

Odabaş, M. E., Çinar, Ç., Akça, G., Araz, İ., Ulusu, T., & Yücel, H. (2011). Short-term antimicrobial properties of mineral trioxide aggregate with incorporated silver-zeolite. *Dental Traumatology, 27*(3), 189-194.

Okabe, T., & Mitchell, R. J. (1996). Setting reactions in dental amalgam Part 2. The kinetics of amalgamation. *Critical Reviews in Oral Biology and Medicine, 7*(1), 23-35.

Okabe, T., Yamashita, T., Nakajima, H., Berglund, A., Zhao, L., Guo, I., & Ferracane, J. L. (1994). Reduced mercury vapor release from dental amalgams prepared with binary Hg-In liquid alloys. *Journal of Dental Research, 73*(11), 1711-1716.

Osborne, J. W., & Summitt, J. B. (1995). Mechanical properties and clinical performance of a gallium restorative material. *Operative Dentistry, 20*, 241-241.

Pal, A., Shah, S., & Devi, S. (2009). Microwave-assisted synthesis of silver nanoparticles using ethanol as a reducing agent. *Materials Chemistry and Physics, 114*(2-3), 530-532.

Pal, J., & Deb, M. K. (2012). Microwave synthesis of polymer coated silver nanoparticles by glucose as reducing agent. *Indian journal of Chemistry, 51*, 821-824.

Park, J., Joo, J., Kwon, S. G., Jang, Y., & Hyeon, T. (2007). Synthesis of monodisperse spherical nanocrystals. *Angewandte Chemie International Edition, 46*(25), 4630-4660.

Patra, J. K., & Baek, K. H. (2014). Green nanobiotechnology: Factors affecting synthesis and characterization techniques. *Journal of Nanomaterials, 2014*(219), 1-12.

Pease, R. F., & Chou, S. Y. (2008). Lithography and Other Patterning Techniques for Future Electronics. *Proceedings of the IEEE, 96*(2), 248-270.

Petersen, P. E., Baez, R., Kwan, S., & Ogawa, H. (2010). Future use of materials for dental restoration: Report of the meeting convened at WHO HQ, Geneva, Switzerland 16th to 17th November 2009: World Health Organization.

Phan, V. N., Lan, H., Thuy, N. T., Hien, T. M., Huy, T. Q., Van Quy, N., Chinh, H. D., Tung, L. M., Tuan, P. A., & Lam, V. D. (2013). Characterization and antimicrobial activity of silver nanoparticles prepared by a thermal decomposition technique. *Applied Physics A, 113*(3), 613-621.

Phillips, R. W., Avery, D. R., Mehra, R., Swartz, M. L., & McCune, R. J. (1972). Observations on a composite resin for Class II restorations: Two-year report. *Journal of Prosthetic Dentistry, 28*(2), 164-169.

Pinto, V. V., Ferreira, M. J., Silva, R., Santos, H. A., Silva, F., & Pereira, C. M. (2010). Long time effect on the stability of silver nanoparticles in aqueous medium: effect of the synthesis and storage conditions. *Colloids Surfaces A: Physicochemical and Engineering Aspects, 364*(1-3), 19-25.

Plasmans, P. J. J. M., Creugers, N. H. J., & Mulder, J. (1998). Long-term survival of extensive amalgam restorations. *Journal of Dental Research, 77*(3), 453-460.

Powell, L. V., Johnson, G. H., & Bales, D. J. (1989). Effect of admixed indium on mercury vapor release from dental amalgam. *Journal of Dental Research, 68*(8), 1231-1233.

Powers, J. M., & Sakaguchi, R. L. (2006). *Craig's restorative dental materials* (12th ed. ed.). St. Louis, Mo.: Mosby Elsevier.

Prabhu, S., & Poulose, E. K. (2012). Silver nanoparticles: mechanism of antimicrobial action, synthesis, medical applications, and toxicity effects. *International Nano Letters, 2*(1), 1-10.

Prathna, T., Chandrasekaran, N., Raichur, A. M., & Mukherjee, A. (2011). Biomimetic synthesis of silver nanoparticles by Citrus limon (lemon) aqueous extract and theoretical prediction of particle size. *Colloids and Surfaces B: Biointerfaces, 82*(1), 152-159.

Priyadarsini, S., Mukherjee, S., & Mishra, M. (2018). Nanoparticles used in dentistry: A review. *Journal of Oral Biology and Craniofacial Research, 8*(1), 58-67.

Qin, Y., Ji, X., Jing, J., Liu, H., Wu, H., & Yang, W. (2010). Size control over spherical silver nanoparticles by ascorbic acid reduction. *Colloids Surfaces A: Physicochemical and Engineering Aspects, 372*(1-3), 172-176.

Radakrishnan, D. (2008). Silverfil dental amalgam. from https://www.silverfilusa.com/certificationsstudies

Rai, M., Yadav, A., & Gade, A. (2009). Silver nanoparticles as a new generation of antimicrobials. *Biotechnology Advances, 27*(1), 76-83.

Reddy, A. S., Chen, C. Y., Baker, S. C., Chen, C. C., Jean, J. S., Fan, C. W., Chen, H. R., & Wang, J. C. (2009). Synthesis of silver nanoparticles using surfactin: A biosurfactant as stabilizing agent. *Materials Letters, 63*(15), 1227-1230.

Richardson, G. M., Wilson, R., Allard, D., Purtill, C., Douma, S., & Graviere, J. (2011). Mercury exposure and risks from dental amalgam in the US population, post-2000. *Science of the Total Environment, 409*(20), 4257-4268.

Saghiri, M. A., Banava, S., Sabzian, M. A., Gutmann, J. L., Asatourian, A., Ramezani, G. H., Garcia-Godoy, F., Sheibani, N., & Biology. (2014). Correlation between long-term in vivo amalgam restorations and the presence of heavy elements in the dental pulp. *Journal of Trace Elements in Medicine, 28*(2), 200-204.

Sakaguchi, R. L., Ferracane, J., & Powers, J. M. (2018). *Craig's restorative dental materials* (14th ed.). St. Missouri: Elsevier Health Sciences.

Samiei, M., Aghazadeh, M., Lotfi, M., Shakoei, S., Aghazadeh, Z., & Pakdel, S. M. V. (2013). Antimicrobial efficacy of mineral trioxide aggregate with and without silver nanoparticles. *Iranian Endodontic Journal, 8*(4), 166-170.

Sarraf, M., Dabbagh, A., Abdul Razak, B., Mahmoodian, R., Nasiri-Tabrizi, B., Hosseini, H. R. M., Saber-Samandari, S., Abu Kasim, N. H., Abdullah, H., & Sukiman, N. L. (2018a). Highly-ordered TiO2 nanotubes decorated with Ag2O nanoparticles for improved biofunctionality of Ti6Al4V. *Surface and Coatings Technology, 349*, 1008-1017.

Sarraf, M., Dabbagh, A., Abdul Razak, B., Nasiri-Tabrizi, B., Hosseini, H. R. M., Saber-Samandari, S., Abu Kasim, N. H., Yean, L. K., & Sukiman, N. L. (2018b). Silver oxide nanoparticles-decorated tantala nanotubes for enhanced antibacterial activity and osseointegration of Ti6Al4V. *Materials & Design, 154*, 28-40.

Shaini, F. J., Fleming, G. J. P., Shortall, A. C. C., & Marquis, P. M. (2001). A comparison of the mechanical properties of a gallium-based alloy with a spherical high-copper amalgam. *Dental Materials, 17*(2), 142-148.

Sharma, V. K., Yngard, R. A., & Lin, Y. (2009). Silver nanoparticles: Green synthesis and their antimicrobial activities. *Advances in Colloid Interface Science, 145*(1), 83-96.

Singh, P., Kim, Y. J., Zhang, D., & Yang, D. C. (2016). Biological synthesis of nanoparticles from plants and microorganisms. *Trends in Biotechnology, 34*(7), 588-599.

Sobczak Kupiec, A., Malina, D., Wzorek, Z., & Zimowska, M. (2011). Influence of silver nitrate concentration on the properties of silver nanoparticles. *Micro and Nano Letters, 6*(8), 656-660.

Sodagar, A., Akhavan, A., Hashemi, E., Arab, S., Pourhajibagher, M., Sodagar, K., Kharrazifard, M. J., & Bahador, A. (2016). Evaluation of the antibacterial activity of a conventional orthodontic composite containing silver/hydroxyapatite nanoparticles. *Progress in Orthodontics, 17*, 40.

Solanki, G. (2012). High copper amalgam alloys in dentistry. *International Journal of Pharmacological Research, 2*(1), 66-68.

Solanki, G. (2017). Uses of high copper amalgam alloys in dentistry. *International Journal of Drug Research and Technology, 2*(3), 222-224.

Song, J. Y., & Kim, B. S. (2009). Rapid biological synthesis of silver nanoparticles using plant leaf extracts. In D. Weuster-Botz (Ed.), Bioprocess and Biosystems Engineering (Vol. 32, pp. 79): Springer Berlin Heidelberg.

Songping, W., & Shuyuan, M. (2005). Preparation of ultrafine silver powder using ascorbic acid as reducing agent and its application in MLCI. *Materials Chemistry and Physics, 89*(2-3), 423-427.

Städtler, P. (1991). Dental amalgam. I: Conventional and non-gamma-2 amalgams. *International Journal of Clinical, Pharmacology, Therapy, Toxicology and Applied Pharmacology, 29*(4), 161-163.

Stencel, R., Kasperski, J., Pakieła, W., Mertas, A., Bobela, E., Barszczewska Rybarek, I., & Chladek, G. (2018). Properties of Experimental Dental Composites Containing Antibacterial Silver-Releasing Filler. *Materials, 11*(6), 1031.

Takahashi, H., Finger, W. J., Endo, T., Kanehira, M., Koottathape, N., Komatsu, M., & Balkenhol, M. (2011). Comparative evaluation of mechanical characteristics of nanofiller containing resin composites. *American Journal of Dentistry, 24*(5), 264-270.

Thomas, G. P. (2013). Amalgam-chemical composition, mechanical properties and common applications. . Retrieved from https://www.azom.com/article.aspx?ArticleID=8081

Tien, D. C., Tseng, K. H., Liao, C. Y., Huang, J. C., & Tsung, T. T. (2008). Discovery of ionic silver in silver nanoparticle suspension fabricated by arc discharge method. *Journal of Alloys and Compounds, 463*(1-2), 408-411.

Tolaymat, T. M., El Badawy, A. M., Genaidy, A., Scheckel, K. G., Luxton, T. P., & Suidan, M. (2010). An evidence-based environmental perspective of manufactured silver nanoparticle in syntheses and applications: A systematic review and critical appraisal of peer-reviewed scientific papers. *Science of the Total Environment, 408*(5), 999-1006.

Tran, Q. H., & Le, A. T. (2013). Silver nanoparticles: synthesis, properties, toxicology, applications and perspectives. *Advances in Natural Sciences: Nanoscience and Nanotechnology, 4*, 033001.

Tsuda, T., Yorifuji, T., Takao, S., Miyai, M., & Babazono, A. (2009). Minamata disease: Catastrophic poisoning due to a failed public health response. *Journal of Public Health Policy, 30*(1), 54-67.

UNEP. (2013). Report of the intergovernmental negotiating committee to prepare a global legally binding instrument on mercury on the work of its fifth session. .

Uo, M., Berglund, A., Cardenas, J., Pohl, L., Watari, F., Bergman, M., & Sjöberg, S. (2003). Surface analysis of dental amalgams by X-ray photoelectron spectroscopy and X-ray diffraction. *Dental Materials, 19*(7), 639-644.

Upadhyay, D., Panchal, M. A., Dubey, R. S., & Srivastava, V. K. (2006). Corrosion of alloys used in dentistry: A review. *Materials Science and Engineering: A, 432*(1-2), 1-11.

Van Nieuwenhuysen, J. P., D'Hoore, W., Carvalho, J., & Qvist, V. (2003). Long-term evaluation of extensive restorations in permanent teeth. *Journal of Dentistry, 31*(6), 395-405.

Venkatesham, M., Ayodhya, D., Madhusudhan, A., Babu, N. V., & Veerabhadram, G. (2014). A novel green one-step synthesis of silver nanoparticles using chitosan: catalytic activity and antimicrobial studies. *Applied Nanoscience, 4*(1), 113-119.

Verma, A., & Mehata, M. S. (2016). Controllable synthesis of silver nanoparticles using Neem leaves and their antimicrobial activity. *Journal of Radiation Research and Applied Sciences, 9*(1), 109-115.

Verma, S., Gokhale, R., & Burgess, D. J. (2009). A comparative study of top-down and bottom-up approaches for the preparation of micro/nanosuspensions. *International Journal of Pharmaceutics, 380*(1-2), 216-222.

Vigneshwaran, N., Ashtaputre, N. M., Varadarajan, P. V., Nachane, R. P., Paralikar, K. M., & Balasubramanya, R. H. (2007). Biological synthesis of silver nanoparticles using the fungus Aspergillus flavus. *Materials Letters, 61*(6), 1413-1418.

Wang, D., Song, C., Hu, Z., & Zhou, X. (2005). Synthesis of silver nanoparticles with flake-like shapes. *Materials Letters, 59*(14-15), 1760-1763.

Wang, K., Chin, P. J., Yeh, C. F., & Gan, D. (2015). The orientation relationships and interfaces of $Ag_3Sn$ and $Ag_4Sn$ on Ag and a discussion of their formation sequence. *Thin Solid Films, 589*, 27-31.

Wanger, C. D., Riggs, W., Davis, L., Moulder, J., & Muilenberg, G. (1992). Handbook of X-ray Photoelectron Spectroscopy. Perkin-Elmer Corp. Eden Prairie, Minnesota, USA.

Wani, I. A., Ganguly, A., Ahmed, J., & Ahmad, T. (2011). Silver nanoparticles: Ultrasonic wave assisted synthesis, optical characterization and surface area studies. *Materials Letters, 65*(3), 520-522.

Wani, I. A., Khatoon, S., Ganguly, A., Ahmed, J., Ganguli, A. K., & Ahmad, T. (2010). Silver nanoparticles: Large scale solvothermal synthesis and optical properties. *Materials Research Bulletin, 45*(8), 1033-1038.

Watkins, J. H., Nakajima, H., Hanaoka, K., Zhao, L., Iwamoto, T., & Okabe, T. (1995). Effect of zinc on strength and fatigue resistance of amalgam. *Dental Materials, 11*(1), 24-33.

Wijnhoven, S. W. P., Peijnenburg, W. J. G. M., Herberts, C. A., Hagens, W. I., Oomen, A. G., Heugens, E. H. W., Roszek, B., Bisschops, J., Gosens, I., & Van De Meent, D. (2009). Nano-silver–A review of available data and knowledge gaps in human and environmental risk assessment. *Nanotoxicology, 3*(2), 109-138.

WordPress Theme. (2014). Pocket Dentristry. from http://pocketdentistry.com/2-1-dental-amalgams/

World Health Organization. (1991). *Environmental health criteria 118*. Paper presented at the International Programme on Chemical Safety, Geneva, Switzerland.

Xu, L., Shen, J., Lu, C., Chen, Y., & Hou, W. (2009). Self-assembled three-dimensional architectures of Y2 (WO4) 3: Eu: controlled synthesis, growth mechanism, and shape-dependent luminescence properties. *Crystal Growth and Design, 9*(7), 3129-3136.

Yahya, N., Puspitasari, P., & Latiff, N. R. A. (2013). Hardness improvement of dental amalgam using zinc oxide and aluminum oxide nanoparticles. In A. Öchsner, L. F. M. da Silva & H. Altenbach (Eds.), *Characterization and Development of Biosystems and Biomaterials* (pp. 9-32). Berlin Heidelberg: Springer-Verlag.

Yin, B., Ma, H., Wang, S., & Chen, S. (2003). Electrochemical synthesis of silver nanoparticles under protection of poly (N-vinylpyrrolidone). *The Journal of Physical Chemistry B, 107*(34), 8898-8904.

Yoshida, K., Tanagawa, M., Matsumoto, S., Yamada, T., & Atsuta, M. (1999). Antibacterial activity of resin composites with silver-containing materials. *European Journal of Oral Sciences, 107*(4), 290-296.

Zhao, L., Wang, H., Huo, K., Cui, L., Zhang, W., Ni, H., Zhang, Y., Wu, Z., & Chu, P. K. (2011). Antibacterial nano-structured titania coating incorporated with silver nanoparticles. *Biomaterials, 32*(24), 5706-5716.

Zhou, K., Dong, C., Zhang, X., Shi, L., Chen, Z., Xu, Y., & Cai, H. (2015). Preparation and characterization of nanosilver-doped porous hydroxyapatite scaffolds. *Ceramics International, 41*(1), 1671-1676.

Zhu, J., Liu, S., Palchik, O., Koltypin, Y., & Gedanken, A. (2000). Shape-controlled synthesis of silver nanoparticles by pulse sonoelectrochemical methods. *Langmuir, 16*(16), 6396-6399.

Zimmer, H., Ludwig, H., Bader, M., Bailer, J., Eickholz, P., Staehle, H. J., & Triebig, G. (2002). Determination of mercury in blood, urine and saliva for the biological monitoring of an exposure from amalgam fillings in a group with self-reported adverse health effects. *International Journal of Hygiene and Environmental Health Perspectives, 205*(3), 205-211.

## LIST OF PUBLICATIONS AND PAPERS PRESENTED

### Chapter in Book

**Ramasindarum, C.,** Balakrishnan, V., Abu Kasim, N. H., & Yarmo, M. A. (2013). *Structural and compositional characterisation of Silverfil amalgam*. In: Öchsner A., da Silva L., Altenbach H. (eds) *Characterization and Development of Biosystems and Biomaterials. Advanced Structured Materials* (vol 29, 153-166.), *Springer, Berlin, Heidelberg.,* (Non ISI-Cited Publication)

# Structural and Compositional Characterization of Silverfil Amalgam

**Chanthiriga Ramasindarum, Vengadaesvaran Balakrishnan, Noor Hayaty Abu Kasim and Mohd Ambar Yarmo**

**Abstract** Silverfil™ (Silverfil dental Products, Malaysia) is a commercially available dental amalgam which is based on silver (Ag) and mercury (Hg) only. The objective of this study was to determine the structural state and chemical composition of the starting materials and presence of mercury in the resulting amalgam. All the starting materials of the Silverfil amalgam were characterized using Field Emission Scanning Electron Microscopy (FESEM-EDX), X-Ray Diffraction (XRD) and X-Ray Photoelectron Spectroscopy (XPS). Analysis using FESEM depicts that amalgam ($Ag_2Hg_3$) clusters were formed as a matrix consisting of crystalline solid. The EDX analysis showed that all the chemical composition of the starting materials consists of Ag and Hg only. The XRD analysis also revealed that Ag and Hg form as isometric (cubic)-hexoctahedral with unit cells of 10.06 Å. This value is similar to a naturally occurring mineral called "Moschellandsbergite" which is found in the district of Landsberg in Germany. The XPS analysis showed that there was no free mercury ($Hg^0$) present in the starting material. When the resulting amalgam was analysed, the binding energy of

C. Ramasindarum · N. H. Abu Kasim
Department of Conservative Dentistry,
University Malaya, 50603 Kuala Lumpur, Malaysia
e-mail: chanthi@um.edu.my

N. H. Abu Kasim
e-mail: nhayaty@um.edu.my

V. Balakrishnan (✉)
Department of Physic, University Malaya,
50603 Kuala Lumpur, Malaysia
e-mail: venga@um.edu.my

M. A. Yarmo
School of Chemical Science and Food Technology,
Universiti Kebangsaan Malaysia, 43600 Bangi, Malaysia
e-mail: ambar@pkrisc.cc.ukm.my

A. Öchsner et al. (eds.), *Characterization and Development of Biosystems and Biomaterials*, Advanced Structured Materials 29,
DOI: 10.1007/978-3-642-31470-4_10, © Springer-Verlag Berlin Heidelberg 2013

**Proceedings**

1. **Ramasindarum, C.,** Balakrishnan, V., Abu Kasim, N. H., & Yarmo, M. A. (2011). *Structural and compositional characterisation of Silverfil amalgam*. Paper presented at the 5th International Conference on Advanced Computational Engineering and Experimenting, ACE-X 2011, Algarve, Portugal. (SCOPUS-Cited Publication).

2. **Ramasindarum, C.,** Abu Kasim, N. H., & Balakrishnan, V., and Yarmo, M. A. (2011). *Diametral tensile strength and microhardness of two different amalgams.* J Dent Res 90B, Abst. 162 (www.dentalresearch.org) (ISI- Cited Publication).

3. **Ramasindarum, C.,** Abu Kasim, N. H., Balakrishnan, V., & Yarmo, M. A. (2011). *Structural and compositional characterisation of Silverfil™ amalgam*. J Dent Res 90A, Abst. 162 (www.dentalresearch.org) (ISI- Cited Publication)

**Attended Conferences**

1. The effect of nanosilver particles on the physico-mechanical properties of Silverfil$^{TM}$ a free mercury dental amalgam. University of Malaya Three Minute Thesis Competition (UM3MT), Faculty of Dentistry, University Malays, Kuala Lumpur. 24th April 2018.
2. Synthesis, Microstructure and Mechanical Properties of Nanosilver Amalgam. 4$^{th}$ International Conference on Functional Materials and Devices (ICFMD 2013). Penang, Malaysia. 8-11 April 2013 (Oral presentation).
3. Diametral Tensile Strength & Microhardness of Three Different Amalgams. 25$^{th}$ IADR SEA Division Meeting. Singapore. 28-30 October 2011 (Poster presentation).